

**DOT/FAA/TC-19/50, P2**

Federal Aviation Administration  
William J. Hughes Technical Center  
Aviation Research Division  
Atlantic City International Airport  
New Jersey 08405

# **Development of a Tabulated Material Model for Composite Material Failure, MAT213**

## **Part 2: Experimental Tests to Characterize the Behavior and Properties of T800-F3900 Toray Composite**

January 2020

Final Report

This document is available to the U.S. public through the National Technical Information Services (NTIS), Springfield, Virginia 22161.

This document is also available from the Federal Aviation Administration William J. Hughes Technical Center at [actlibrary.tc.faa.gov](http://actlibrary.tc.faa.gov).



U.S. Department of Transportation  
**Federal Aviation Administration**

## **NOTICE**

This document is disseminated under the sponsorship of the U.S. Department of Transportation in the interest of information exchange. The U.S. Government assumes no liability for the contents or use thereof. The U.S. Government does not endorse products or manufacturers. Trade or manufacturers' names appear herein solely because they are considered essential to the objective of this report. The findings and conclusions in this report are those of the author(s) and do not necessarily represent the views of the funding agency. This document does not constitute FAA policy. Consult the FAA sponsoring organization listed on the Technical Documentation page as to its use.

This report is available at the Federal Aviation Administration William J. Hughes Technical Center's Full-Text Technical Reports page: [actlibrary.tc.faa.gov](http://actlibrary.tc.faa.gov) in Adobe Acrobat portable document format (PDF).

**Technical Report Documentation Page**

1. Report No. DOT/FAA/TC-19/50, P2		2. Government Accession No.		3. Recipient's Catalog No.	
4. Title and Subtitle  Development of a Tabulated Material Model for Composite Material Failure, MAT213  Part 2: Experimental Tests to Characterize the Behavior and Properties of T800-F3900 Toray Composite				5. Report Date January 2020	
				6. Performing Organization Code	
7. Author(s) Bilal Khaled, Loukham Shyamsunder, Nathan Schmidt, Canio Hoffarth and Subramaniam Rajan				8. Performing Organization Report No.	
9. Performing Organization Name and Address School of Sustainable Engineering and the Built Environment Arizona State University 660 South College Ave Tempe, AZ 85281-3005				10. Work Unit No. (TRAIS)	
				11. Contract or Grant No. FAA Grant 12-G-001 NASA Contract NN15CA32	
12. Sponsoring Agency Name and Address  U.S. Department of Transportation Federal Aviation Administration FAA New England Regional Office 1200 District Ave Burlington, MA 01803				13. Type of Report and Period Covered  Final Report	
				14. Sponsoring Agency Code AIR-6A0	
15. Supplementary Notes  The Federal Aviation Administration Aviation William J. Hughes Technical Center Research Division COR was Daniel Cordasco and the NASA Glenn Research Center Contracting Officer Representative was Robert Goldberg					
16. Abstract  One of the challenges in building a predictive numerical model for composites is the ability to model accurately the behavior of the structure, especially under impact loading. This report describes a newly developed orthotropic material model that has three distinct sub-models for deformation, damage, and failure of general composites. This model has been implemented in the commercial finite element program—LS-DYNA—as *MAT_213 (*MAT_COMPOSITE_TABULATED_PLASTICITY_DAMAGE). Tabulated data can be generated for this model using laboratory tests or via virtual testing. The yield function is a modified form of the Tsai-Wu failure model. A non-associated plastic flow is used. Rate and temperature dependence are supported along with tension-compression asymmetric behavior. The damage sub-model enables uncoupled and coupled parameters to be defined. Strain equivalence between the true and the effective stress space permits decoupling of the plasticity and damage calculations. The failure modeling is currently being enhanced, however, the initial version in this report describes some of the most commonly used failure criteria, including principal strain, Tsai-Wu, and a generalized tabulated laminate failure criterion. Part 1 describes the experimental procedures and results from characterizing a widely used aerospace composite—T800-F3900. Part 2 discusses the theory, implementation, verification, and validation of the MAT213 material model using the T800-F3900 composite as a test case. Verification tests are carried out using single and multiple element models. Validation tests are carried out using data from impact tests carried out at NASA-GRC, which involve T800-F3900 composite panels. Part 3 discusses the probabilistic modeling implementation in LS-DYNA to support MAT213 (via *DEFINE_STOCHASTIC_VARIATION_MAT213) and compares the results from deterministic and probabilistic modeling of impact events.					
17. Key Words  Orthotropic plasticity, material characterization testing, damage, failure, cohesive zone modeling, explicit finite element analysis, probabilistic modeling, impact simulations. Composite failure, LSDYNA, MAT213, Tabulated material model.			18. Distribution Statement  This document is available to the U.S. public through the National Technical Information Service (NTIS), Springfield, Virginia 22161. This document is also available from the Federal Aviation Administration William J. Hughes Technical Center at <a href="http://actlibrary.tc.faa.gov">actlibrary.tc.faa.gov</a> .		
19. Security Classif. (of this report) Unclassified		20. Security Classif. (of this page) Unclassified		21. No. of Pages	22. Price

## TABLE OF CONTENTS

1	OVERVIEW.....	1
2	INPUT FOR MAT213 MATERIAL MODEL AND REQUIRED MATERIAL CHARACTERIZATION TESTS .....	2
2.1	SAMPLE PREPARATION.....	2
2.2	TEST MACHINES, FIXTURES, EQUIPMENT, AND SOFTWARE .....	6
2.3	TYPICAL TEST PROCEDURE .....	10
2.4	POST-PROCESSING OF TEST DATA .....	11
3	QS-RT TEST DETAILS AND RESULTS.....	14
3.1	TEST T1: IN-PLANE 0° TENSION TEST.....	14
3.2	TEST T2: IN-PLANE 90° TENSION TEST.....	18
3.3	TEST T3: OUT-OF-PLANE TENSION TEST .....	23
3.4	TEST T4: IN-PLANE 0° COMPRESSION TEST .....	28
3.5	TEST T5: IN-PLANE 90° COMPRESSION TEST .....	31
3.6	TEST T6: OUT-OF-PLANE COMPRESSION TEST .....	35
3.7	TEST T7: SHEAR TEST IN THE 1-2 PLANE.....	39
3.8	TEST T8: SHEAR TEST IN THE 2-3 PLANE.....	44
3.9	TEST T9: SHEAR TEST IN THE 1-3 PLANE.....	48
3.10	TEST T10: 45° OFF-AXIS TENSION TEST IN THE 1-2 PLANE .....	52
3.11	T11 TEST: 45° OFF-AXIS COMPRESSION TEST IN THE 2-3 PLANE .....	55
3.12	TEST T12: OFF-AXIS COMPRESSION TEST 45° IN THE 1-3 PLANE .....	59
3.13	TEST T13: MASS DENSITY TEST .....	63
3.14	TEST T14: VOLUME FRACTION TEST .....	66
4	DAMAGE CHARACTERIZATION TEST DETAILS AND RESULTS .....	69
4.1	BACKGROUND .....	69
4.2	EXPERIMENTAL METHODS .....	72
4.2.1	UNCOUPLED EXPERIMENTS.....	72
4.2.2	COUPLED EXPERIMENTS.....	74
4.2.3	COMPUTING ELASTIC MODULUS .....	76
4.3	EXPERIMENTAL RESULTS.....	80
4.3.1	UNCOUPLED 2-DIRECTION TENSION.....	80
4.3.2	UNCOUPLED 1-2 PLANE SHEAR .....	81
4.3.3	UNCOUPLED 2-DIRECTION COMPRESSION.....	86
4.3.4	COUPLED 2-DIRECTION COMPRESSION 2-DIRECTION TENSION ...	90
4.3.5	COUPLED 2-DIRECTION COMPRESSION 2-1 PLANE SHEAR.....	94
4.3.6	REMAINING DAMAGE CHARACTERIZATION EXPERIMENTS .....	104
5	CONCLUDING REMARKS .....	105
6	REFERENCES.....	106
	APPENDIX A—ANALYSIS OF DIC-OBTAINED STRAIN FIELD .....	112

## LIST OF FIGURES

Figure 1-1. Principal material directions	1
Figure 2.1-1. Optical microscopy images of finished edges	4
Figure 2.1-2. Double lap shear test specimen	5
Figure 2.1-3. Close up of a typical speckled surface	6
Figure 2.2-1. Experimental equipment	9
Figure 2.2-2. Typical strain gage section	10
Figure 3.1-1. Typical specimen geometry and layout	14
Figure 3.1-2. 1-direction tension specimens prior to testing	15
Figure 3.1-3. 1-direction tension specimens after testing	16
Figure 3.1-4. 1-direction tension stress-strain curves	17
Figure 3.2-1(a). Typical specimen geometry and layout (dimensions in mm)	18
Figure 3.2-1(b). Modified specimen geometry and layout	18
Figure 3.2-2. 2-direction tension specimens prior to testing	19
Figure 3.2-3. 2-direction tension specimens after testing	19
Figure 3.2-4. Transverse strain plot	20
Figure 3.2-5. Longitudinal strain plot	21
Figure 3.2-6. Determination of Poisson's ratio	21
Figure 3.2-7. 2-direction tension stress-strain curves	22
Figure 3.3-1. Typical specimen geometry and layout	23
Figure 3.3-2. Fiberglass tab layup geometry	24
Figure 3.3-3. 3-direction tension test experimental setup	24
Figure 3.3-4. 3-direction tension specimens prior to testing	25
Figure 3.3-5. 3-direction tension specimens after testing	26
Figure 3.3-6. 3-direction tension stress-strain curves	27
Figure 3.4-1. Typical specimen geometry and layout	28
Figure 3.4-2. 1-direction compression specimens after testing	29
Figure 3.4-3. 1-direction compression stress-strain curves	30
Figure 3.5-1. Typical specimen geometry and layout	31
Figure 3.5-2. 2-direction compression specimens after testing	33
Figure 3.5-3. 2-direction compression stress-strain curves	34
Figure 3.6-1. Typical specimen geometry and layout	35
Figure 3.6-2. 3-direction compression specimens prior to testing	36
Figure 3.6-3. 3-direction compression specimens after testing	37
Figure 3.6-4. 3-direction compression stress-strain curves	38
Figure 3.7-1. Typical specimen geometry	39
Figure 3.7-2. ASTM definition of shear failure	40
Figure 3.7-3. ASTM acceptable failure modes	40
Figure 3.7-4. 1-2 plane shear specimens prior to testing	41
Figure 3.7-5. 1-2 plane shear specimens after testing	42
Figure 3.7-6. 1-2 plane shear stress-tensorial strain curves	43
Figure 3.8-1. Typical specimen geometry and layout	44
Figure 3.8-2. 2-3 plane shear specimens prior to testing	45
Figure 3.8-3. 2-3 plane shear specimens after testing	46
Figure 3.8-4. 2-3 plane shear stress-tensorial strain curves	47

Figure 3.9-1. Typical specimen geometry and layout	48
Figure 3.9-2. 1-3 plane shear specimens prior to testing	49
Figure 3.9-3. 1-3 plane shear specimens after testing	50
Figure 3.9-4. 1-3 plane shear stress-tensorial strain curves	51
Figure 3.10-1. Specimen geometry and layout	52
Figure 3.10-2. 1-2 plane 45° off-axis tension specimens prior to testing	53
Figure 3.10-3. 1-2 plane 45° off-axis tension specimens after testing	53
Figure 3.10-4. 1-2 plane 45° off-axis tension stress-strain curves	54
Figure 3.11-1. Specimen geometry and layout	55
Figure 3.11-2. 2-3 plane 45° off-axis compression test specimens prior to testing	56
Figure 3.11-3. 2-3 plane 45° off-axis compression test specimens after testing	57
Figure 3.11-4. 2-3 plane 45° off-axis compression stress-strain curves	58
Figure 3.12-1. Specimen geometry and layout	59
Figure 3.12-2. 1-3 plane 45° off-axis compression test specimens prior to testing	60
Figure 3.12-3. 1-3 plane 45° off-axis compression test specimens after testing	61
Figure 3.12-4. 1-3 plane 45° off-axis compression stress-strain curves	62
Figure 3.13-1. Specific gravity test	63
Figure 3.14-1. ImageJ volume fraction analysis 16-Ply analysis zone	66
Figure 3.14-2. ImageJ volume fraction analysis original and processed images	67
Figure 4.2-1. Loading-unloading steps	73
Figure 4.2-2. Uncoupled 2-direction tension test specimen	73
Figure 4.2-3. Uncoupled 2-direction compression test specimen	74
Figure 4.2-4. Uncoupled 1-2 plane shear test specimen	74
Figure 4.2-5. Loading-unloading steps	75
Figure 4.2-6. Specimen dimensions for coupled normal-normal tests	75
Figure 4.2-7. Specimen dimensions for coupled normal-shear tests	76
Figure 4.2-8. Standard cycle for the coupled test	77
Figure 4.2-9. Individual load and unload paths the tension cycle	78
Figure 4.3-1. Uncoupled 2-direction tension test	80
Figure 4.3-2. (a) 1-2 shear specimen (b) 2-1 shear specimen	81
Figure 4.3-3. Uncoupled 1-2 plane shear experimental curves	81
Figure 4.3-4. Uncoupled 1-2 plane shear damage curves	83
Figure 4.3-5. Damage vs. total strain	84
Figure 4.3-6. Uncoupled 1-2 plane shear specimens after failure	85
Figure 4.3-7. Uncoupled 2-direction compression experimental curves	86
Figure 4.3-8. Uncoupled 2-direction compression damage curves	87
Figure 4.3-9. Uncoupled 2-direction compression specimens after failure	89
Figure 4.3-10. Experimental stress-strain curves	90
Figure 4.3-11. Coupled 2-direction compression 2-direction tension damage curves	91
Figure 4.3-12. Coupled 2-direction compression 2-direction tension specimens	93
Figure 4.3-13. Specimen dimensions for coupled 2-direction 2-1 plane shear tests	94
Figure 4.3-14. Investigative 2-direction compression test using 2-1 plane shear	95
Figure 4.3-15. Coupled 2-direction compression 2-1 plane shear	96
Figure 4.3-16. Strain field of C2-S21 coupled	97
Figure 4.3-17. Strain comparison of the C2-S21 investigative compression test	98
Figure 4.3-18. 1-2 shear specimen and 2-1 shear specimen	99

Figure 4.3-19. 1-2 and 2-1 plane shear stress-strain	99
Figure 4.3-20. Coupled 2-direction compression 1-2 plane shear	101
Figure 4.3-21. Coupled 2-direction compression 1-2 plane shear damage curves	102
Figure 4.3-22. Coupled 2-direction compression 2-direction tension specimens	103
Figure 4.3-23. Specimen geometry	104
Figure A.1-1. TF16-5 strain fields	114

## LIST OF TABLES

Table 1-1. T800/F3900 Manufacturer Reported Material Properties	1
Table 2-1. Summary of Test Suite	2
Table 2-2. Panels Used for Tests	2
Table 2.1-1. Waterjet Specifications	3
Table 2.1-2. 80-Grit (US Std) Specifications	3
Table 2.1-3. Grinding Wheel Specifications	3
Table 2.1-4. 46 Grit (Grinding Wheel) Specifications	4
Table 2.1-5. Adhesive Strength Study Results	5
Table 2.4-1. Descriptions of the Parameters Used in this Report	11
Table 3.1-1. 1-Direction Tension Test Specimen Dimensions	14
Table 3.1-2. Summary of 1-Direction Tension Test Results	17
Table 3.2-1. 2-Direction Tension Test Specimen Dimensions	18
Table 3.2-2. Summary of 2-Direction Tension Test Results	20
Table 3.3-1. 3-Direction Tension Test Specimen Dimensions	23
Table 3.3-2. Summary of 3-Direction Tension Test Results	27
Table 3.4-1. 1-Direction Compression Test Specimen Dimensions	28
Table 3.4-2. Summary of 1-Direction Compression Test Results	29
Table 3.5-1. 1-Direction Compression Test Specimen Dimensions	31
Table 3.5-2. Summary of 2-Direction Compression Test Results	33
Table 3.6-1. 3-Direction Compression Test Specimen Dimensions	35
Table 3.6-2. Summary of the 3-Direction Compression Test Results	38
Table 3.7-1. 1-2 Plane Shear Test Specimen Dimensions	39
Table 3.7-2. Summary of the 1-2 Plane Shear Test Results	43
Table 3.8-1. 2-3 Plane Shear Test Specimen Dimensions	44
Table 3.8-2. Summary of the 2-3 Plane Shear Test Results	46
Table 3.9-1. 2-3 Plane Shear Test Specimen Dimensions	48
Table 3.9-2. Summary of 1-3 Plane Shear Test Results	51
Table 3.10-1. 1-2 Plane 45° Off-Axis Tension Test Specimen Dimensions	52
Table 3.10-2. Summary of 1-2 Plane 45° Off-Axis Tension Test Results	54
Table 3.11-1. 2-3 Plane 45° Off-Axis Compression Test Specimen Dimensions	55
Table 3.11-2. Summary of 2-3 Plane 45° Off-Axis Compression Test Results	57
Table 3.12-1. 1-3 Plane 45° Off-Axis Compression Test Specimen Dimensions	59
Table 3.12-2. Summary of 1-3 Plane 45° Off-Axis Compression Test Results	62
Table 3.13-1. Specific Gravity	64
Table 3.13-2. Specific Gravity Summary and Statistics	65
Table 3.14-1. Volume Fraction Results 16-Ply, 200x	67
Table 3.14-2. Volume Fraction Results 16-Ply, 400x	67
Table 3.14-3. Volume Fraction Results 16-Ply, 500x	68
Table 4.1-1. Uncoupled Normal and Shear Damage Parameters	70
Table 4.1-2. Coupled Normal-Normal Damage Parameters	71
Table 4.1-3. Coupled Normal-Shear Damage Parameters	71
Table 4.1-4. Coupled Shear-Normal Damage Parameters	71
Table 4.1-5. Damaged Modulus and Plastic Strain (normal stress-strain relationship)	71
Table 4.1-6. Damaged Modulus and Plastic Strain (shear stress-strain relationship)	72

Table 4.2-1. Summary of Tension Moduli	79
Table 4.3-1. Uncoupled 1-2 Plane Shear Summary of Results	82
Table 4.3-2. Uncoupled 2-direction Compression Damage Parameters	88
Table 4.3-3. Coupled 2-direction Compression 2-direction Tension Damage	92
Table 4.3-4. Remaining Damage Characterization Experiments	104
Table A.1-1. Summary of the Maximum Strains for Each Test at Peak Stress	115

## LIST OF ACRONYMS

ASU	Arizona State University
FAA	Federal Aviation Administration
GRC	Glenn Research Center
GMU	George Mason University
NASA	National Aeronautics and Space Administration

## EXECUTIVE SUMMARY

It is a challenge to build a predictive numerical model for composites that accurately models the behavior of the structure, especially under impact loading. This report describes a new orthotropic material model with three distinct sub-models for deformation, damage, and failure of general composites. This model was implemented in the commercial finite element program,—LS-DYNA—as \*MAT\_213 (\*MAT\_COMPOSITE\_TABULATED\_PLASTICITY\_DAMAGE). You can generate tabulated data for this model using laboratory tests or virtual testing. The yield function is a modified form of the Tsai-Wu failure model with a non-associated plastic flow. Rate and temperature dependence are supported along with tension-compression asymmetric behavior. The damage sub-model enables the definition of uncoupled and coupled parameters. Strain equivalence between the true and the effective stress space enables decoupling of the plasticity and damage calculations. Failure modeling is currently being enhanced. This report describes the most commonly used failure criteria in the initial version of the model, including principal strain, Tsai-Wu, and a generalized tabulated laminate failure criterion.

Part 1 describes the experimental procedures and results from characterizing a widely used aerospace composite—T800-F3900. Part 2 describes the theory, implementation, verification, and validation of the MAT213 material model using the T800-F3900 composite as a test case. Verification tests use one or more element models. Validation tests use data from impact tests at NASA-GRC with T800-F3900 composite panels. Part 3 describes the probabilistic modeling implementation in LS-DYNA to support MAT213 (via \*DEFINE\_STOCHASTIC\_VARIATION\_MAT213). It compares the results from deterministic and probabilistic modeling of impact events.

# 1 OVERVIEW

This document summarizes the test procedures for characterizing the quasi-static (QS), room temperature (RT) behavior of T800-F3900 composite material manufactured by Toray Composites, Seattle, WA. The overall objective is to develop a framework for creating MAT213 material input to use in the LS-DYNA program [1]. Details of the MAT213 material model and its implementation are available publicly [2,3,4].

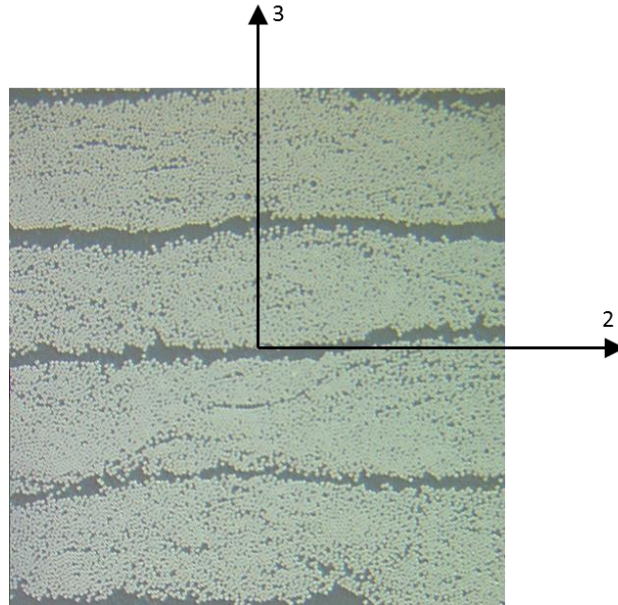


Figure 1-1. Principal material directions shown in the optical microscopy image with unidirectional fibers oriented in the 1-direction

The T800-F3900 composite is a unidirectional carbon fiber/epoxy resin composite system (figure 1-1). The material properties reported by Toray Composites shown in table 1-1 are averages of multiple replicates.

Table 1-1. T800/F3900 Manufacturer Reported Material Properties

<b>Characteristic</b>	<b>Reported Value</b>
Resin Content Beginning (%)	34.8
Resin Content Ending (%)	35.4
Ultimate Tensile Strength (psi)	434 000
Tensile Modulus (psi)	22 000 000
Tensile Strain at Failure (in/in)	0.0177
Ultimate Compressive Strength (psi)	214 000

## 2 INPUT FOR MAT213 MATERIAL MODEL AND REQUIRED MATERIAL CHARACTERIZATION TESTS

Characterization of the composite behavior requires 12 stress-strain curves as summarized in table 2-1. Three different panel types were used to create the test specimens. The panels chosen to create the respective specimens are shown in table 2-1. The panel dimensions are shown in table 2-2.

Table 2-1. Summary of Test Suite

Test ID	Description	ASTM (Panel Type)
T1	Tension 1-direction	D3039 (PT1)
T2	Tension 2-direction	D3039 (PT1)
T3	Tension 3-direction	D7291 (PT3)
T4	Compression 1-direction	D3410 (PT1)
T5	Compression 2-direction	D3410 (PT1)
T6	Compression 3-direction	D7291 (PT3)
T7	Shear 1-2 plane	D5379/M-12 (PT2)
T8	Shear 2-3 plane	D5379/M-12 (PT3)
T9	Shear 1-3 plane	D5379/M-12 (PT3)
T10	Off-axis tension (45°, 1-2 plane)	D3039 (PT1)
T11	Off-axis compression (45°, 2-3 plane)	D3039 (PT3)
T12	Off-axis compression (45°, 1-3 plane)	D3039 (PT3)
T13	Density	D791 (PT1, PT2, PT3)

Table 2-2. Panels Used for Tests

Panel Type	Nominal Dimensions (length x width)	Nominal Thickness, mm (# of plies)
PT1	12" x 24"	3.1 (16)
PT2	12" x 12"	4.7 (24)
PT3	12" x 12"	18.4 (96)

### 2.1 SAMPLE PREPARATION

Waterjet is used to cut the samples. The waterjet specifications for the three different panel thicknesses (16, 24, and 96-ply) are shown in table 2.1-1. Specifications of the abrasive used in the waterjet are shown in table 2.1-2. When necessary, the waterjet cut edges are ground using a grinding wheel matching the specifications shown in table 2.1-3. Particle size statistics of the abrasive used on the grinding wheel are shown in table 2.1-4. Test samples were generated with planar cut edges and free of any visible damage.

Table 2.1-1. Waterjet Specifications

	<b>16-ply Samples</b>	<b>24-ply Samples</b>	<b>96-ply Samples</b>
Approximate Thickness (in)	0.125	0.182	0.728
Abrasive Size (grit)	80 (US Std)	80 (US Std)	80 (US Std)
Nozzle Diameter (in)	0.03	0.03	0.03
Minimum Nozzle Pressure (psi)	30000	30000	30000
Maximum Nozzle Pressure (psi)	45000	45000	45000
Cut Speed (in/min)			
Quality 1	135.43	94.3	21.42
Quality 2	116.15	80.88	18.37
Quality 3	72.87	50.74	11.53
Quality 4	52.34	36.45	8.28
Quality 5	40.5	28.2	6.41

Table 2.1-2. 80-Grit (US Std) Specifications

<b>Sieve Size (US Std)</b>	<b>Sieve Mesh Diameter (in)</b>	<b>% Retained</b>
8	0.0937	0
12	0.0661	0
14	0.0555	0
16	0.0469	0
20	0.0331	0
30	0.0234	0
40	0.0165	0-5
50	0.0117	10-35
60	0.0098	20-40
80	0.007	20-50
120	0.0049	0-15
Pan	-	0-3

Table 2.1-3. Grinding Wheel Specifications

Frequency of Rotation (rpm)	~3500
Abrasive Grit (grit)	46 (US Std)
Tolerance (in)	±0.005
Operation	Manual

Table 2.1-4. 46 Grit (Grinding Wheel) Specifications

Minimum Particle Size (in)	0.0095
Maximum Particle Size (in)	0.022
Average Particle Size (in)	0.014

Figure 2.1-1 shows images of a typical cut sample captured using an optical microscope under various magnifications.

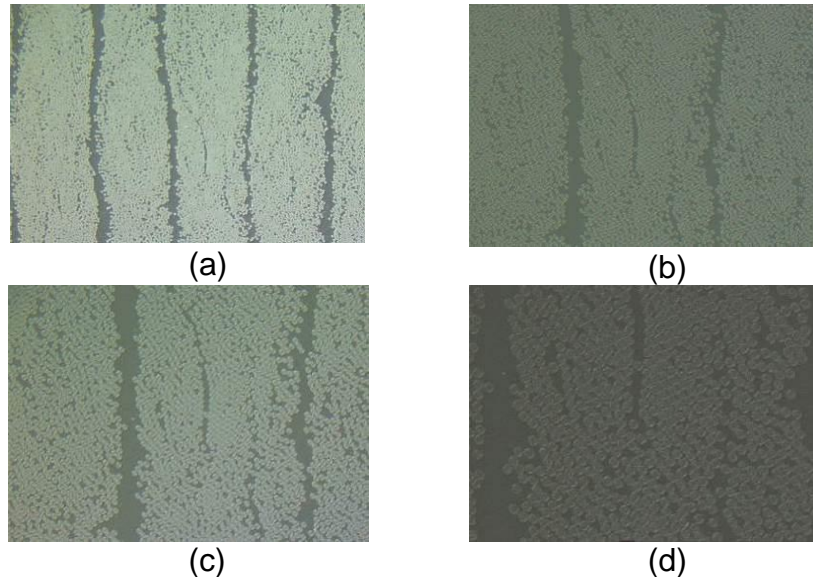


Figure 2.1-1. Optical microscopy images of finished edges after grinding (a) 200x, (b) 400x, (c) 500x, (d) 1000x

When required, G10 fiberglass tabs<sup>1</sup> are used with the sample. The fiberglass tabs act as compliant surfaces that prevent specimens from crushing when placed in the hydraulic grips. They also act as stiffening elements when conducting shear tests. The tabs are bonded to the specified specimen surfaces using a two-part epoxy adhesive.

3M DP460 Scotch Weld toughened two-part epoxy<sup>2</sup> bonds fiberglass tabs to the specimens. The guidelines in ASTM D3528-96 were applied to the adhesive strength study using a double lap shear test. The study determines the strength of the bond between fiberglass and fiberglass. Figure 2.1-2 shows the specimen dimensions and layout used in the experiments. The top and bottom hatched regions show where the specimen was gripped with hydraulic grips. The hatched gage section region shows where the shear strength study takes place.

<sup>1</sup> G10, FR4 Laminate Sheets 36"x 48", Epoxyglas™; NEMA Grade FR4, Mil-I-24768/27, <http://www.accum.com/>  
<sup>2</sup><http://multimedia.3m.com/mws/media/661220/3mtm-scotch-weld-tm-epoxy-adhesive-dp460-ns-and-off-white.pdf>

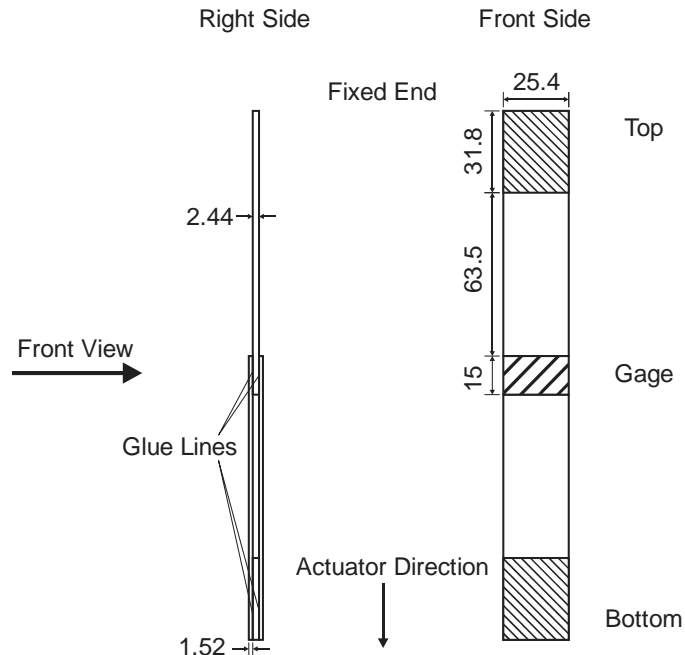


Figure 2.1-2. Double lap shear test specimen (all dimensions in mm)

The average strength of the adhesive characterization study and average strength reported by the manufacturer are shown in table 2.1-5.

Table 2.1-5. Adhesive Strength Study Results

Test	Substrate	Maximum Stress (psi)
ASU	G10 Fiberglass	3423
3M	Aluminum	4500
	Phenolic <sup>3</sup>	1400
	PVC	500

Steps taken to fully prepare the specimens for testing follow. All specimens are prepared similarly unless otherwise noted.

1. The regions on a typical specimen have bonded fiberglass tabs. The surfaces of the fiberglass tabs are bonded to the specimen and lightly sanded using 120 grit sandpaper. Sanding the surfaces ensures a complete bond between the specimen and tabs.
2. The sanded surfaces are cleaned using cotton swabs soaked with isopropyl alcohol. The surfaces are air dried until there is no visible moisture on the bonding surfaces.

<sup>3</sup> Substrate failure

3. The 3M epoxy is mixed according to the manufacturer's recommendation. A thin layer of the mixed epoxy is applied to the prepared surface of the tabs using a wooden applicator.
4. The tabs are then placed on the specimen and positioned until the surfaces of the specimen and the tabs are in complete contact and aligned properly in the desired region.
5. The specimens are cured at room temperature and atmospheric pressure for 24 hours.
6. The gage region of the specimen is painted and speckled. Speckling of the specimen involves first spraying the surface of the specimen with a layer of white paint with a flat finish. Paint is sprayed onto the surface until the specimen can no longer be seen. The paint must dry completely at room temperature.
7. After the white paint dries, black paint with a flat finish is sprayed onto the dry white paint. The black paint is sprayed in a random array of black dots deposited on the white area of the specimen.
8. After being painted, the specimens are cured for another 24 hours as recommended by the manufacturer. A close-up of a typical speckled surface is shown in figure 2.1-3.

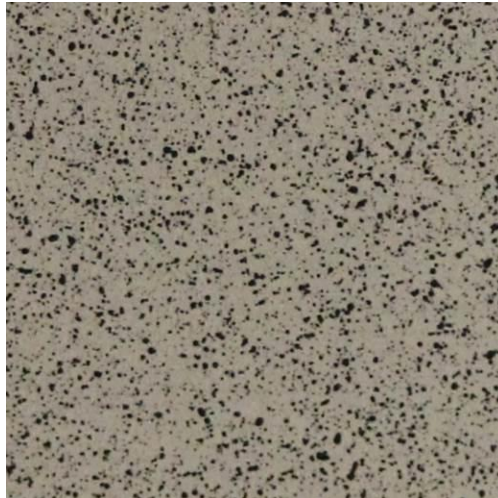


Figure 2.1-3. Close up of a typical speckled surface

## 2.2 TEST MACHINES, FIXTURES, EQUIPMENT, AND SOFTWARE

All experiments are performed using the same test frame and camera system. Post processing of the experimental images is performed using the same software as follows.

*Test Frame:* The experimental procedure is performed using an MTS 810 universal testing frame (figure 2.2-1(a)). Flat tension specimens are held in the frame with MTS 647.10A hydraulic grips (figure 2.2-1(b)). The hydraulic grips are aligned by clamping a rigid, flat steel plate and allowing the heads to freely rotate into position. After aligning the hydraulic grips, the specimen is placed into the test frame. Verticality of the specimen is ensured by using a laser alignment system (figure 2.2-1(c)). The specimen

is gripped up to the end of the fiberglass tabs. Shear specimens are held in the test frame using a Wyoming Test Fixtures losipescu shear test fixture<sup>4</sup> as shown in figure 2.2-1(d). Compression cubes are bonded to custom fixtures (figure 2.2-1(e) and machined out of A2 tool steel using Loctite liquid super glue<sup>5</sup>. Alignment of the specimen is ensured using 0.2" deep square notches machined into the center of the fixtures as shown in figure 2.2-1(f). Flat (in-plane) compression specimens were tested using a Wyoming Test Fixtures combined loading compression fixture (CLC) as shown in figure 2.2-1(g) and figure 2.2-1(h). The CLC fixture transfers load into the compression specimens through both shear load transfer and end load transfer, which lessens the need for excessive clamping forces.

Force data is gathered using an MTS 661.21A-03 load cell, last calibrated by an MTS technician on October 16, 2015. All experiments are performed under displacement control conditions. The displacement rate refers to the rate of displacement of the test frame actuator. The rate is set using the MTS system controller.



(a)



(b)



(c)



(d)

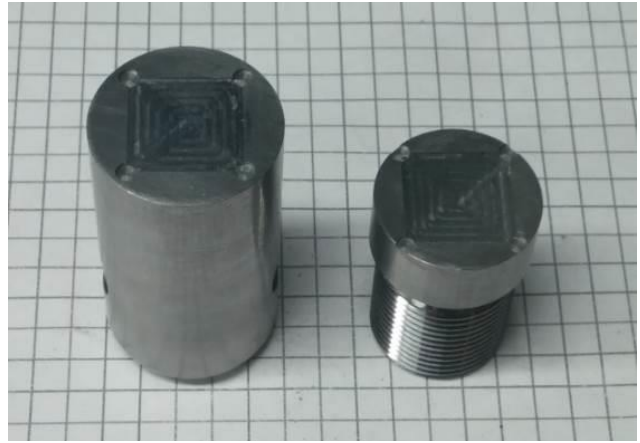
---

<sup>4</sup> <http://www.wyomingtestfixtures.com/Products/a1.html>

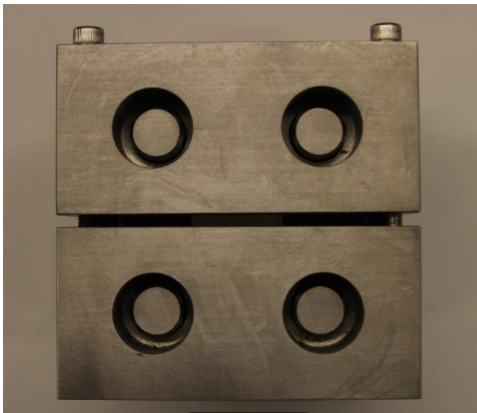
<sup>5</sup> [http://www.loctiteproducts.com/p/4/2/sg\\_bottle/overview/Loctite-Super-Glue-Longneck-Bottle.htm](http://www.loctiteproducts.com/p/4/2/sg_bottle/overview/Loctite-Super-Glue-Longneck-Bottle.htm)



(e)



(f)



(g)



(h)



(i)



(j)

Figure 2.2-1. Experimental equipment (a) Test frame, (b) Hydraulic grips, (c) Specimen alignment, (d) Iosipescu shear test fixture, (e) Compression cube fixture, (f) Custom fixture for compression tests, (g) CLC compression fixture (top), (h) CLC fixture front showing C2 specimen, (i) two DIC cameras and high-speed camera, and (j) LED lighting fixture

*Digital Image Correlation (DIC) Equipment:* Two Point Grey Grasshopper 3<sup>6</sup> cameras are used to capture images of the specimen during the experiment as shown in figure 2.2-1(i). LED lamps properly illuminate the specimen during the experiment. The cameras and lights are fixed to the same frame (figure 2.1-1(j)). The frame is leveled using a bubble level to ensure the field of view of the cameras is both horizontal and vertical, respectively. A high-speed camera is used to capture the specimen state at the moment of failure (figure 2.2-1(i)). Unless otherwise noted, images are captured at five second intervals throughout the experiment using Vic-Snap 8 [5] to obtain the strain field on the surface of the specimen.

*Post Processing:* The images captured during the experiment are processed to obtain a full strain field using Vic-3D v7. The Lagrangian definition of strain is chosen to perform the analysis. Functionality within the Vic-3D software is used to smooth the strain data with a decay filter algorithm. For the initial processing, the entire speckled region of the specimen is analyzed. After the analysis and smoothing, a smaller region with constant strain is taken as the representative strain induced in the specimen during the experiment. The region of interest is typically chosen so that the strain field is as uniform in that region as possible. Typically, this region is away from the edges of the specimen and away from areas of strain concentrations that may be present where the specimens are gripped. In this report, the area or region from which the strain values

---

<sup>6</sup> <https://www.ptgrey.com/grasshopper3-gige-vision-cameras>

are obtained and reported is referred to as the *strain gage section* (SGS). Sample images are shown in figure 2.2-2.

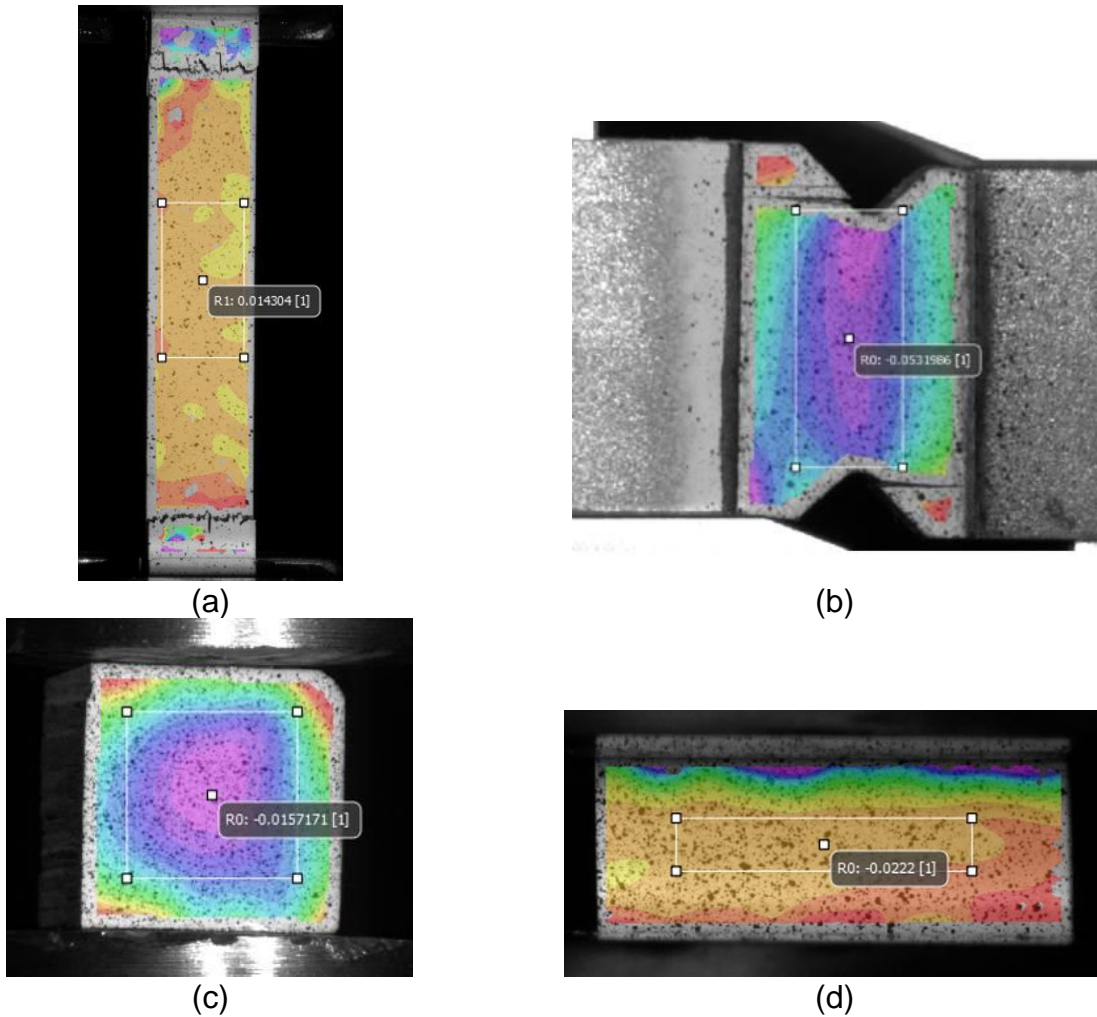


Figure 2.2-2. Typical strain gage section (a) Tension specimens, (b) Shear specimens, (c) Compression specimens (cube), (d) Compression specimens (flat panel)

*Measurement Instruments:* Several instruments were used to obtain specimen dimensions, specimen mass, and optical microscope images. Specimen dimensions were measured using a Pittsburgh 4" Digital Caliper. The caliper has a resolution of 0.0005 in. All optical microscopy images were obtained using an Olympus MX50 optical microscope.

### 2.3 TYPICAL TEST PROCEDURE

The procedure for conducting experiments is the same for each specimen unless otherwise noted. For all experiments, prior to loading the specimen, the DIC system is calibrated using Vic 3D v7. Calibration is done only when the cameras must be moved or if new fixtures will cause the plane of the specimen to move away from where the cameras were calibrated.

## 2.4 POST-PROCESSING OF TEST DATA

After the experiments are completed, force data is obtained as a function of time from the MTS controller, and strain data is obtained as a function of time from DIC analysis. The stress in the specimen is taken as the average stress across the respective cross section of the specimen. For tension and compression specimens, the cross section perpendicular to the direction of loading is used to calculate the cross-sectional area. The average stress is calculated using the following equation

$$\sigma = \frac{F}{A} \quad (1)$$

where  $F$  is the normal force reported by the load cell at the current time-step, and  $A$  is the cross-sectional area. For shear specimens, the surface between the notches, through the thickness of the specimen, is used to calculate the cross-sectional area. The average stress is calculated using the following equation

$$\tau = \frac{V}{A} \quad (2)$$

where  $V$  is the shear force reported by the load cell at the current time-step, and  $A$  is the cross-sectional area.

The strain reported from Vic 3D v7 in the region of interest is used with the calculated stress to generate a true stress-strain curve for any given specimen. After stress-strain curves for several replicates are obtained, a *model curve* used as input for MAT 213 is generated. The *model curve* is obtained in three steps. First, the average ultimate strain is calculated by averaging the ultimate strain obtained from each specimen. Second, for a given strain value, the average of the stress values from all the replicates is obtained. Last, this process is continued until the average ultimate strain is reached for each specimen either shortening or lengthening (via extrapolation) the individual stress-strain curves to that point. Extrapolation of a curve is done by performing a linear regression on the last five percent of the curve and using the resulting equation to extrapolate to the end point.

In addition to the model curve used as input for MAT 213, several parameters are obtained from the stress strain curves of each individual specimen to determine the consistency of the data. Table 2.4-1 describes each parameter and how they are obtained from the available data.

Table 2.4-1. Descriptions of the Parameters Used in this Report

<b>Parameter</b>	<b>Definition</b>	<b>Method</b>
Loading rate	Constant rate at which the actuator on the test frame is displaced.	Chosen by the experimenter as a fixed parameter at the beginning of

		the procedure. The rate is prescribed as a displacement over a certain time period.
Strain rate	The rate at which strain is induced in the specimen during a given experiment.	The strain measure of interest is plotted as a function of time and the average strain rate during the experiment is obtained by performing a linear regression. The slope of the resulting best fit line is taken as the average strain rate.
Modulus	The slope of the initial linear region of the true stress-strain curve.	The analyst determines the region that is most linear in the initial portion of the curve and performs a linear regression on the data. The slope of the resulting best fit line is taken as the modulus.
Poisson's ratio	The negative ratio of transverse strain to normal strain.	Both elastic and plastic Poisson's ratios may be obtained by plotting transverse strain as a function of normal strain. The analyst determines where the onset of plasticity occurs from the stress-strain curve. The corresponding normal strain point on the transverse strain-normal strain curve is used as the point that separates the elastic and plastic zones. A linear regression is performed on each zone separately and the slope is taken as the respective Poisson's ratio.
Peak stress	Maximum stress achieved during a given experiment.	Selected from stress data obtained through scaling the force data reported by the load cell.
Ultimate strain	Strain measured at peak stress.	Selected as the largest strain when the specimen exhibits brittle failure with no post-peak strength.
Failure strain	Strain measured when the specimen fails.	Selected as the strain when there is a large drop in stress and the specimen no longer loads back up to that peak stress point. Typically, this is when the test is terminated and used when the specimen does not exhibit brittle failure.
Transverse strain	Strain induced in the specimen perpendicular to the direction of loading in tension and compression tests. In shear tests, it is defined as strain induced in the specimen parallel to the movement of the actuator.	Obtained through DIC measurements.
Longitudinal strain	Strain induced in the specimen parallel to the direction of loading in tension and compression tests. In shear tests, it is defined as strain induced in the specimen perpendicular to the movement of the actuator.	Obtained through DIC measurements.

Shear strain	Tensorial shear strain induced in the principal plane being observed.	Obtained through DIC measurements.
--------------	---	------------------------------------

### 3 QS-RT TEST DETAILS AND RESULTS

Details of each test are discussed in this section. Applicable ASTM standards are used. Deviations from the standards for some tests are noted.

#### 3.1 TEST T1: IN-PLANE 0° TENSION TEST

This test is used to generate the tension stress-strain curve in the 1-direction.

*Specimen Geometry:* ASTM D3039 standard is applicable for this test. Due to the high strength in the 1-direction, the specimen thickness is reduced in the gage section to obtain a full curve with failure. The specimen geometry (16-ply thick) and layout is shown in figure 3.1-1. Shaded regions indicate where fiberglass tabs are bonded to the specimen.

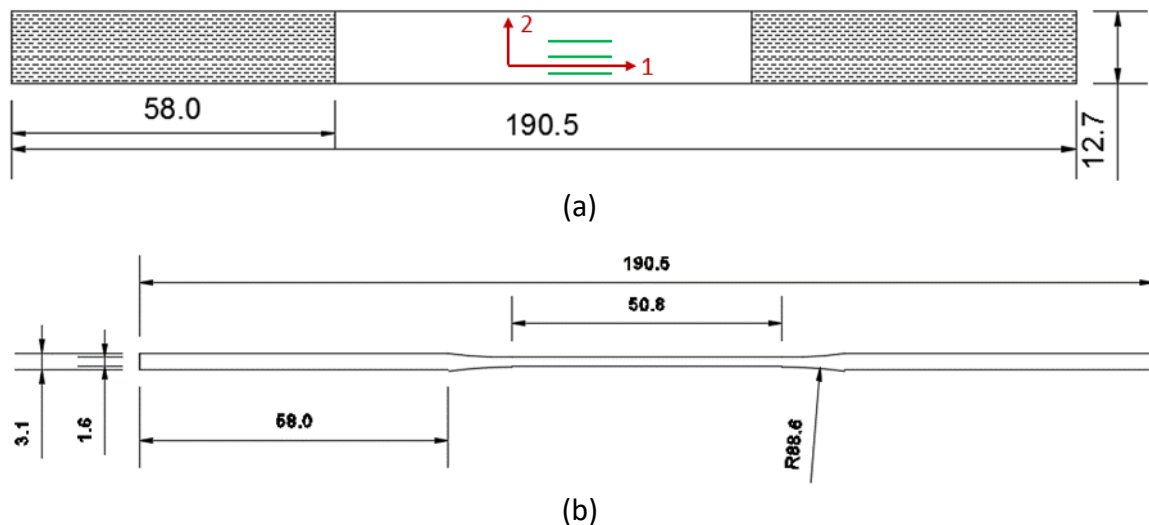


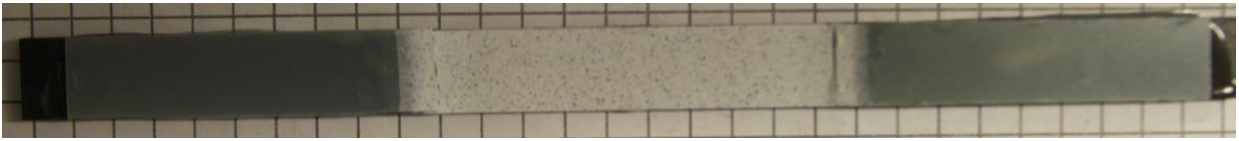
Figure 3.1-1. Typical specimen geometry and layout (a) plan view and (b) elevation view (all dimensions in mm)

The average specimen dimensions in the gage section are shown in table 3.1-1 for the three tested replicates.

Table 3.1-1. 1-Direction Tension Test Specimen Dimensions

Replicate ID	Width (in)	Thickness (in)	Cross Sectional Area (in <sup>2</sup> )
TF16-5	0.5016	0.0633	0.0317
TF16-6	0.5023	0.0643	0.0323
TF16-7	0.5025	0.0648	0.0326

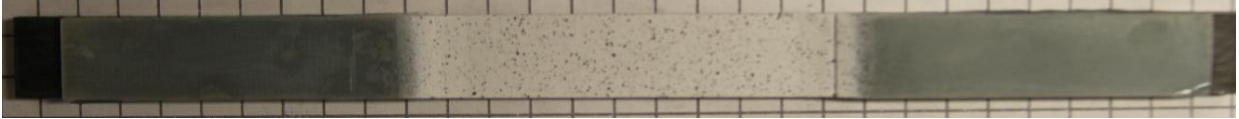
*Specimen Photographs:* The specimen photographs before the tests are shown in figure 3.1-2. Figure 3.1-3 shows the specimens after testing. The specimens exhibited longitudinal cracks in the matrix between the fibers at failure.



(a)

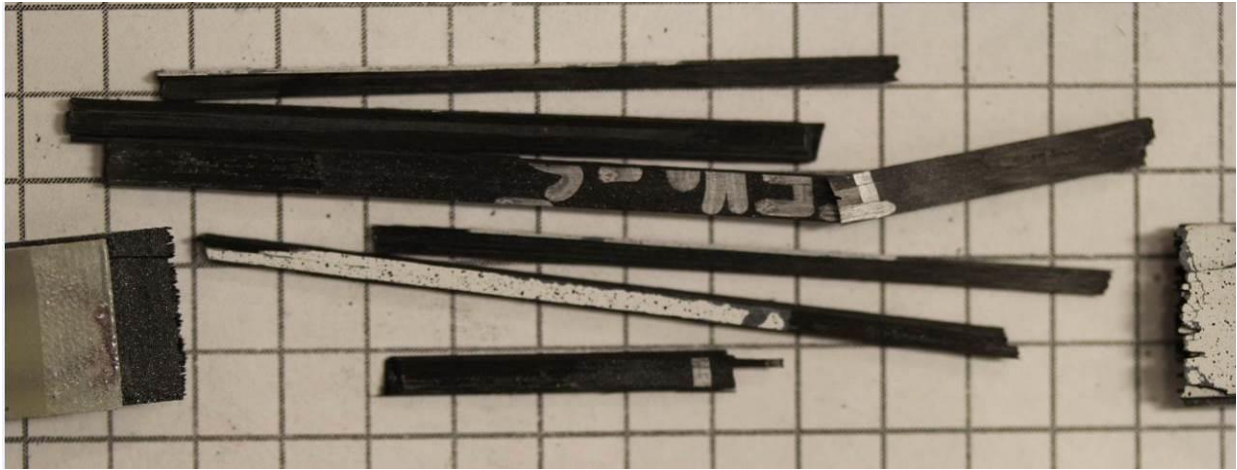


(b)

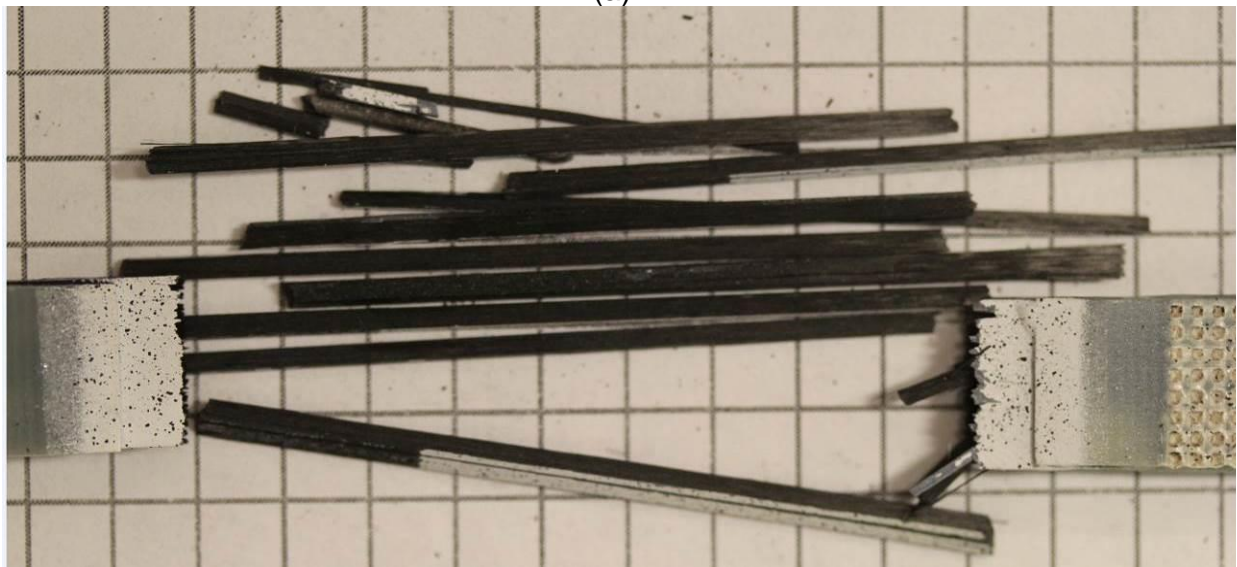


(c)

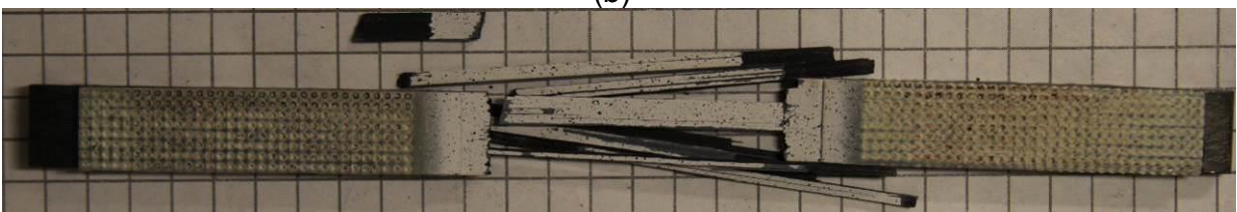
Figure 3.1-2. 1-direction tension specimens before testing (a) TF16-5, (b) TF16-6, (c) TF16-7



(a)



(b)



(c)

Figure 3.1-3. 1-direction tension specimens after testing  
(a) TF16-5, (b) TF16-6, (c) TF16-7

*Test Results:* The summary of the results from the tests is shown in table 3.1-2.

Table 3.1-2. Summary of 1-Direction Tension Test Results

Replicate	Loading Rate (in/min)	Strain Rate $\left(\frac{1}{s}\right)$	E <sub>11</sub> (psi)	Poisson's Ratio (ν <sub>12</sub> )	Ultimate Strain	Peak Stress (psi)
TF16-5	0.03	4.27(10 <sup>-5</sup> )	23 384 440	0.321	0.01579	374 323
TF16-6	0.02	5.00(10 <sup>-5</sup> )	23 121 815	0.319	0.01583	361 434
TF16-7	0.03	4.90(10 <sup>-5</sup> )	23 867 357	0.311	0.01520	362 453
Average	-	-	23 457 871	0.317	0.01560	366 070
Standard Deviation	-	-	378 156	0.005	0.00035	7 165
Coefficient of Variation	-	-	1.6%	1.6%	2.3%	2.0%

Figure 3.1-4 shows the individual stress-strain curves for each of the specimens as well as the model curve.

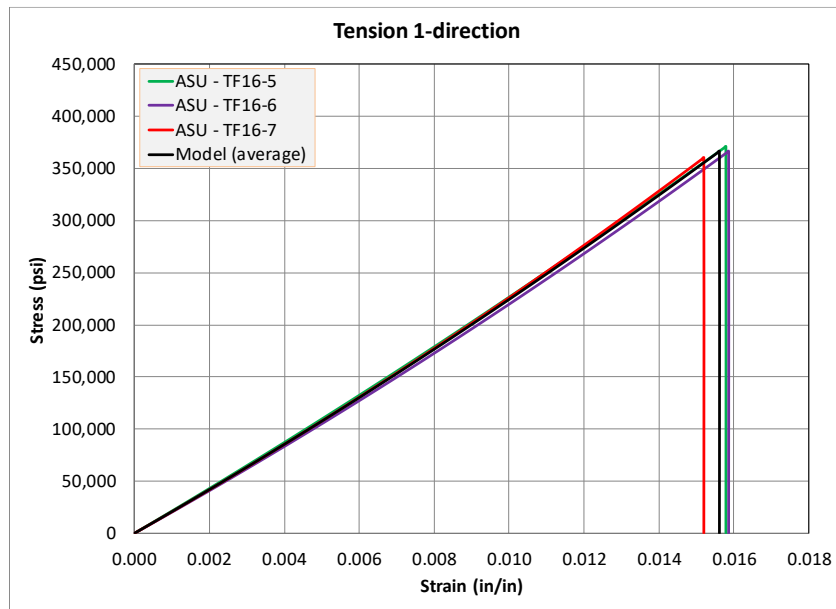


Figure 3.1-4. 1-direction tension stress-strain curves

### 3.2 TEST T2: IN-PLANE 90° TENSION TEST

This test is used to generate the tension stress-strain curve in the 2-direction.

*Specimen Geometry:* The specimen dimensions and layout are shown in figure 3.2-1. The specimen geometry shown in figure 3.2-1(a) is taken from ASTM D3039. The alternative dog bone geometry (figure 3.2-1(b)) was created to try promoting failure in the gage section of the test specimens. Shaded regions indicate where the fiberglass tabs are bonded to the specimen.

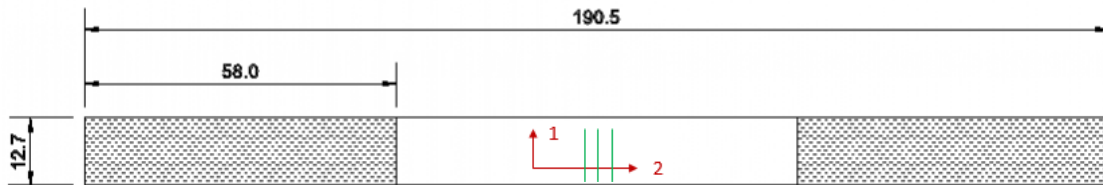


Figure 3.2-1(a). Typical specimen geometry and layout (dimensions in mm)

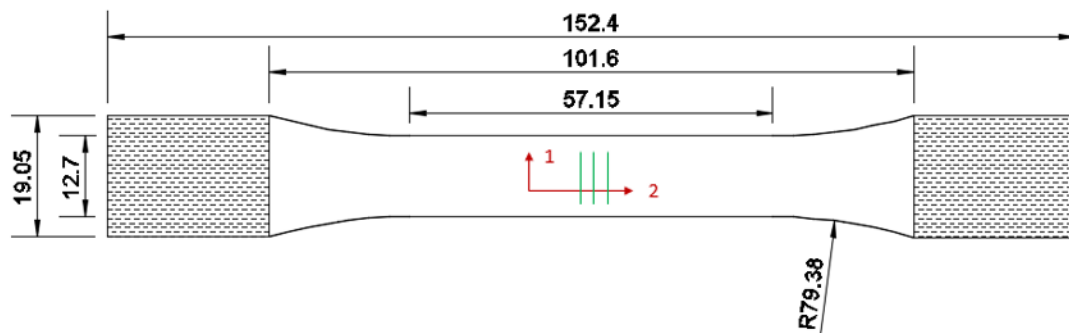


Figure 3.2-1(b). Modified specimen geometry and layout (dimensions in mm)

The average specimen dimensions in the gage section are shown in table 3.2-1 for the four tested replicates.

Table 3.2-1. 2-Direction Tension Test Specimen Dimensions

Replicate	Width (in)	Thickness (in)	Cross Sectional Area (in <sup>2</sup> )
TFT2-3	0.4812	0.1227	0.0591
TFT2-4	0.4999	0.1231	0.0616
TFT2-5	0.4989	0.1231	0.0614
TFT2-6	0.5009	0.1214	0.0608

*Specimen Photographs:* The specimen photographs before the tests are shown in figure 3.2-2. The specimens exhibited brittle failure of the matrix before the tests were terminated and at the point of failure. Figure 3.2-3 shows the specimens after testing.

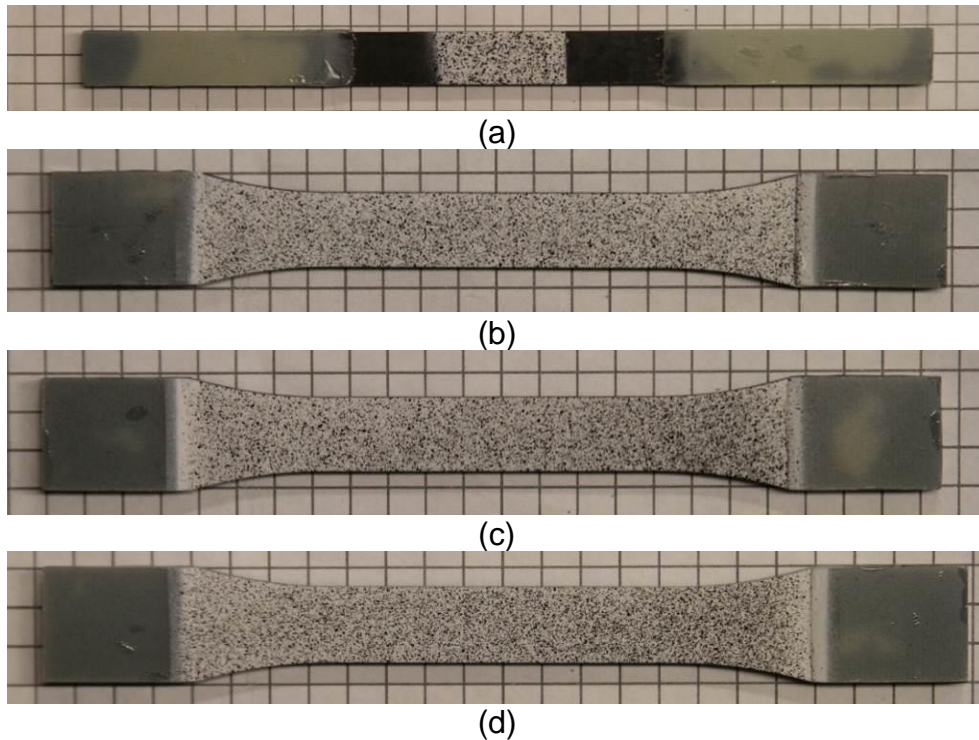


Figure 3.2-2. 2-direction tension specimens before testing (a) TFT2-3, (b) TFT2-4, (c) TFT2-5, (d) TFT2-6

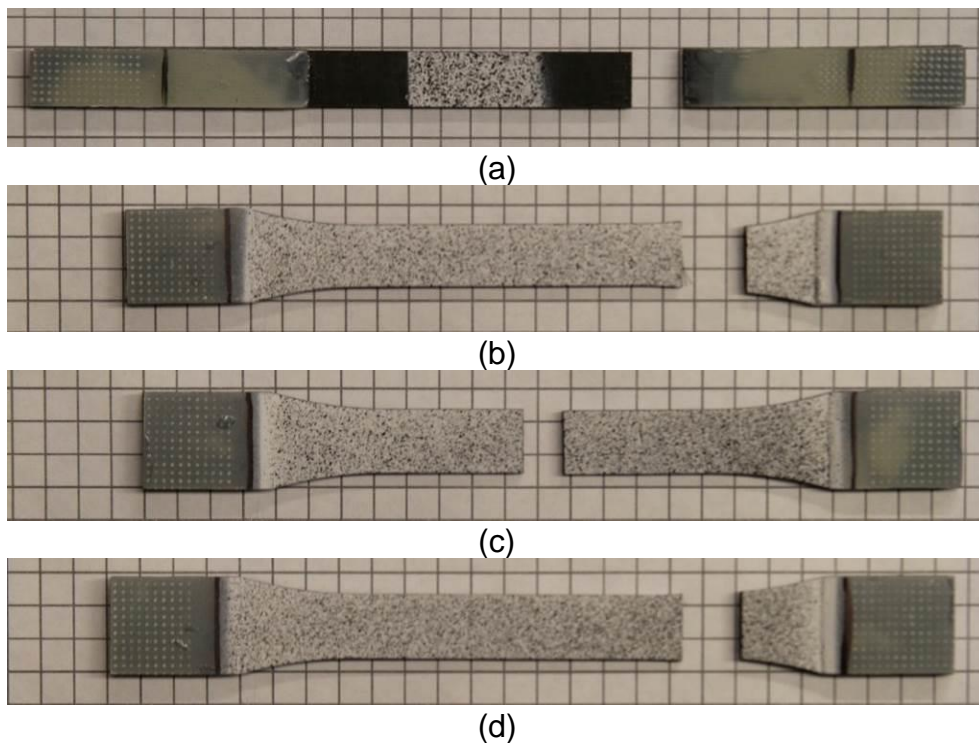


Figure 3.2-3. 2-direction tension specimens after testing (a) TFT2-3, (b) TFT2-4, (c) TFT2-5, (d) TFT2-6

*Test Results:* The summary of the results from the tests is shown in table 3.2-2.

Table 3.2-2. Summary of 2-Direction Tension Test Results

Replicate	Geometry	Loading Rate (in/min)	Strain Rate $\left(\frac{1}{s}\right)$	E <sub>22</sub> (psi)	Poisson's Ratio (ν <sub>21</sub> )	Ultimate Strain	Peak Stress (psi)
TFT2-3	ASTM D3039	0.005	2.21(10 <sup>-5</sup> )	1 055 484	0.0156	0.00590	6 360
TFT2-4	Dog bone	0.0025	9.71(10 <sup>-6</sup> )	1 076 171	0.0155	0.00652	6 647
TFT2-5	Dog bone	0.005	1.92(10 <sup>-5</sup> )	1 069 788	0.0185	0.00641	6 646
TFT2-6	Dog bone	0.005	1.99(10 <sup>-5</sup> )	1 082 595	0.0177	0.00606	6 356
Average	Dog bone	-	-	1 066 413	0.0168	0.00622	6 502
Standard Deviation	-	-	-	14 087	0.0015	0.00029	167
Coefficient of Variation	-	-	-	1.3%	9.0%	4.6%	2.6%

Figures. 3.2-4 and 3.2-5 show the transverse strain and the longitudinal strain values obtained as a function of time from the SGS.

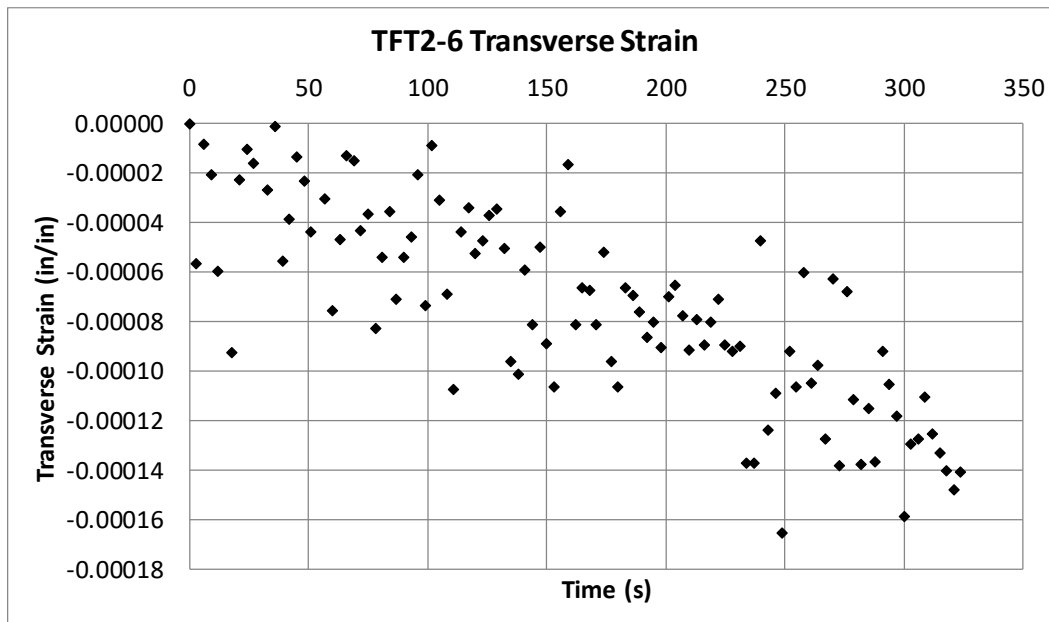


Figure 3.2-4. Transverse strain plot (specimen TFT2-6)

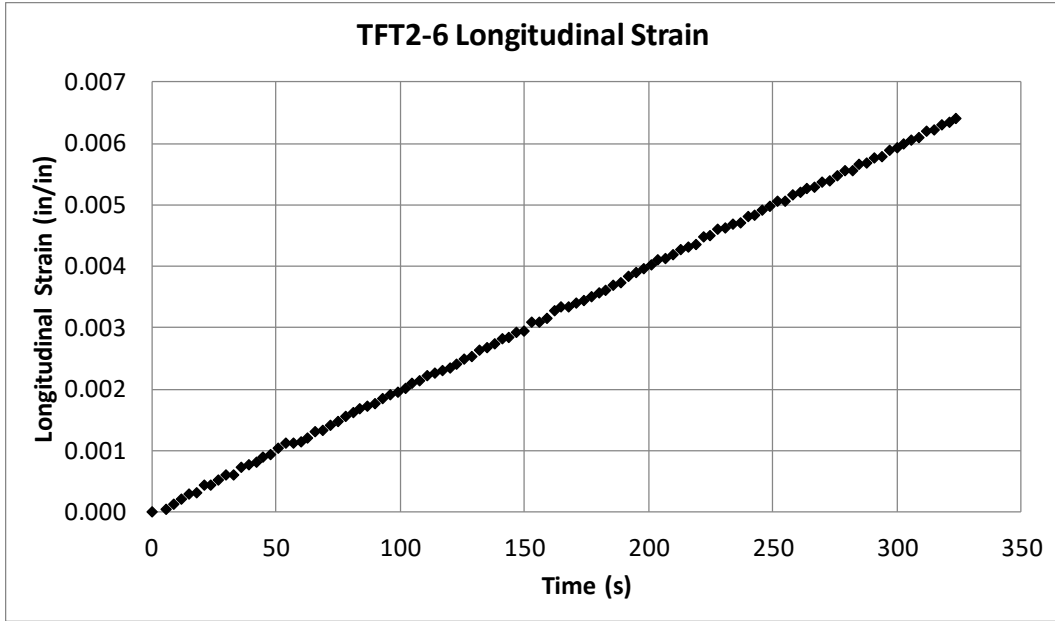


Figure 3.2-5. Longitudinal strain plot (specimen TFT2-6)

The plots shown in figure 3.2-4 and 3.2-5 are combined to generate the plot shown in figure 3.2-6.

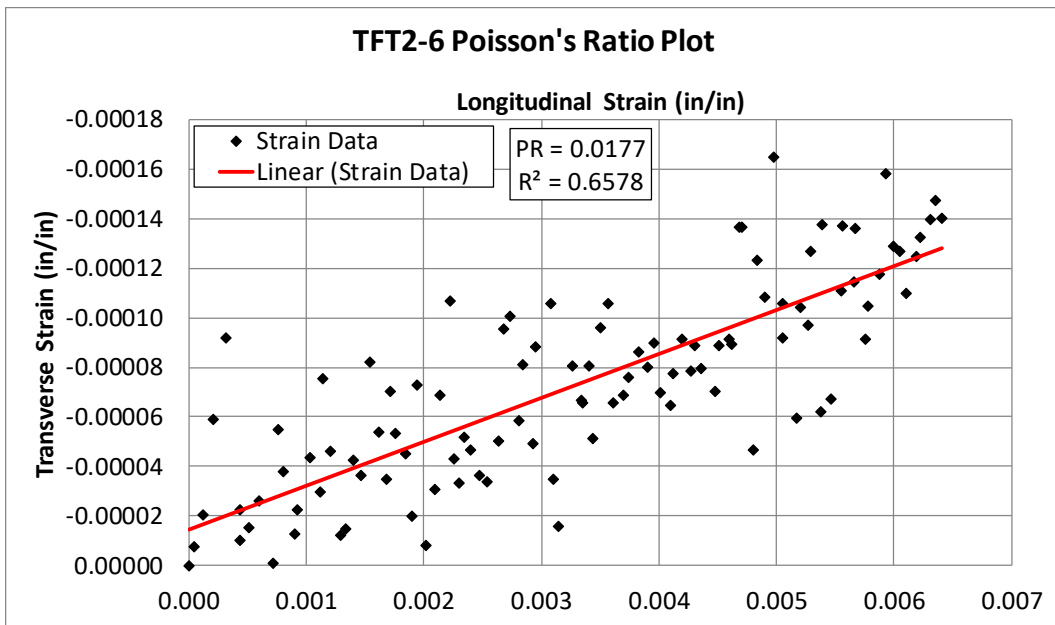


Figure 3.2-6. Determination of Poisson's ratio ( $\nu_{21}$ ) (specimen TFT2-6)

Figure 3.2-7 shows the individual stress-strain curves for each of the specimens as well as the model curve.

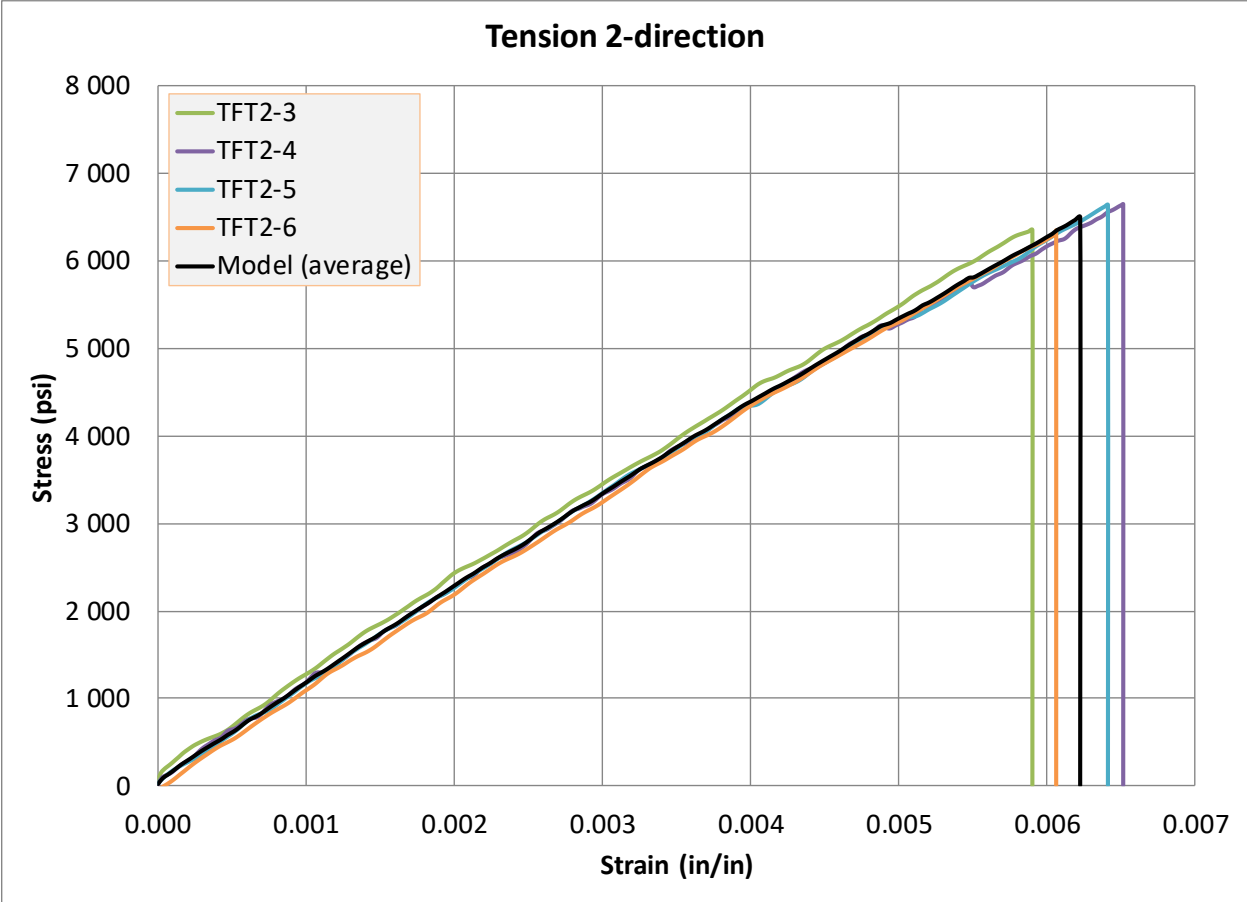


Figure 3.2-7. 2-direction tension stress-strain curves

### 3.3 TEST T3: OUT-OF-PLANE TENSION TEST

This test is used to generate the tension stress-strain curve in the through thickness or 3-direction.

*Specimen Geometry:* The specimen dimensions and layout are shown in figure 3.3-1. ASTM standard could not be followed when creating the specimens because the specimen geometry is dictated by the thickness of the test panel. Only one principal plane is considered when gathering strain data during any given test. However, both the 2-3 and 1-3 planes are considered during separate experiments to discern any differences in experimental data that the speckled plane may yield. Shaded regions indicate where the fiberglass tabs are bonded to the specimen.

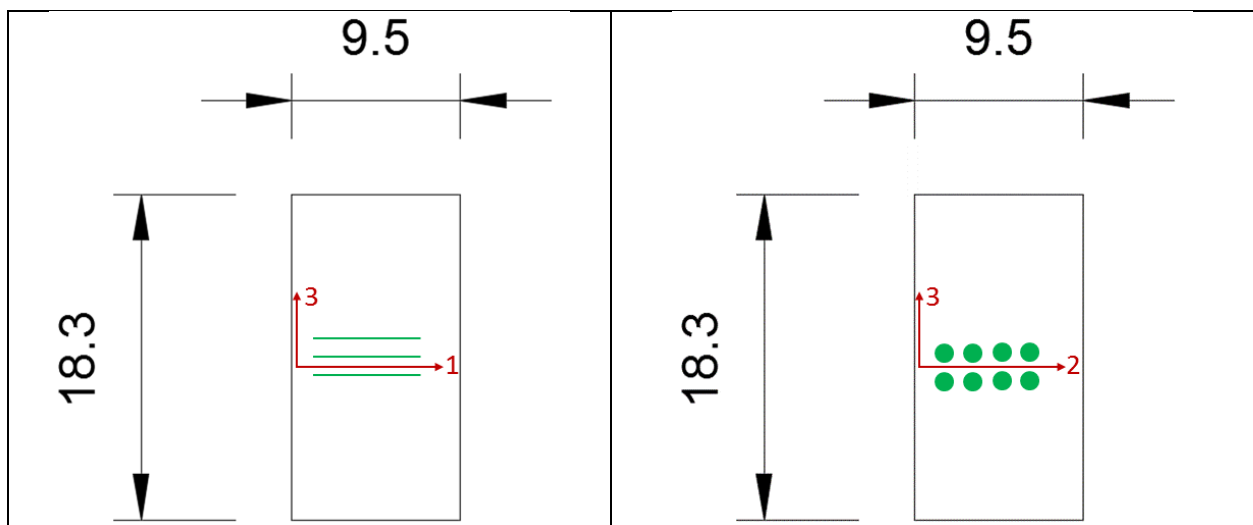


Figure 3.3-1. Typical specimen geometry and layout (dimensions in mm)

The average specimen dimensions in the gage section are shown in table 3.3-1 for the three tested replicates.

Table 3.3-1. 3-Direction Tension Test Specimen Dimensions

Replicate	Width (in)	Thickness (in)	Cross Sectional Area (in <sup>2</sup> )
TFT3-9	0.3707	0.0610	0.0226
TFT3-10	0.3707	0.0595	0.0221
TFT3-13	0.3707	0.0573	0.0213

*Specimen Preparation:* The maximum length of the specimen is dictated by the thickness of the 96-ply panel. Sufficiently long specimens are needed to properly secure the specimen in the hydraulic grips. Three layers of fiberglass tabs were used to create a pocket where the specimen could be inserted. The fiberglass layers were bonded together using Loctite liquid super glue. A notch with the same width and thickness as

the specimen was cut out of the middle layer of the fiberglass layup. Figure 3.3-2 shows the rendering of the fiberglass tabbing system. Approximately one-third of either end of the specimen is then placed inside the pocket and is bonded to the fiberglass tabs using 3M DP460 Scotch Weld toughened two-part epoxy.

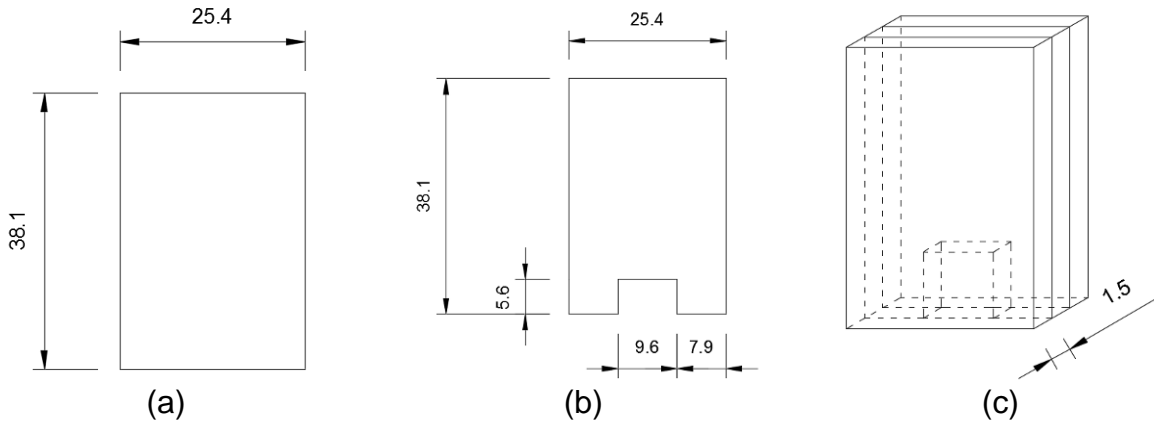


Figure 3.3-2. Fiberglass tab layup geometry (a) Outer layers, (b) Center layer, (c) Overall layup (dimensions in mm)

*Experimental Setup:* The experimental procedure is performed using an MTS 810 universal testing frame (figure 2.2-1(a)). The specimens are held in the frame with MTS 647.10A hydraulic grips (figure 2.2-1(b)). Only the fiberglass tab layup is held by the hydraulic grips. The region of the specimens bonded to the tabs is kept outside of the grips to minimize stress concentrations. Figure 3.3-3 shows the experimental setup.



Figure 3.3-3. 3-direction tension test experimental setup

*Specimen Photographs:* The specimen photographs before the tests are shown in figure 3.3-4. The specimens exhibited brittle failure of the matrix before the tests were terminated and at failure. Figure 3.3-5 shows the specimens after testing.

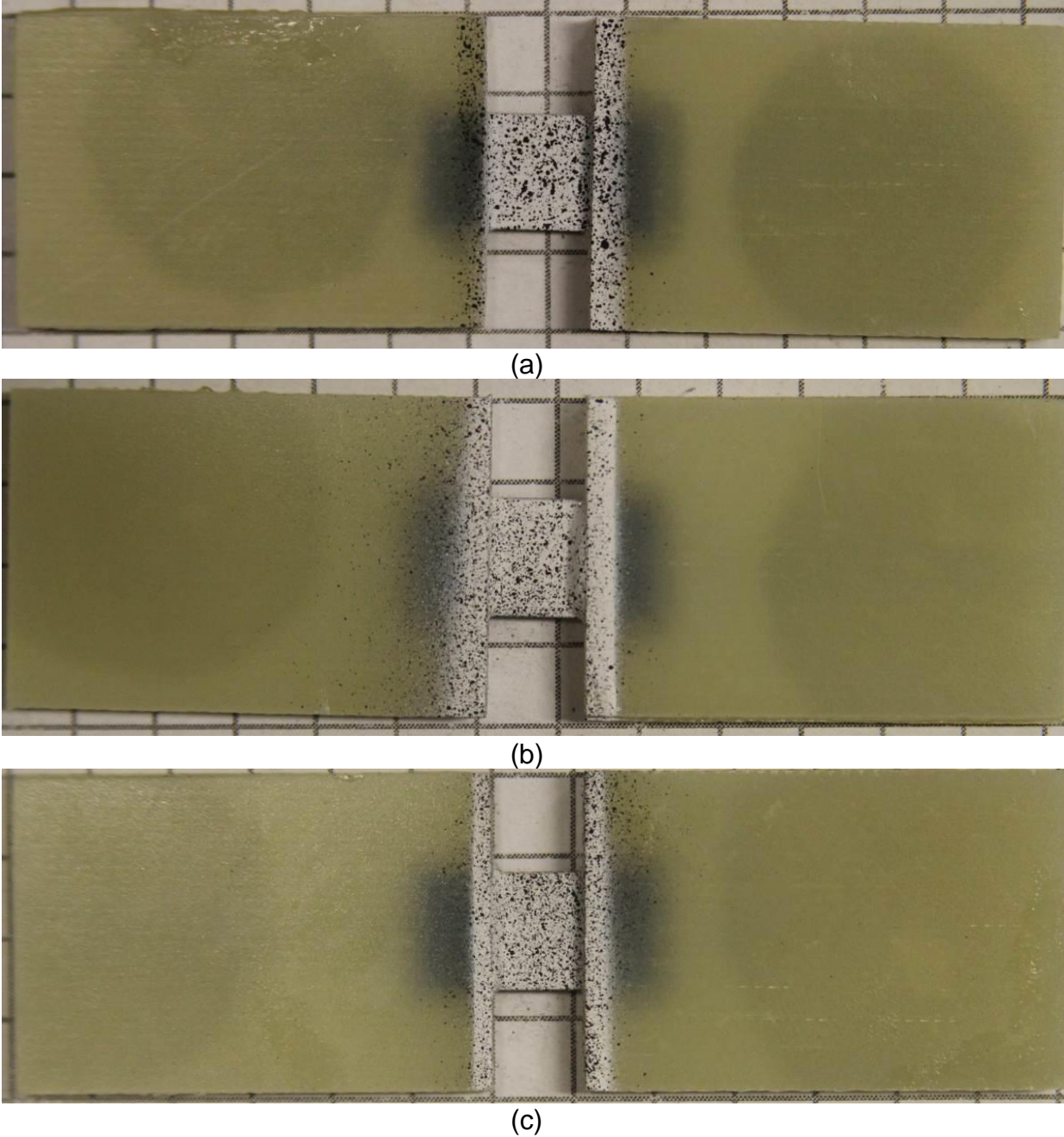
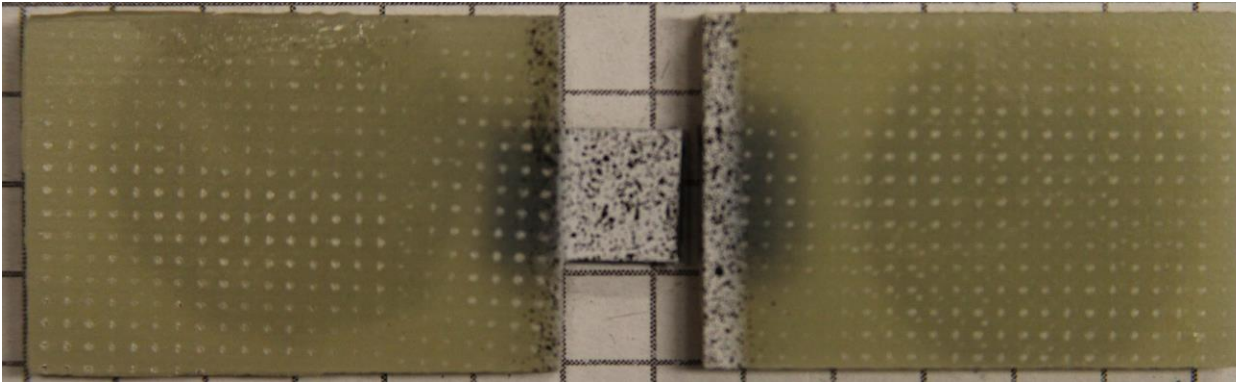
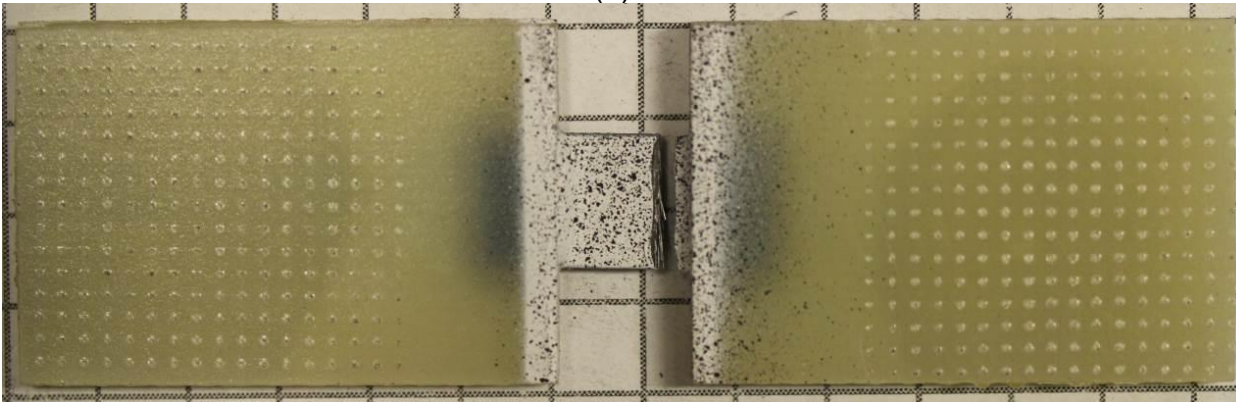


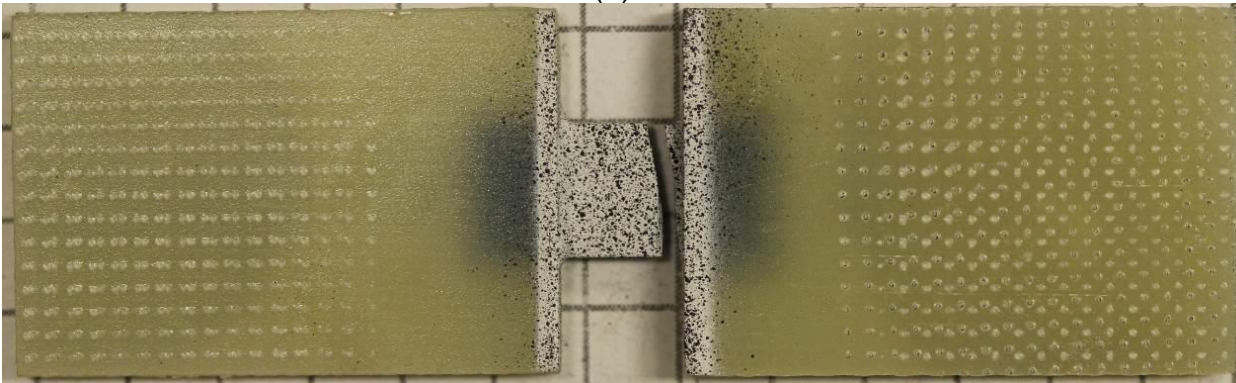
Figure 3.3-4. 3-direction tension specimens prior to testing (a) TFT3-9, (b) TFT3-10, (c) TFT3-13



(a)



(b)



(c)

Figure 3.3-5. 3-direction tension specimens after testing (a) TFT3-9, (b) TFT3-10, (c) TFT3-13

*Test Results:* The summary of the results from the tests is shown in table 3.3-2.

Table 3.3-2. Summary of 3-Direction Tension Test Results

Replicate	Loading Rate (in/min)	Strain Rate $\left(\frac{1}{s}\right)$	$E_{33}$ (psi)	Poisson's Ratio ( $\nu_{31}$ )	Poisson's Ratio ( $\nu_{32}$ )	Ultimate Strain	Peak Stress (psi)
TFT3-9	0.001	$3.3(10)^{-5}$	1 022 475	0.026	-	0.00472	4 469
TFT3-10	0.001	$4.2(10)^{-5}$	915 837	0.027	-	0.00397	3 624
TFT3-13	0.001	$4.0(10)^{-5}$	961 202	-	0.439	0.00395	3 838
Average			966 505	0.027	0.439	0.00421	3 977
Standard Deviation			43 696	0.001	-	0.00036	359
Coefficient of Variation			4.5%	1.9%	0.00%	8.5%	9.0%

Figure 3.3-6 shows the individual stress-strain curves for each of the specimens as well as the model curve.

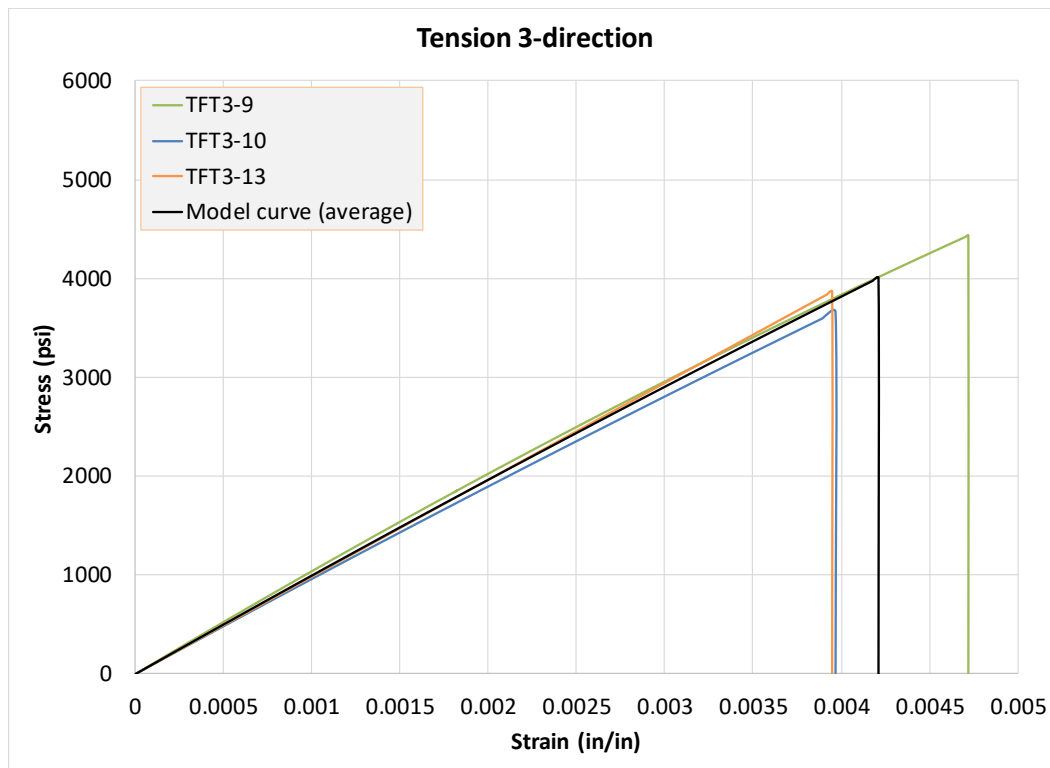


Figure 3.3-6. 3-direction tension stress-strain curves

### 3.4 TEST T4: IN-PLANE 0° COMPRESSION TEST

This test is used to generate the compressive stress-strain curve in the 1-direction.

*Specimen Geometry:* The specimen dimensions and layout are shown in figure 3.4-1. The geometry follows guidelines set by ASTM D3410. The shaded regions indicate where fiberglass tabs are placed.

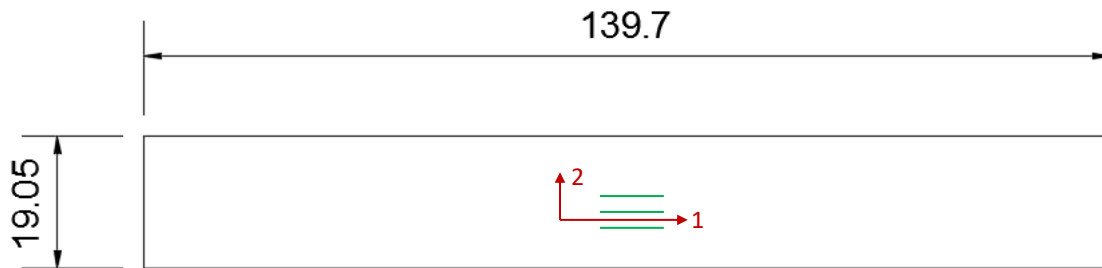


Figure 3.4-1. Typical specimen geometry and layout (dimensions in mm)

The average specimen dimensions in the gage section are shown in table 3.4-1 for the three tested replicates.

Table 3.4-1. 1-Direction Compression Test Specimen Dimensions

Replicate	Width (in)	Thickness (in)	Cross Sectional Area (in <sup>2</sup> )
TFC1-9	0.7525	0.1238	0.0932
TFC1-11	0.7516	0.1219	0.0916
TFC1-12	0.7522	0.1227	0.0923

*Specimen Photographs:* The specimens exhibited failure across the fibers near the gripping region. Failed specimens are shown in figure 3.4-2.

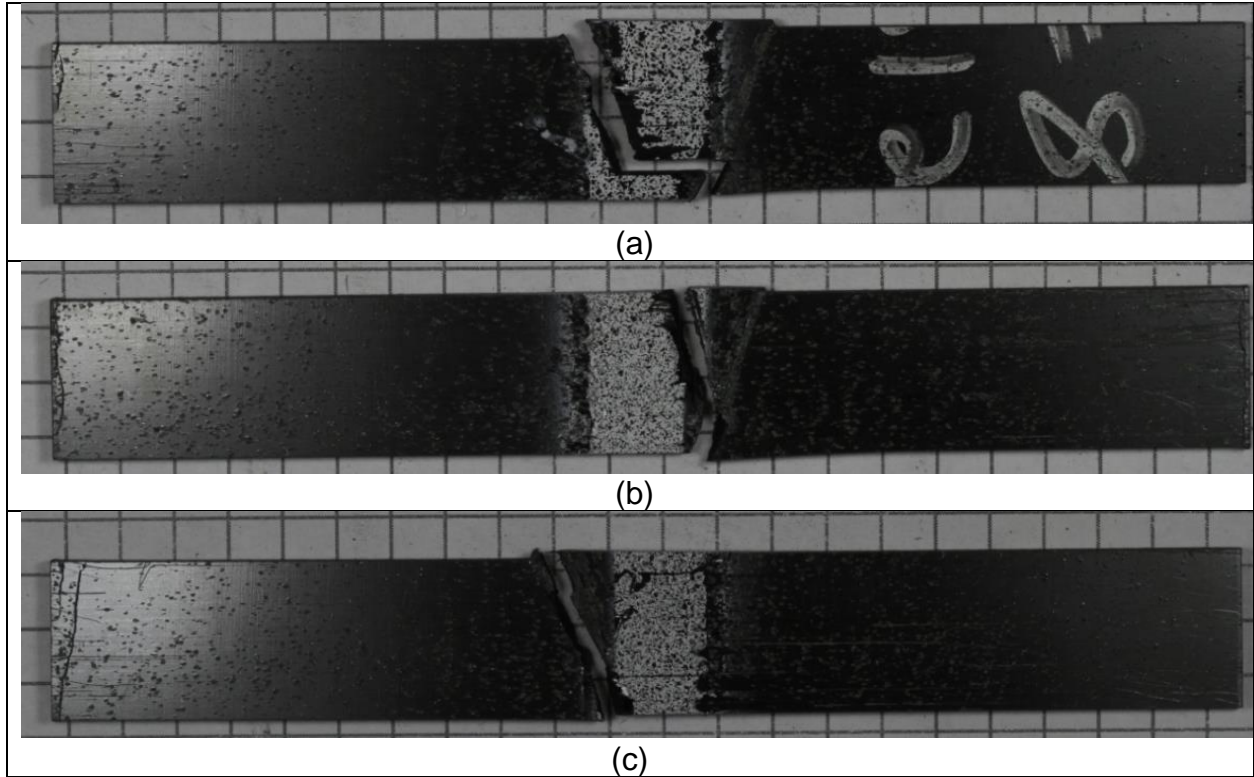


Figure 3.4-2. 1-direction compression specimens after testing (a) TFC1-9, (b) TFC1-11, (c) TFC1-12

*Test Results:* The summary of the results from the tests is shown in table 3.4-2.

Table 3.4-2. Summary of 1-Direction Compression Test Results

Replicate	Loading Rate (in/min)	Strain Rate $\left(\frac{1}{s}\right)$	$E_{11}$ (psi)	Poisson's Ratio ( $\nu_{12}$ )	Ultimate Strain	Peak Stress (psi)
TFC1-9	0.01	$1.65(10^{-5})$	17 533 691	0.417	0.00622	109 736
TFC1-11	0.01	$1.69(10^{-5})$	19 793 053	0.414	0.00509	100 997
TFC1-12	0.01	$1.99(10^{-5})$	18 283 466	0.376	0.00501	90 937
Average	-	-	18 536 737	0.402	0.00544	100 557
Standard Deviation	-	-	939 606	0.018	0.00055	7 681
Coefficient of Variation	-	-	5.07%	4.58%	10.12%	7.64%

Figure 3.4-3 shows the individual stress-strain curves for each of the specimens as well as the model curve.

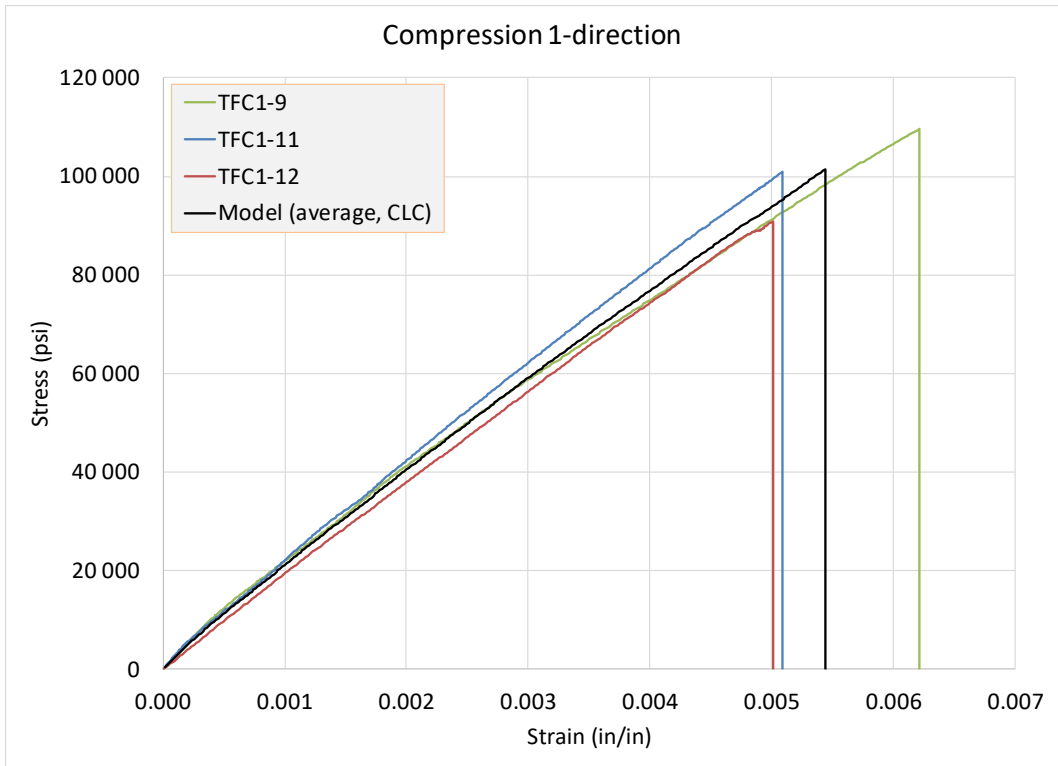


Figure 3.4-3. 1-direction compression stress-strain curves

### 3.5 TEST T5: IN-PLANE 90° COMPRESSION TEST

This test is used to generate the compressive stress-strain curve in the 2-direction.

*Specimen Geometry:* The specimen dimensions and layout are shown in figure 3.5-1. The geometry shown follows guidelines set by ASTM D3410. The shaded regions indicate where fiberglass tabs are bonded to the specimen.

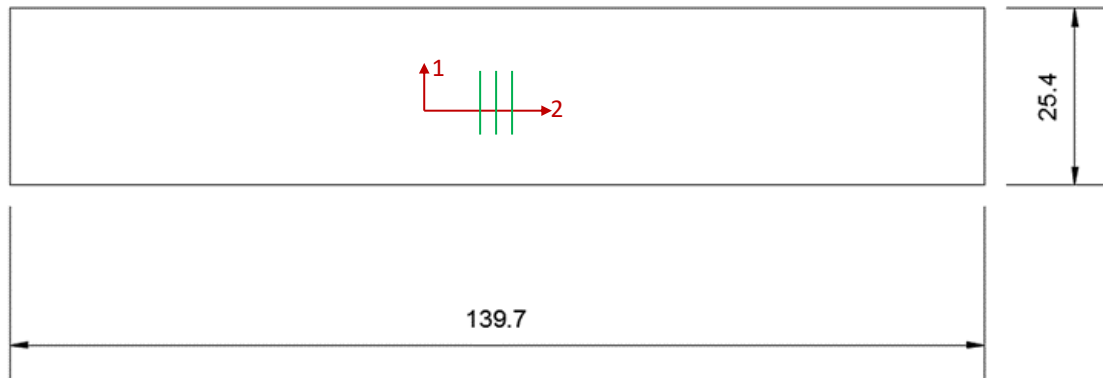


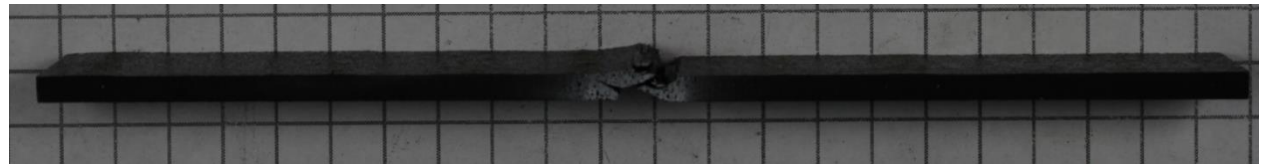
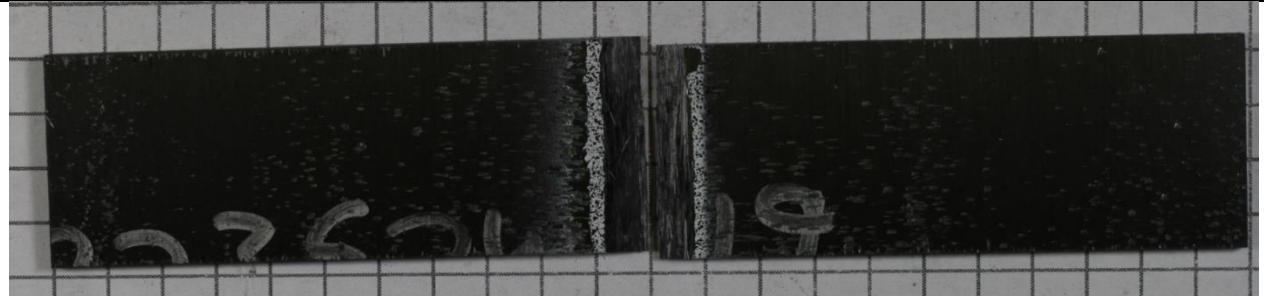
Figure 3.5-1. Typical specimen geometry and layout (all dimensions in mm)

The average specimen dimensions in the gage section are shown in table 3.5-1 for the three tested replicates.

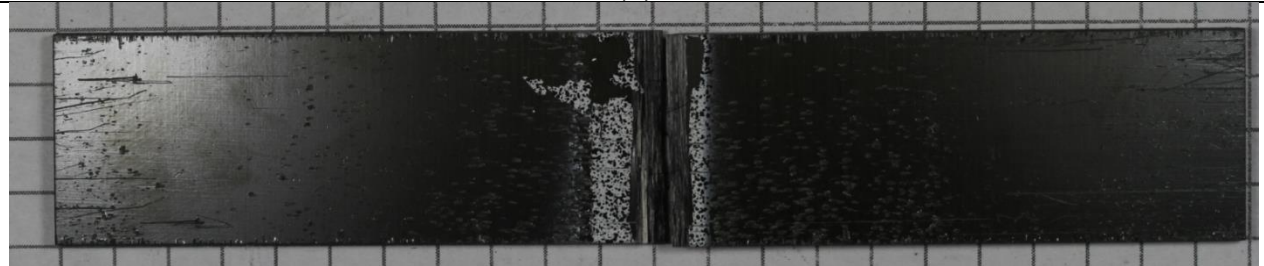
Table 3.5-1. 1-Direction Compression Test Specimen Dimensions

Replicate	Width (in)	Thickness (in)	Cross Sectional Area (in <sup>2</sup> )
TFC2-12	1.0022	0.1218	0.1221
TFC2-13	1.0026	0.1228	0.1231
TFC2-14	1.0028	0.1238	0.1241
TFC2-15	1.0022	0.1231	0.1234
TFC2-16	1.0030	0.1224	0.1228

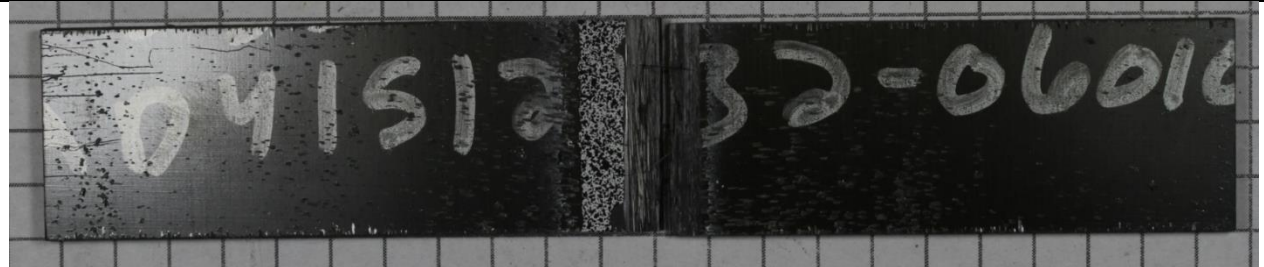
*Specimen Photographs:* The specimens exhibited brittle failure of the matrix before the tests were terminated. Figure 3.5-2 shows the specimens after testing.



(a)



(b)



(c)

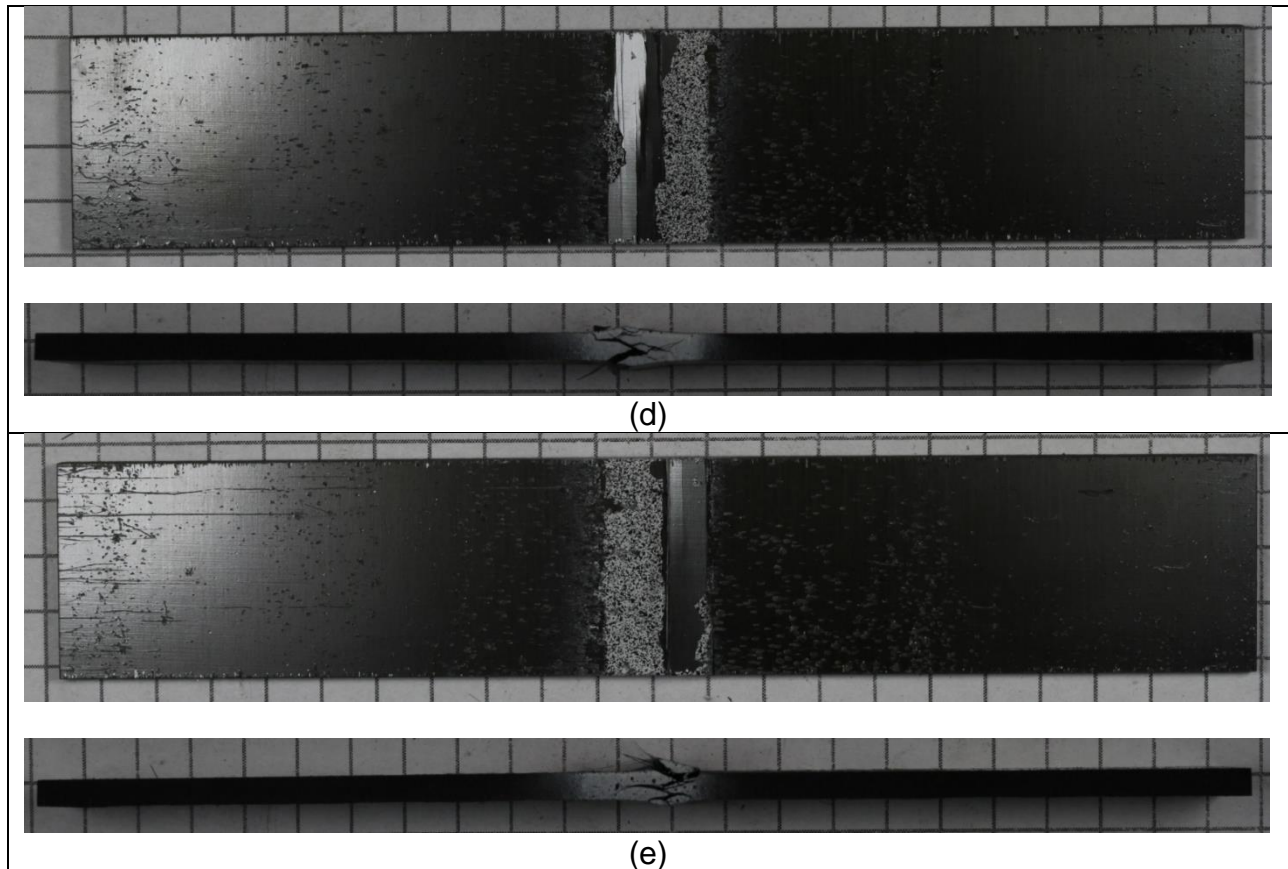


Figure 3.5-2. 2-direction compression specimens after testing (a) TFC2-12, (b) TFC2-13, (c) TFC2-14, (d) TFC2-15, and (e) TFC2-16

Table 3.5-2. Summary of 2-Direction Compression Test Results

Replicate	Loading Rate (in/min)	Strain Rate $\left(\frac{1}{s}\right)$	E <sub>22</sub> (psi)	Poisson's Ratio (ν <sub>21</sub> )	Ultimate Strain	Peak Stress (psi)
TFC2-12	0.005	1.88(10 <sup>-5</sup> )	1 191 648	0.0235	0.02786	24 857
TFC2-13	0.01	4.69(10 <sup>-5</sup> )	1 273 405	0.0148	0.02810	24 778
TFC2-14	0.01	4.13(10 <sup>-5</sup> )	1 123 480	0.0311	0.02687	24 001
TFC2-15	0.005	2.64(10 <sup>-5</sup> )	1 195 899	0.0356	0.02817	24 614
TFC2-16	0.005	2.88(10 <sup>-5</sup> )	1 220 798	0.0372	0.02948	25 393
Average	-	-	1 201 046	0.0284	0.02810	24 728
Standard Deviation	-	-	48 492	0.0083	0.00084	448
Coefficient of Variation	-	-	4.04%	29.21%	2.97%	1.81%

Figure 3.5-3 shows the individual stress-strain curves for each of the specimens as well as the model curve.

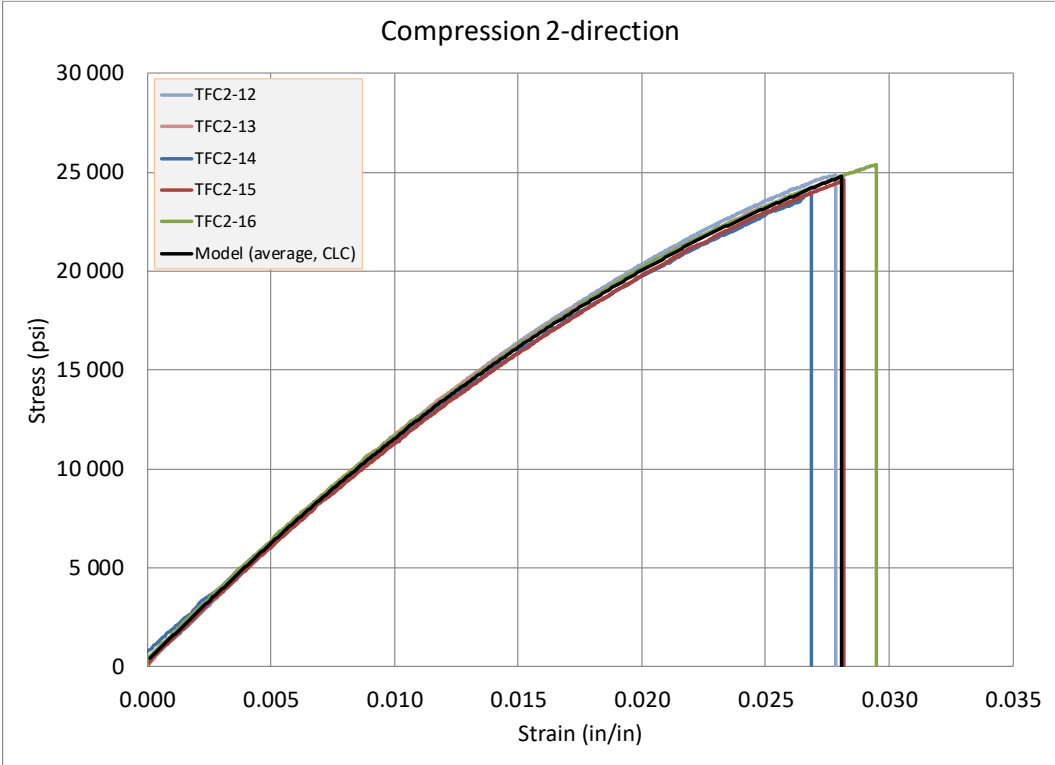


Figure 3.5-3. 2-direction compression stress-strain curves

### 3.6 TEST T6: OUT-OF-PLANE COMPRESSION TEST

This test is used to generate the compressive stress-strain curve in the through thickness or 3-direction.

*Specimen Geometry:* The specimen dimensions and layout are shown in figure 3.6-1. The geometry shown is a modified version of the geometry set forth by ASTM D7291. A cube was used in place of a cylindrical specimen for ease of machining and sample preparation. The dimensions of the cube are less than the dimensions of the cylinder due to the thickness of the available panel. The thickness of the panel determined the other two dimensions, so all three dimensions are the same. ASTM D7291 sets guidelines for through thickness tensile properties. This ASTM document was used because there is no standard available that sets guidelines for obtaining through thickness and compressive properties of fiber reinforced composites. Only one principal plane is considered when gathering strain data during any given test. However, both the 2-3 and 1-3 planes are evaluated during separate experiments for differences in experimental data of the speckled plane.

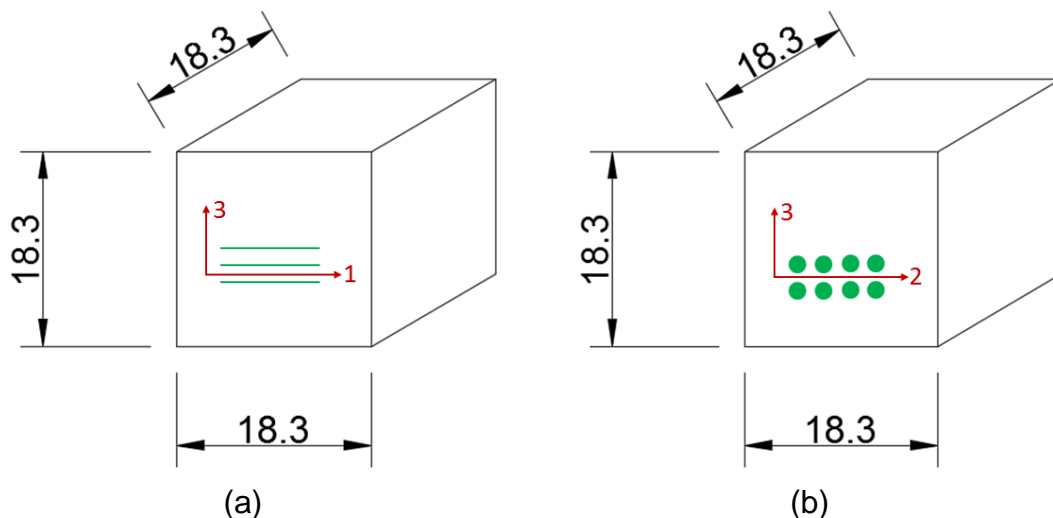


Figure 3.6-1. Typical specimen geometry and layout (a) 1-3 plane speckled and (b) 2-3 plane speckled (all dimensions in mm)

The average specimen dimensions in the gage section are shown in table 3.6-1 for the four tested replicates.

Table 3.6-1. 3-Direction Compression Test Specimen Dimensions

Replicate	Width (in)	Thickness (in)	Cross Sectional Area (in <sup>2</sup> )
TFC3-2	0.7853	0.7857	0.6170
TFC3-5	0.7826	0.7825	0.6124
TFC3-8	0.7888	0.7822	0.6170
TFC3-9	0.7815	0.7809	0.6103

*Specimen Photographs:* The specimen photographs before the tests are shown in figure 3.6-2. The specimens exhibited brittle failure of the matrix in the 2-3 plane before the tests were terminated. Figure 3.6-3 shows the specimens after testing. Each set of photos includes an image of the front, left, and right side of the respective specimen. The front of the specimen is defined as the surface that was speckled.

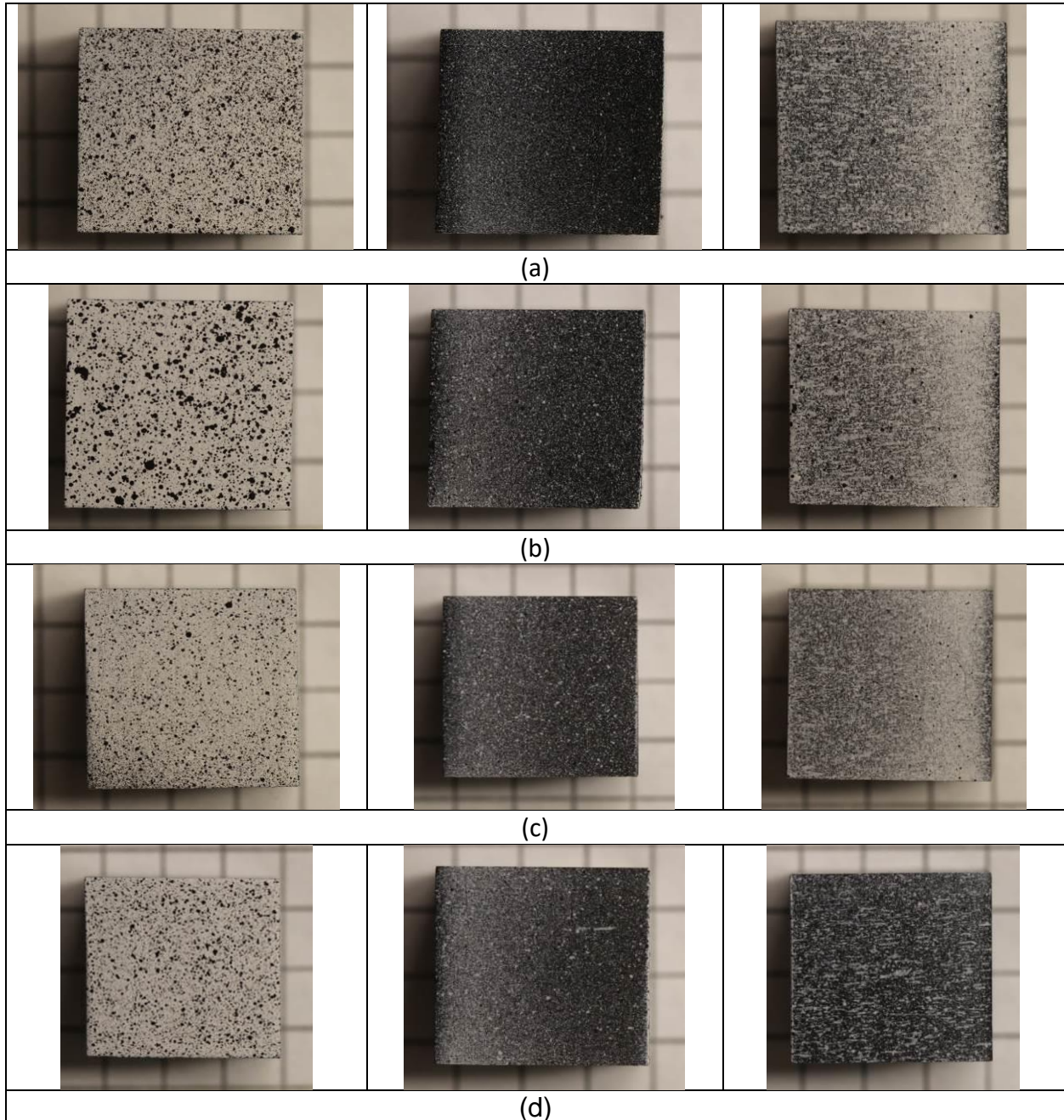


Figure 3.6-2. 3-direction compression specimens prior to testing (a) TFC3-5, (b) TFC3-6, (c) TFC3-8, (d) TFC3-9

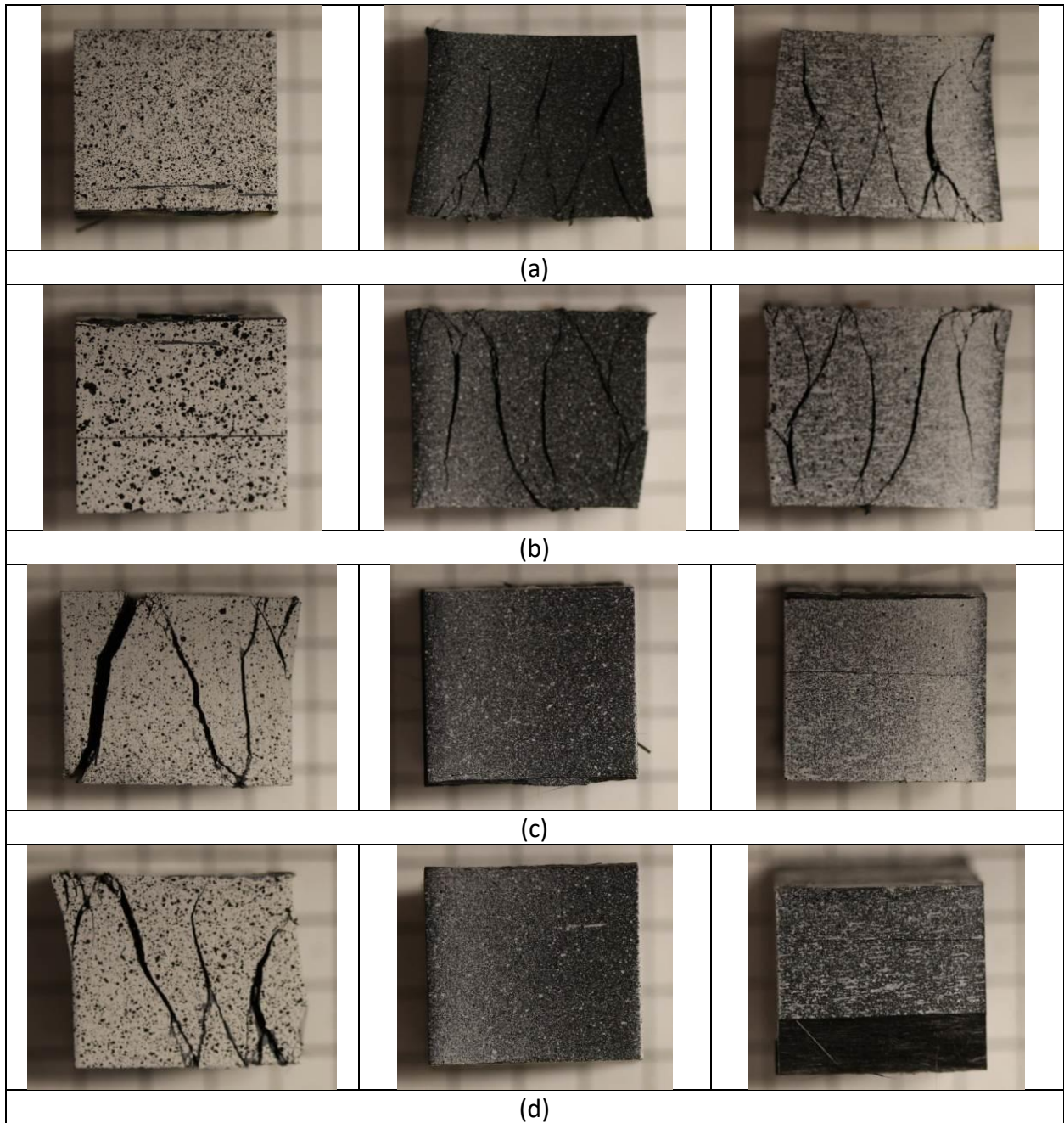


Figure 3.6-3. 3-direction compression specimens after testing (a) TFC3-5, (b) TFC3-6, (c) TFC3-8, (d) TFC3-9

*Test Results:* The summary of the results from the tests is shown in table 3.2-2.

Table 3.6-2. Summary of the 3-Direction Compression Test Results

Replica te	Speck led Plane	Loading Rate (in/min)	Strain Rate (1/s)	$E_{33}$ (psi)	Poiss on's Ratio ( $\nu_{31}$ )	Poiss on's Ratio ( $\nu_{32}$ )	Ultim ate Strain	Peak Stress (psi)
TFC3-5	1-3	0.01	1.09E-05	1 157 898	0.038	-	0.02571	25 441
TFC3-6	1-3	0.01	1.07E-04	1 073 002	0.027	-	0.02612	24 665
TFC3-8	2-3	0.01	4.80E-06	893 155	-	0.699	0.03044	22 168
TFC3-9	2-3	0.01	1.20E-04	1 030 705	-	0.653	0.03196	26 861
Average	-	-	-	1 038 690	0.032	0.676	0.02856	24 784
Standard Deviation	-	-	-	110 502	0.006	0.033	0.00312	1967
Coefficie nt of Variation	-	-	-	10.6%	17.1%	4.9%	10.9%	7.9%

Figure 3.6-4 shows the individual stress-strain curves for each of the specimens as well as the model curve.

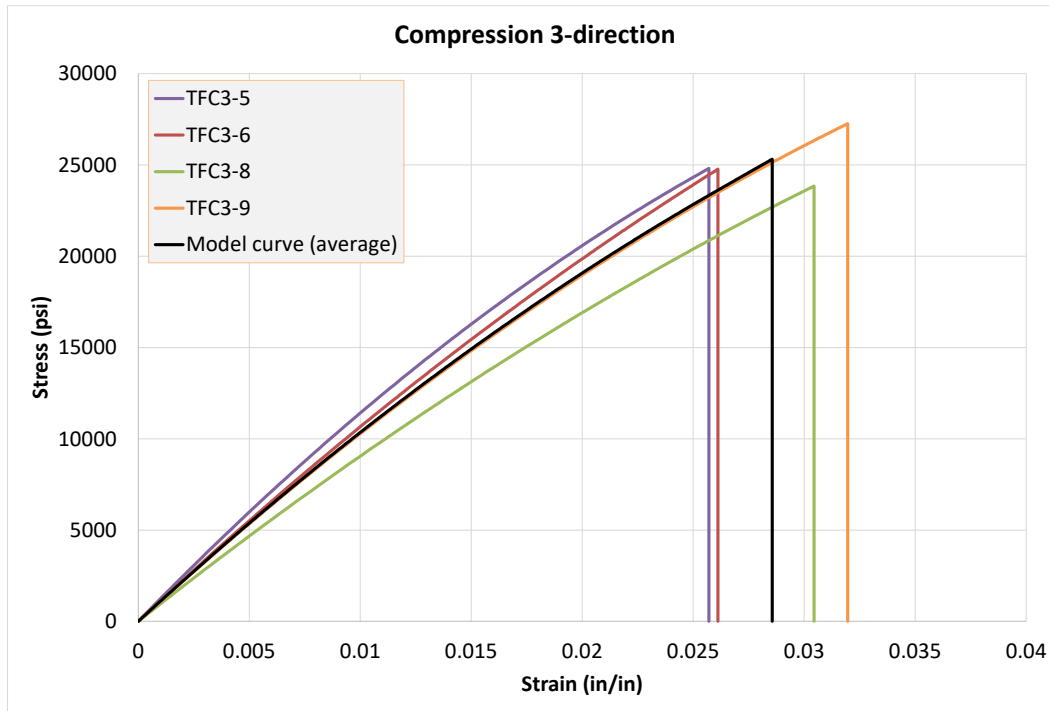


Figure 3.6-4. 3-direction compression stress-strain curves

### 3.7 TEST T7: SHEAR TEST IN THE 1-2 PLANE

This test is used to generate the shear stress-strain curve in the 1-2 plane.

*Specimen Geometry:* The specimen dimensions and layout are shown in figure 3.7-1. The geometry shown meets guidelines set by ASTM D5379/D5379M-12. Shaded regions indicate where fiberglass tabs are bonded to the specimen.

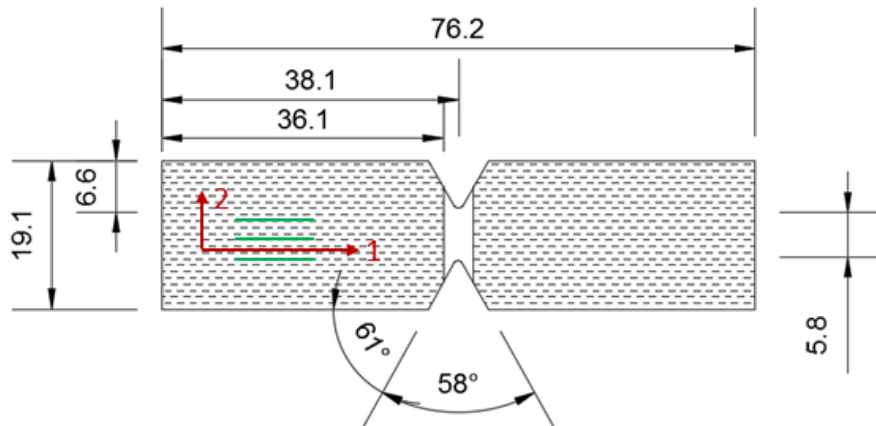


Figure 3.7-1. Typical specimen geometry

Two changes with respect to the ASTM standards should be noted. First, the notches shown in figure 3.7-1 are deeper. Second, the fiberglass tabs terminate closer to the center of the specimen. Both modifications were made to reduce transverse strains and promoting shear failure between the notches.

The average specimen dimensions in the gage section are shown in table 3.7-1 for the three tested replicates. The ligament height is defined as the distance between the notches.

Table 3.7-1. 1-2 Plane Shear Test Specimen Dimensions

Replicate	Ligament Height (in)	Thickness (in)	Cross Sectional Area (in <sup>2</sup> )
TFS12-8	0.2658	0.1823	0.0484
TFS12-9	0.2668	0.1803	0.0481
TFS12-10	0.2618	0.1805	0.0472

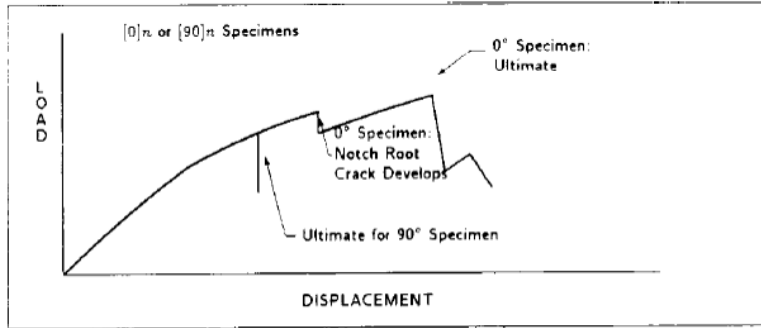


Figure 3.7-2. ASTM definition of shear failure<sup>7</sup>

Figure 3.7-3 shows the modes of failure deemed acceptable by the ASTM standard.

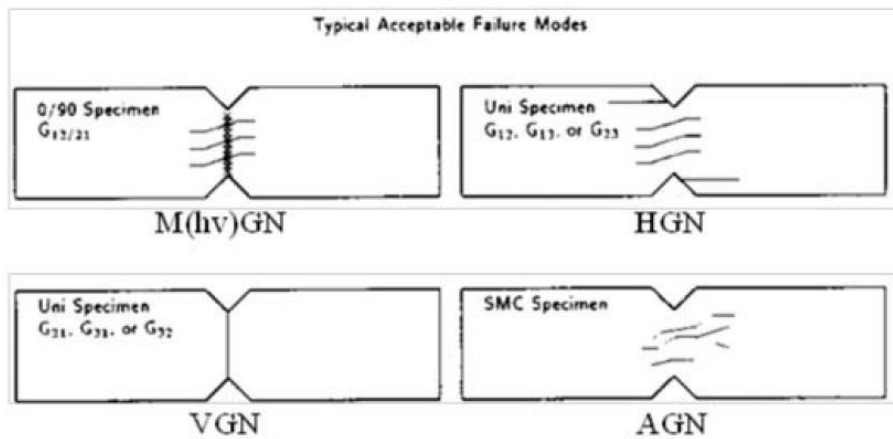
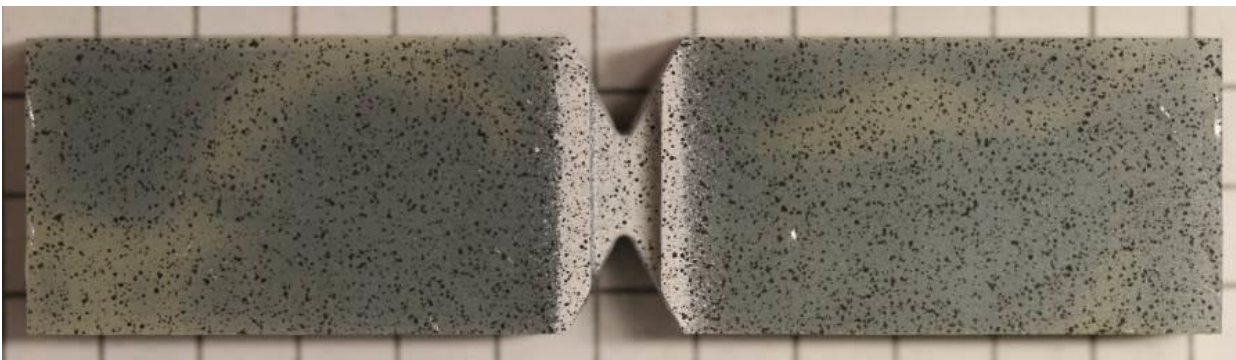


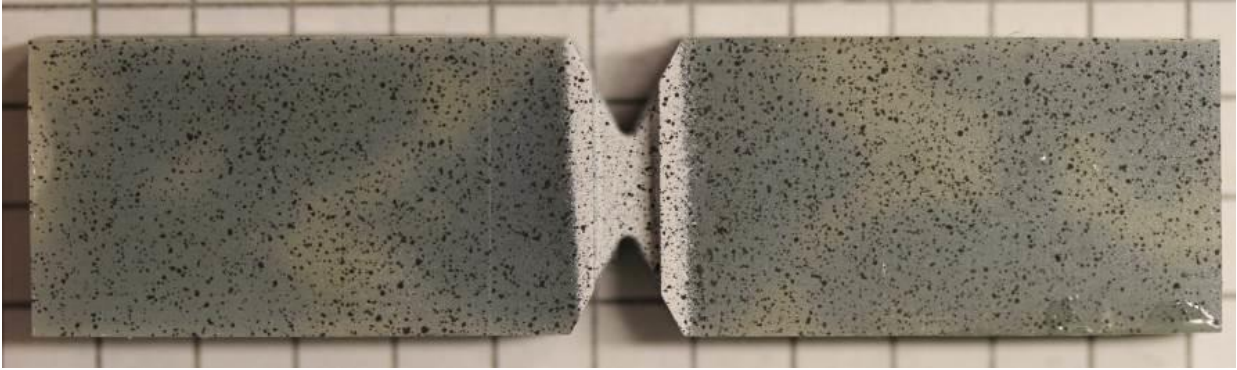
Figure 3.7-3. ASTM acceptable failure modes<sup>7</sup>

*Specimen Photographs:* The specimen photographs before the tests are shown in figure 3.7-4. The specimens exhibited HGN failure as shown in figure 3.7-3. Figure 3.7-5 shows the specimens after testing.

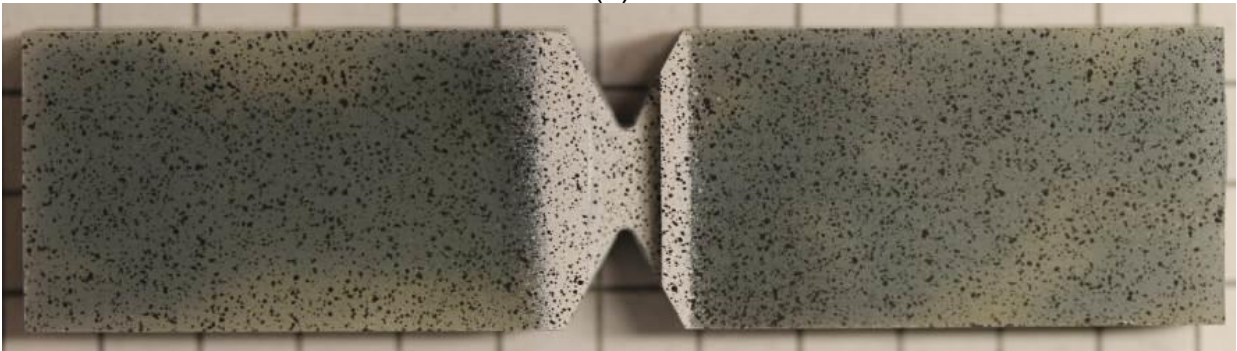


(a)

<sup>7</sup> ASTM D 5379/D5379M-12 Committee (2013). Test Method for Shear Properties of Composite Materials by the V-Notched Beam Method, ASTM International, West Conshohocken, PA.



(b)



(c)

Figure 3.7-4. 1-2 plane shear specimens prior to testing (a) TFS12-8, (b) TFS12-9, (c) TFS12-10



(a)



(b)



(c)

Figure 3.7-5. 1-2 plane shear specimens after testing<sup>8</sup> (a) TFS12-8, (b) TFS12-9, (c) TFS12-10

*Test Results:* The summary of the results from the tests is shown in table 3.7-2. The shear modulus reported in table 3.7-2 is in terms of engineering shear strain not tensorial shear strain. It should be noted that MAT213 requires the stress-tensorial strain curve input from the user and internally converts the curve into stress-engineering strain before computing the shear modulus for use in the program.

---

<sup>8</sup> Small pressure was applied to the tested specimen to show the cracks. Otherwise, the cracks are not visible in the photograph.

Table 3.7-2. Summary of the 1-2 Plane Shear Test Results

Replicate	Loading Rate (in/min)	Tensorial Strain Rate ( $\frac{1}{s}$ )	$G_{12}$ (psi)	Failure Strain (Tensorial)	Peak Stress (psi)
TFS12-8	0.02	0.00065	621 242	0.12946	18 588
TFS12-9	0.02	0.0007	576 658	0.13438	18 547
TFS12-10	0.02	0.00075	540 568	0.13817	18 875
Average	-	-	579 489	0.13400	18 670
Standard Deviation	-	-	40 411	0.00437	179
Coefficient of Variation	-	-	7.0%	3.3%	1.0%

Figure 3.7-6 shows the individual stress-strain curves for each of the specimens as well as the model curve.

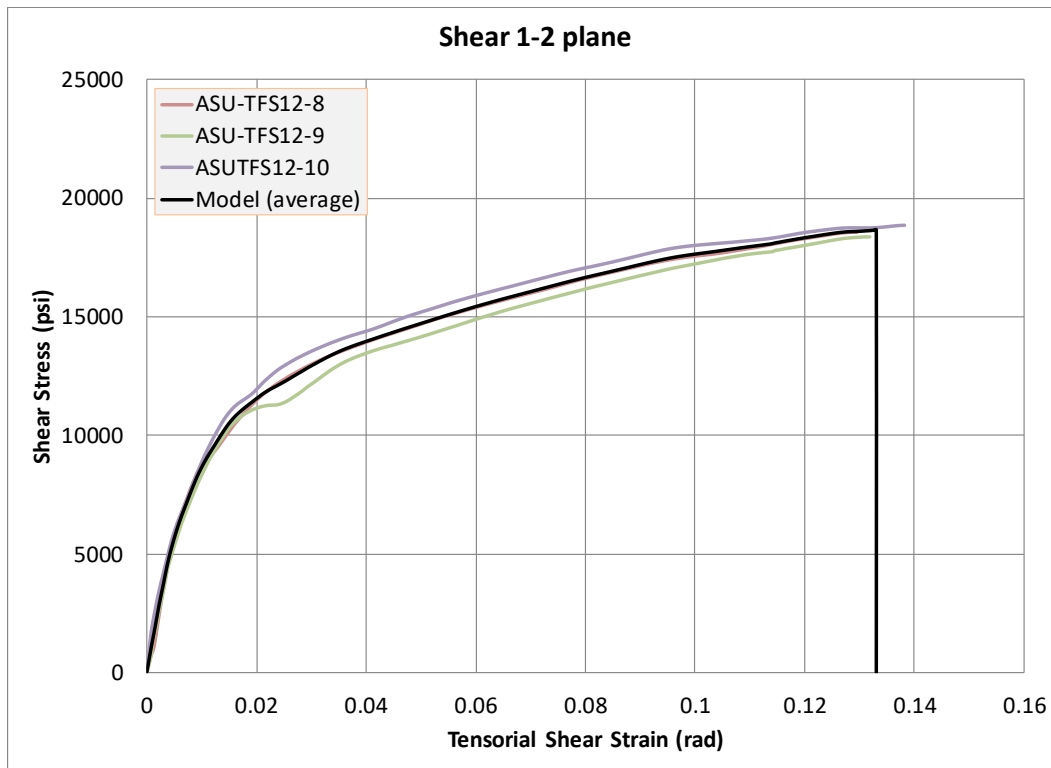


Figure 3.7-6. 1-2 plane shear stress-tensorial strain curves

### 3.8 TEST T8: SHEAR TEST IN THE 2-3 PLANE

This test is used to generate the shear stress-strain curve in the 2-3 plane.

*Specimen Geometry:* The specimen dimensions and layout are shown in figure 3.8-1. The geometry shown meets guidelines set by ASTM D5379/D5379M-12. Shaded regions indicate where fiberglass tabs are bonded to the specimen.

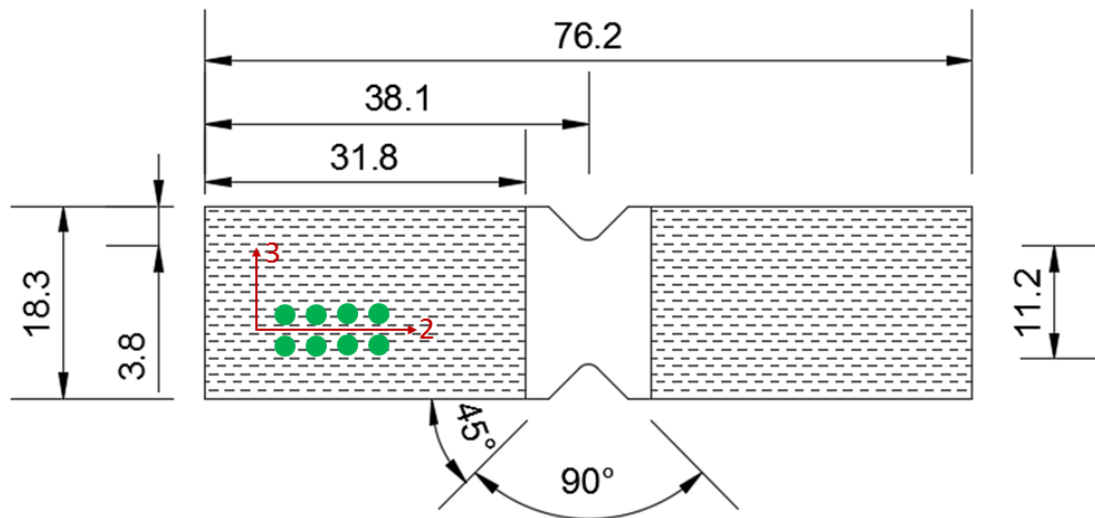


Figure 3.8-1. Typical specimen geometry and layout

The average specimen dimensions between the notches are shown in table 3.8-1 for the three tested replicates. The ligament height is defined as the distance between the notches.

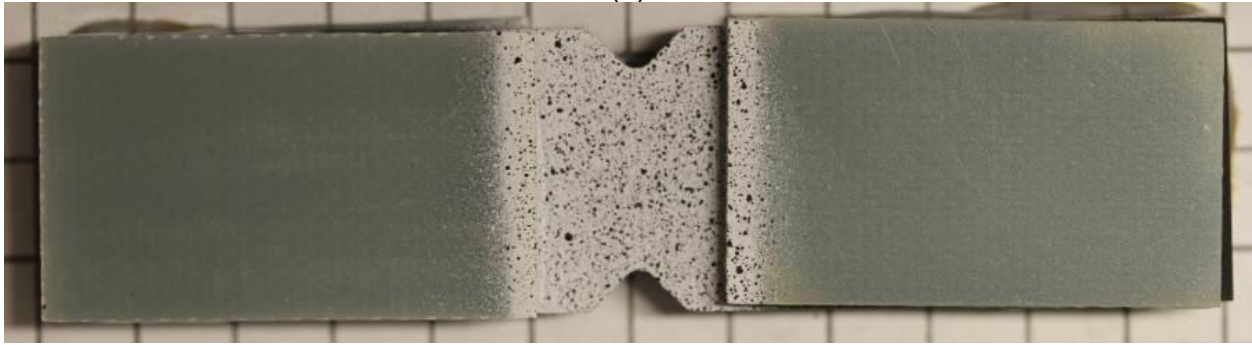
Table 3.8-1. 2-3 Plane Shear Test Specimen Dimensions

Replicate	Ligament Height (in)	Thickness (in)	Cross Sectional Area (in <sup>2</sup> )
TFS23-3	0.4945	0.1100	0.0544
TFS23-5	0.5113	0.1275	0.0652
TFS23-9	0.4605	0.1205	0.0555

*Specimen Photographs:* The specimen photographs before the tests are shown in figure 3.8-2. The specimens exhibited HGN failure as shown in figure 3.7-3. Figure 3.8-3 shows the specimens after testing.



(a)

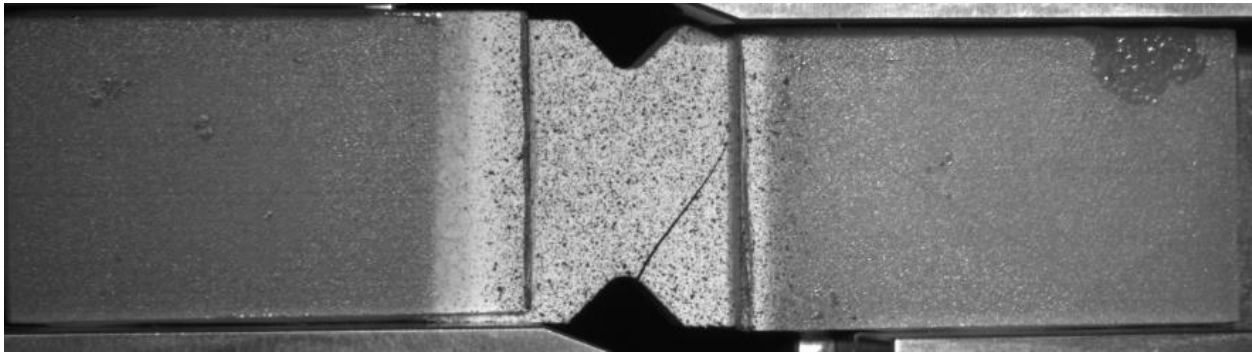


(b)



(c)

Figure 3.8-2. 2-3 plane shear specimens prior to testing (a) TFS23-3, (b) TFS23-5, (c) TFS23-9



(a)

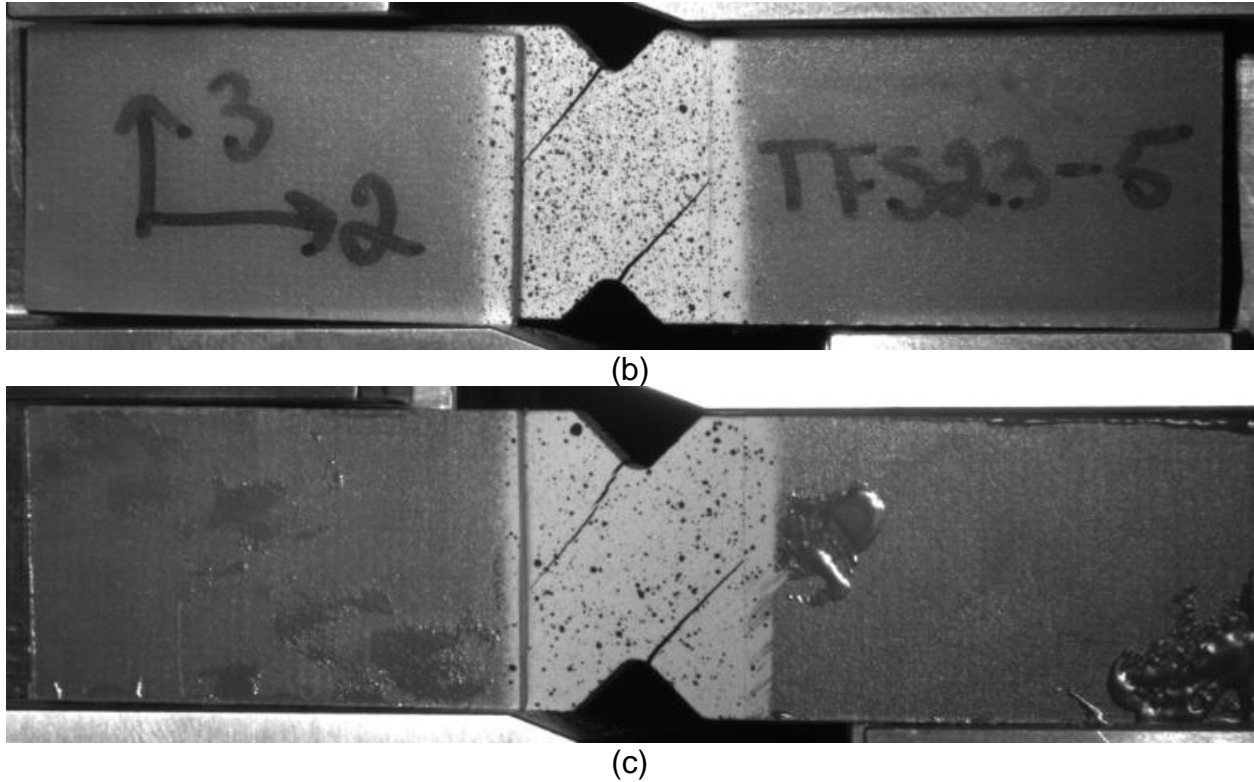


Figure 3.8-3. 2-3 plane shear specimens after testing (a) TFS23-3, (b) TFS23-5, (c) TFS23-9

*Test Results:* The summary of the results from the tests is shown in table 3.8-2. The shear modulus reported in table 3.8-2 is in terms of engineering shear strain not tensorial shear strain. It should be noted that MAT213 requires stress-tensorial strain curve input from the user and internally converts the curve into stress-engineering strain before computing the shear modulus for use in the program.

Table 3.8-2. Summary of the 2-3 Plane Shear Test Results

Replicate	Loading Rate (in/min)	Tensorial Strain Rate ( $1/s$ )	$G_{23}$ (psi)	Ultimate Strain (Tensorial)	Peak Stress (psi)
TFS23-3	0.001	$5.00(10^{-6})$	343 467	0.00428	2 881
TFS23-5	0.001	$4.50(10^{-6})$	340 488	0.00420	2 866
TFS23-9	0.001	$5.00(10^{-6})$	322 828	0.00435	2 702
Average	-	-	335 594	0.00428	2 816
Standard Deviation	-	-	11 156	0.00007	99
Coefficient of Variation	-	-	3.3%	1.7%	3.5%

Figure 3.8-4 shows the individual stress-strain curves for each of the specimens as well as the model curve.

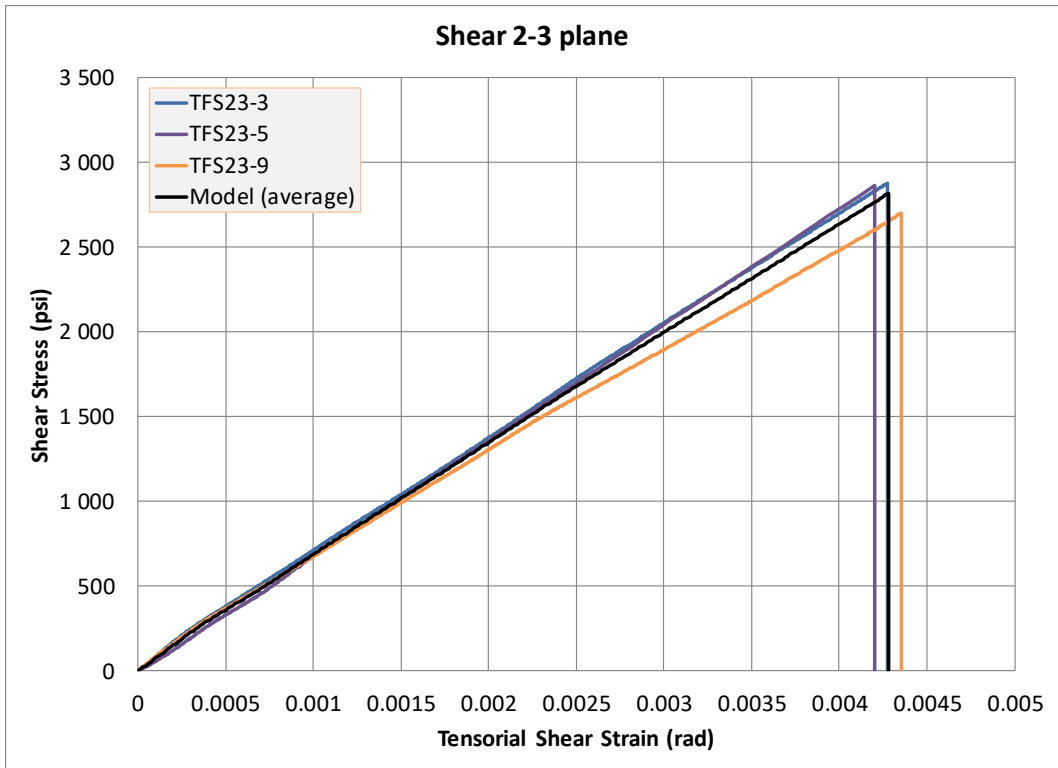


Figure 3.8-4. 2-3 plane shear stress-tensorial strain curves

### 3.9 TEST T9: SHEAR TEST IN THE 1-3 PLANE

This test is used to generate the shear stress-strain curve in the 1-3 plane.

*Specimen Geometry:* The specimen dimensions and layout are shown in figure 3.9-1. The geometry shown meets guidelines set by ASTM D5379/D5379M-12. Shaded regions indicate where fiberglass tabs are bonded to the specimen.

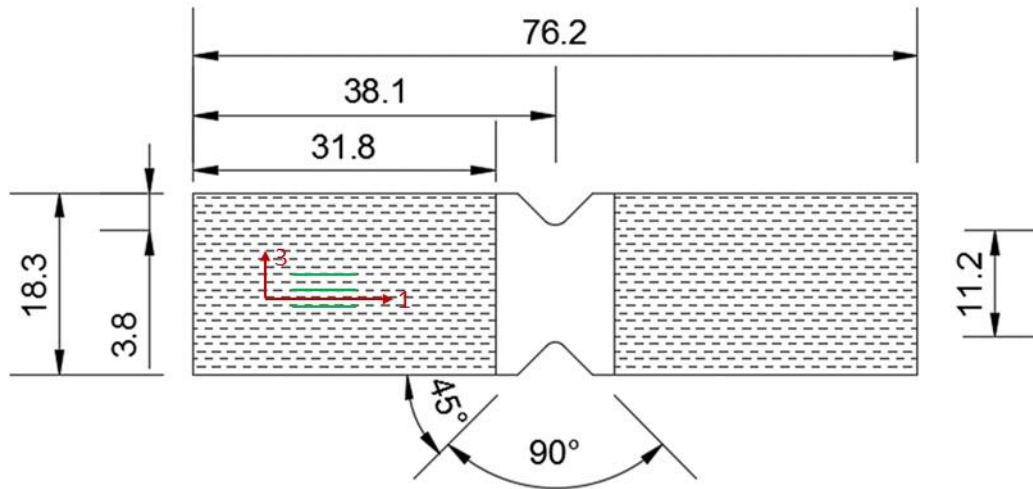


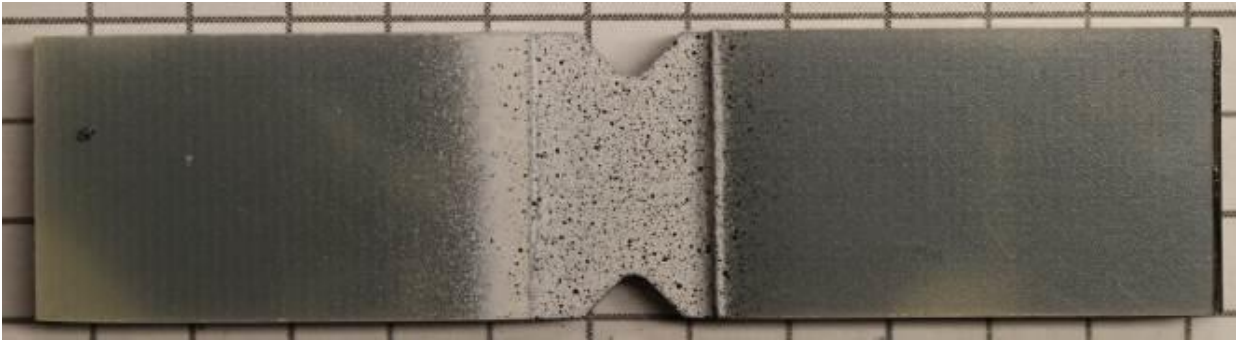
Figure 3.9-1. Typical specimen geometry and layout

The average specimen dimensions between the notches are shown in table 3.9-1 for the four tested replicates. The ligament height is defined as the distance between the notches.

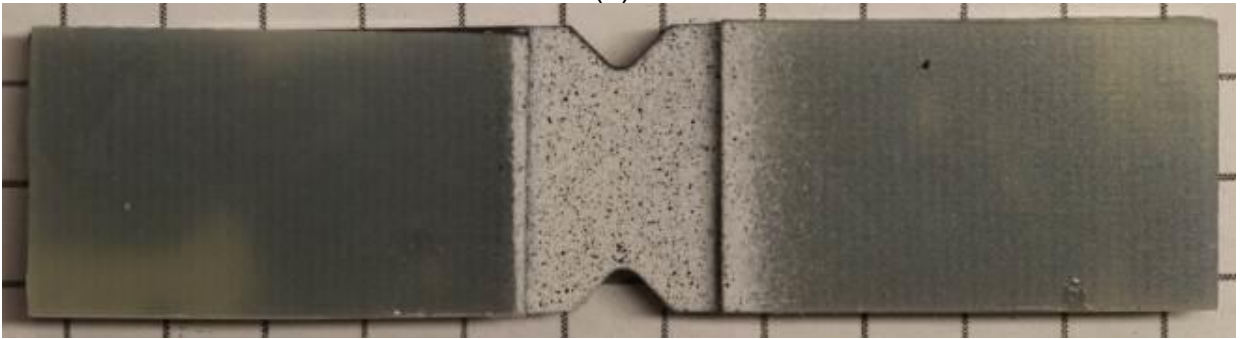
Table 3.9-1. 2-3 Plane Shear Test Specimen Dimensions

Replicate	Ligament Height (in)	Thickness (in)	Cross Sectional Area (in <sup>2</sup> )
TFS13-1	0.5108	0.1228	0.0627
TFS13-2	0.5093	0.1225	0.0624
TFS13-3	0.4945	0.1160	0.0574
TFS13-4	0.4935	0.1160	0.0572

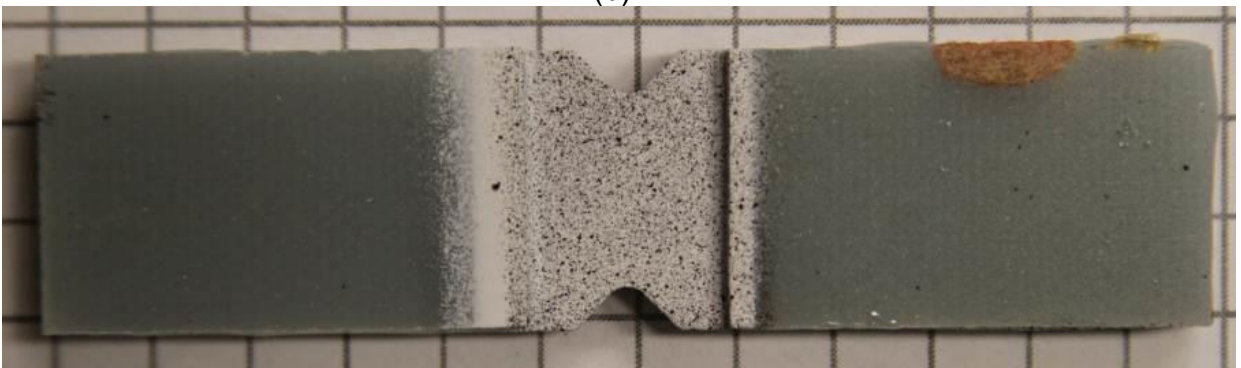
*Specimen Photographs:* The specimen photographs before the tests are shown in figure 3.9-2. The specimens exhibited HGN failure as shown in figure 3.7-3. Figure 3.9-3 shows the specimens after testing.



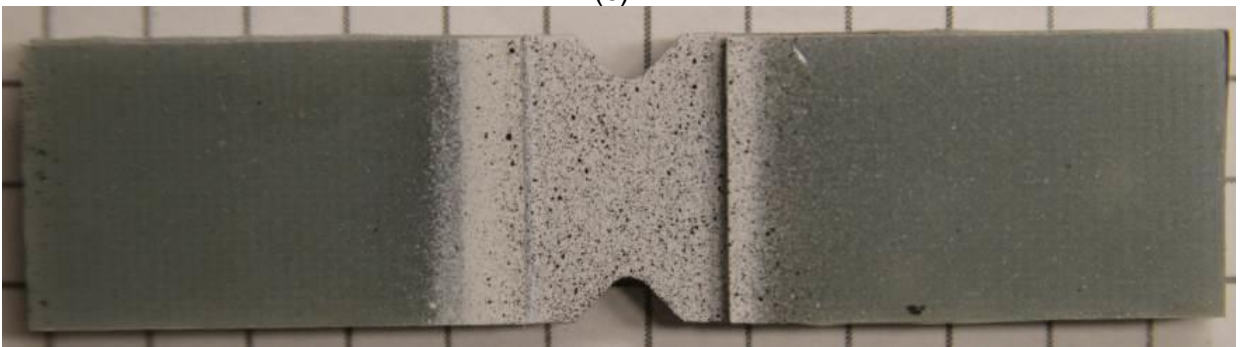
(a)



(b)

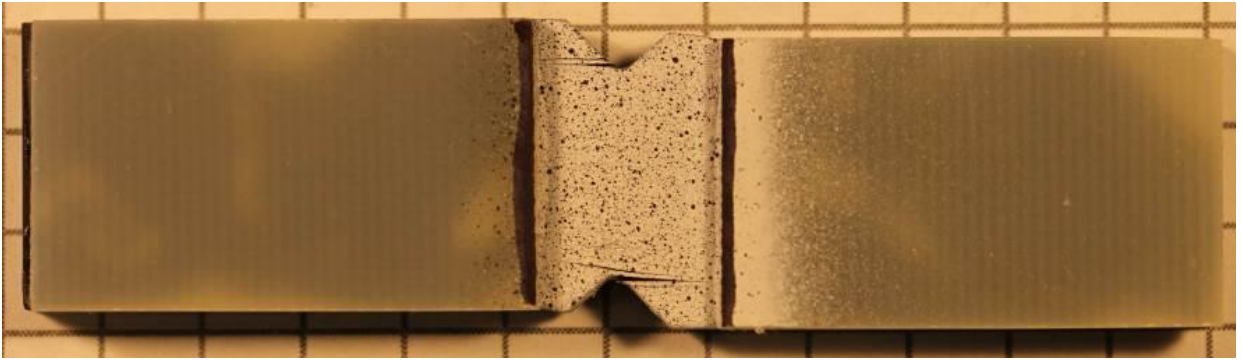


(c)

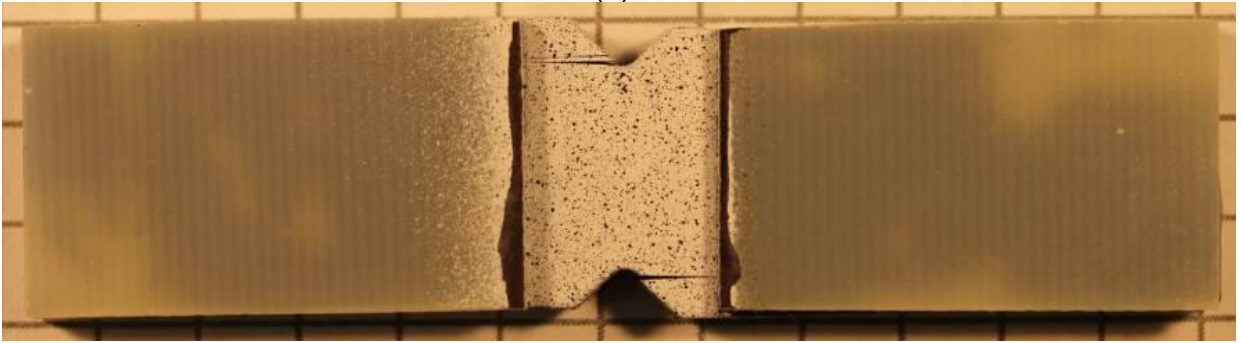


(d)

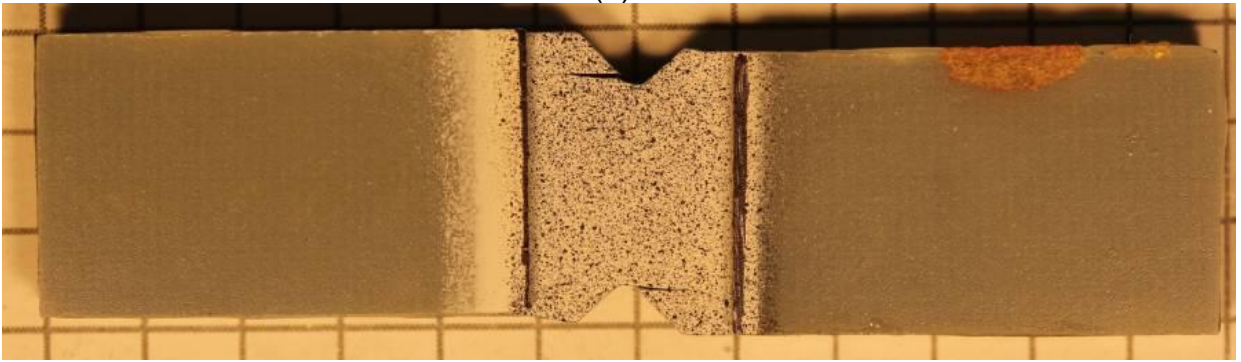
Figure 3.9-2. 1-3 plane shear specimens prior to testing (a) TFS13-1, (b) TFS13-2, (c) TFS13-3, (d) TFS13-4



(a)



(b)



(c)



(d)

Figure 3.9-3. 1-3 plane shear specimens after testing (a) TFS13-1, (b) TFS13-2, (c) TFS13-3, (d) TFS13-4

*Test Results:* The summary of the results from the tests is shown in table 3.9-2. The shear modulus reported in table 3.9-2 is in terms of engineering shear strain not tensorial shear strain. It should be noted that MAT213 requires stress-tensorial strain curve input from the user and internally converts the curve into stress-engineering strain before computing the shear modulus for use in the program.

Table 3.9-2. Summary of 1-3 Plane Shear Test Results

Replicate	Loading Rate (in/min)	Tensorial Strain Rate ( $1/s$ )	$G_{13}$ (psi)	Failure Strain (Tensorial)	Peak Stress (psi)
TFS13-1	0.05	$1.00(10^{-3})$	345 941	0.07511	11 837
TFS13-2	0.05	$8.00(10^{-4})$	341 301	0.06827	12 146
TFS13-3	0.05	$9.00(10^{-4})$	358 760	0.07608	13 070
TFS13-4	0.04	$7.50(10^{-4})$	344 951	0.06213	12 623
Average	-	-	347 738	0.07040	12 419
Standard Deviation	-	-	7 614	0.00651	541
Coefficient of Variation	-	-	2.2%	9.3%	4.4%

Figure 3.9-4 shows the individual stress-strain curves for each of the specimens as well as the model curve.

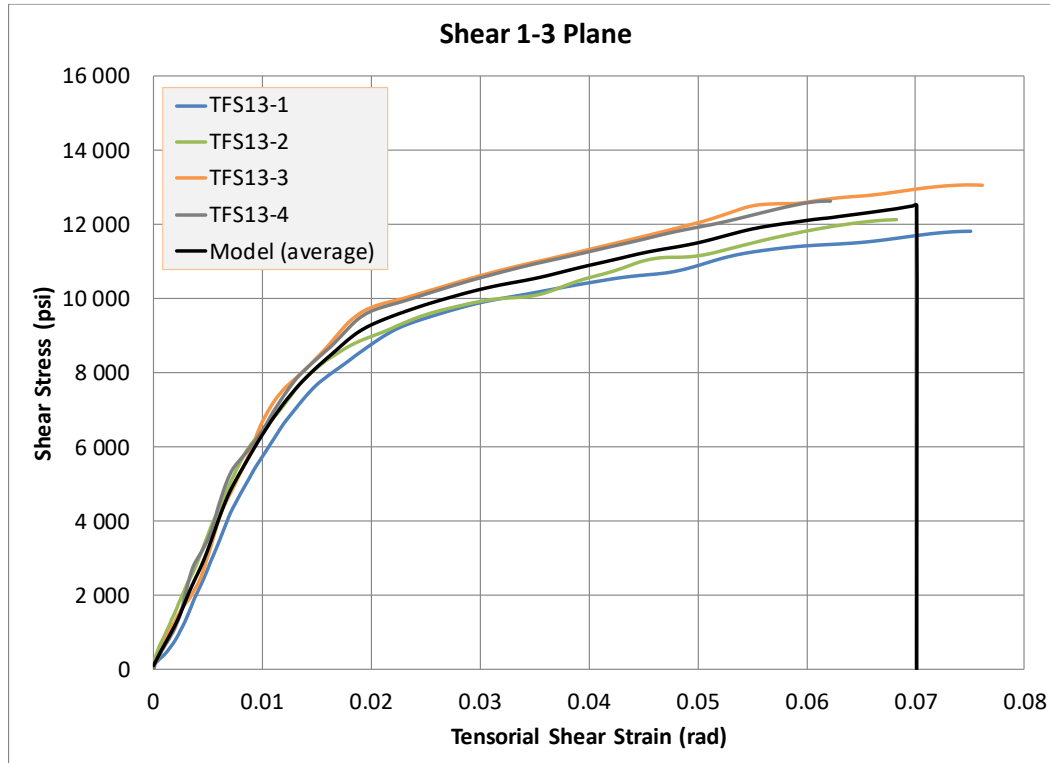


Figure 3.9-4. 1-3 plane shear stress-tensorial strain curves

### 3.10 TEST T10: 45° OFF-AXIS TENSION TEST IN THE 1-2 PLANE

This test is used to generate the 45° off-axis tension stress-strain curve in the 1-2 plane.

*Specimen Geometry:* The specimen dimensions and layout are shown in figure 3.10-1. The specimen geometry shown in figure 3.10-1(a) is taken from ASTM D3039. The alternative geometry (figure 3.10-1(b)) was created to try to promote failure in the gage section of the test specimens. Shaded regions indicate where the fiberglass tabs are bonded to the specimen.

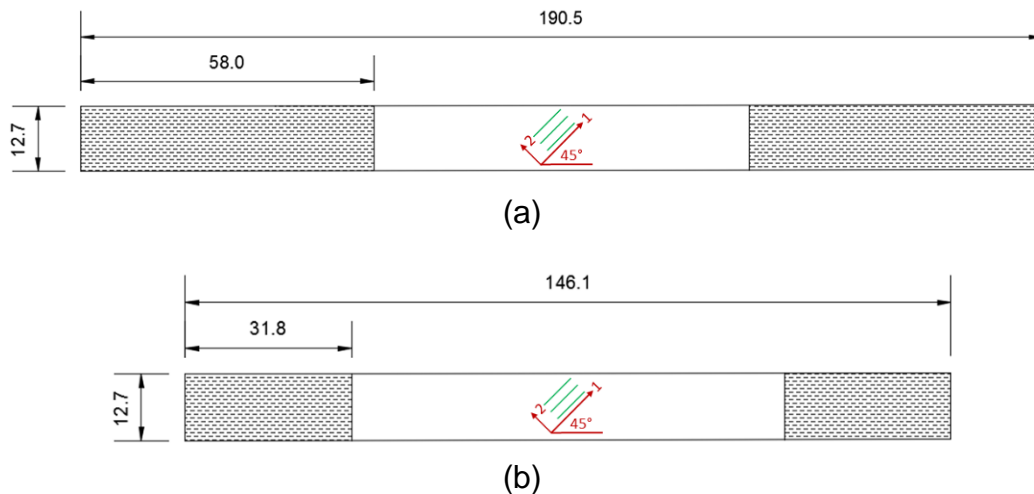


Figure 3.10-1. Specimen geometry and layout (a) ASTM geometry, (b) Alternative geometry

The average specimen dimensions in the gage section are shown in table 3.10-1 for the four tested replicates.

Table 3.10-1. 1-2 Plane 45° Off-Axis Tension Test Specimen Dimensions

Replicate	Width (in)	Thickness (in)	Cross Sectional Area (in <sup>2</sup> )
TFO12-3	0.4983	0.1240	0.0618
TFO12-4	0.4989	0.1234	0.0615
TFO12-5	0.4917	0.1229	0.0604
TFO12-6	0.4907	0.1233	0.0605

*Specimen Photographs:* The specimen photographs before the tests are shown in figure 3.10-2. The specimens exhibited failure in the matrix between and at the angle of the fibers before the tests ended. Figure 3.10-3 shows the specimens after testing.

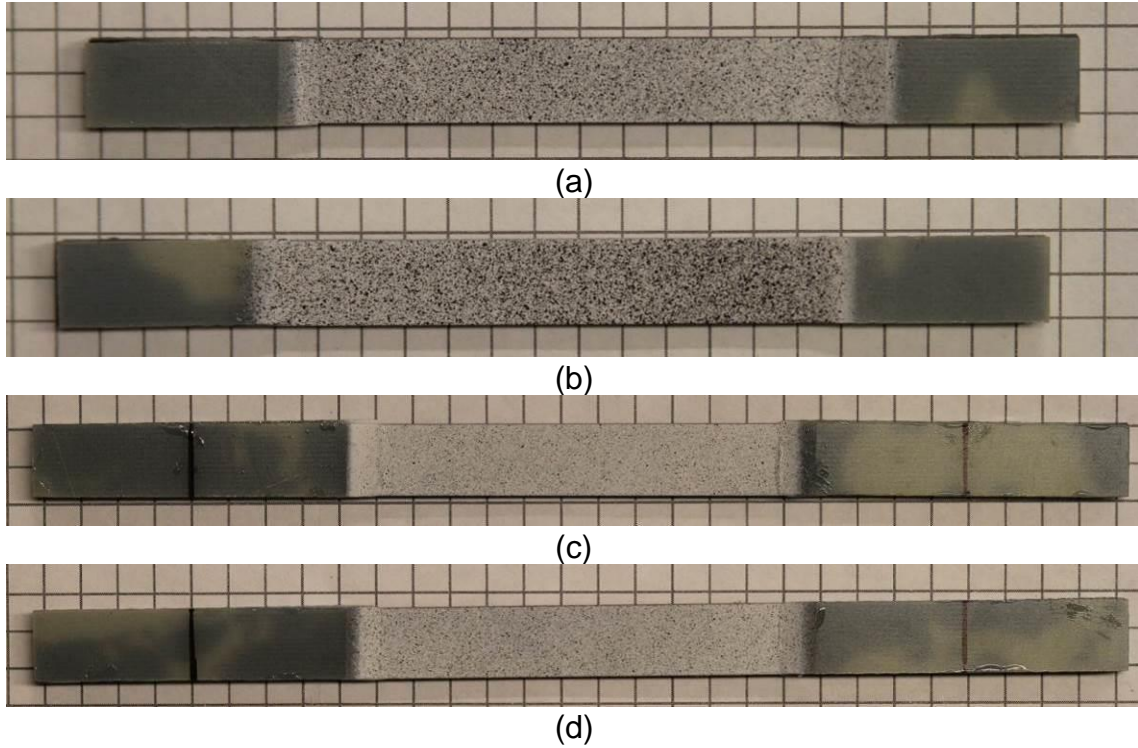


Figure 3.10-2. 1-2 plane 45° off-axis tension specimens prior to testing (a) TFO12-3, (b) TFO12-4, (c) TFO12-5, (d) TFO12-6

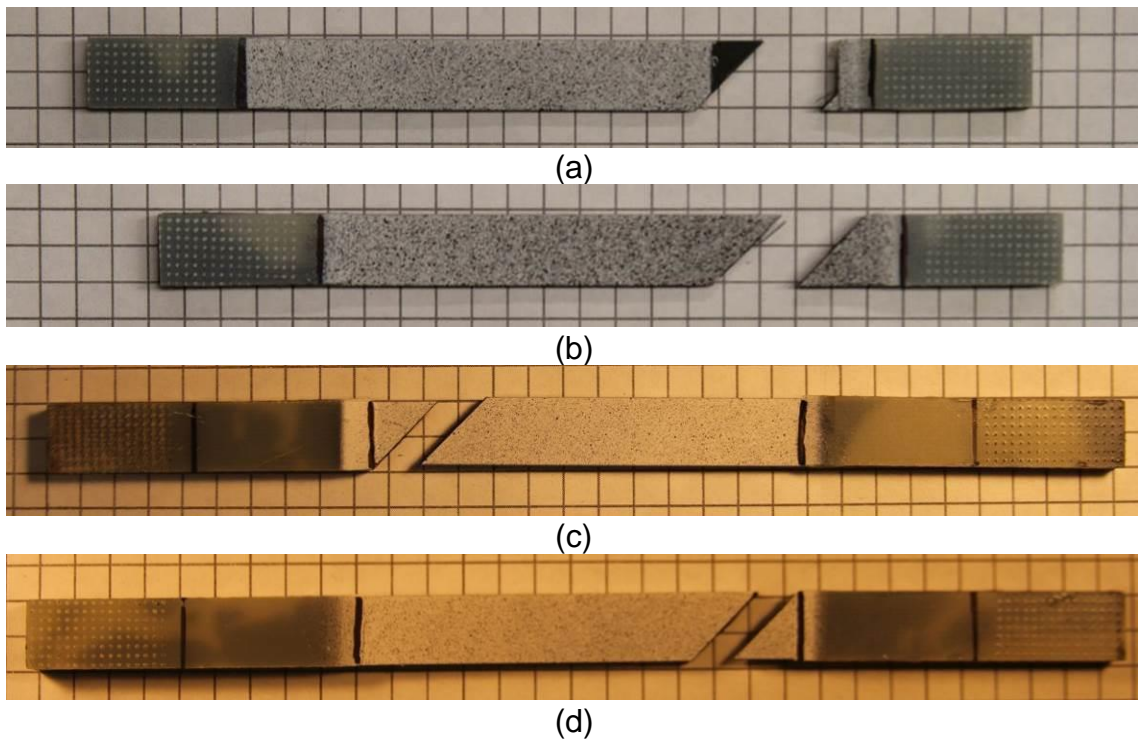


Figure 3.10-3. 1-2 plane 45° off-axis tension specimens after testing (a) TFO12-3, (b) TFO12-4, (c) TFO12-5, (d) TFO12-6

Test Results: The summary of the results from the tests is shown in table 3.10-2.

Table 3.10-2. Summary of 1-2 Plane 45° Off-Axis Tension Test Results

Replicate	Loading Rate (in/min)	Strain Rate ( $\frac{1}{s}$ )	Modulus (psi)	Ultimate Strain	Peak Stress (psi)
TFO12-3	0.02	8.00(10 <sup>-5</sup> )	1 581 087	0.00635	8 919
TFO12-4	0.02	8.00(10 <sup>-5</sup> )	1 513 604	0.00759	9 642
TFO12-5	0.02	8.00(10 <sup>-5</sup> )	1 500 341	0.00712	8 997
TFO12-6	0.02	4.00(10 <sup>-5</sup> )	1 465 136	0.00797	9 411
Average	-	-	1 515 042	0.00726	9 242
Standard Deviation	-	-	48 548	0.00070	343
Coefficient of Variation	-	-	3.2%	9.6%	3.7%

Figure 3.10-4 shows the individual stress-strain curves for each of the specimens as well as the model curve.

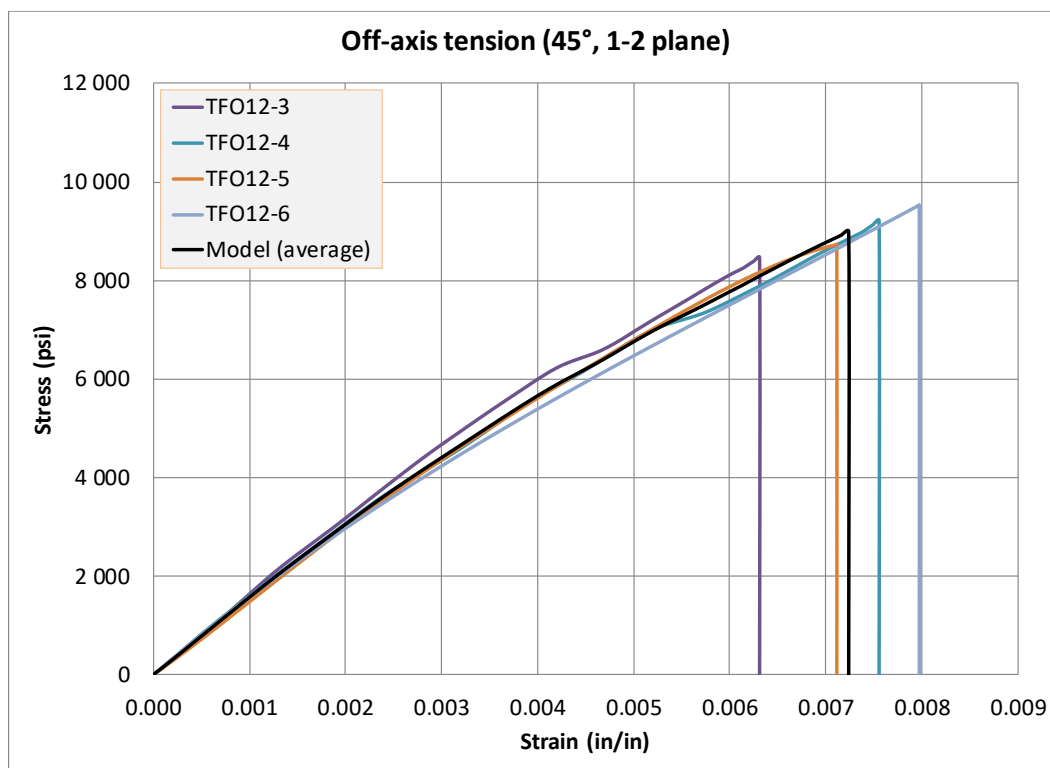


Figure 3.10-4. 1-2 plane 45° off-axis tension stress-strain curves

### 3.11 T11 TEST: 45° OFF-AXIS COMPRESSION TEST IN THE 2-3 PLANE

This test is used to generate the 45° off-axis compression stress-strain curve in the 2-3 plane.

*Specimen Geometry:* The specimen dimensions and layout are shown in figure 3.11-1. The geometry shown is a modified version of the geometry set by ASTM D7291. A cube was substituted for a cylindrical specimen for ease of machining and sample preparation. However, due to the limitation of the maximum specimen size presented by the thickness of the available panels, the size of the specimen was modified by making the specimens' dimensions smaller. ASTM D7291 sets guidelines for through thickness tensile properties. This ASTM was used because there is no standard available that sets guidelines for obtaining through thickness compressive properties of fiber reinforced composites.

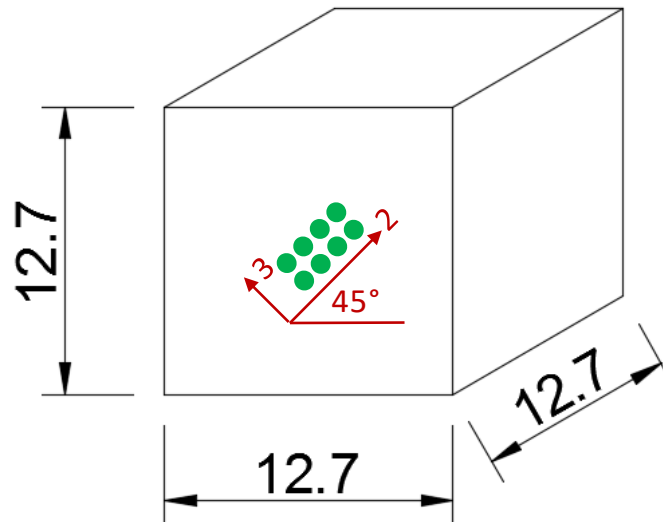


Figure 3.11-1. Specimen geometry and layout

The average specimen dimensions in the gage section are shown in table 3.11-1 for the three tested replicates.

Table 3.11-1. 2-3 Plane 45° Off-Axis Compression Test Specimen Dimensions

Replicate	Width (in)	Thickness (in)	Cross Sectional Area (in <sup>2</sup> )
TFO23-3	0.5457	0.5179	0.2826
TFO23-4	0.5142	0.5043	0.2593
TFO23-5	0.5309	0.5113	0.2715

*Specimen Photographs:* The specimen photographs before the tests are shown in figure 3.11-2. The specimens exhibited brittle failure of the matrix in the 2-3 plane before the

tests were terminated. Figure 3.11-3 shows the specimens after testing. Each set of photos includes an image of the front, left, and right side of the respective specimen. The front of the specimen is defined as the surface that was speckled for the purpose of capturing the strain field throughout the experiment.

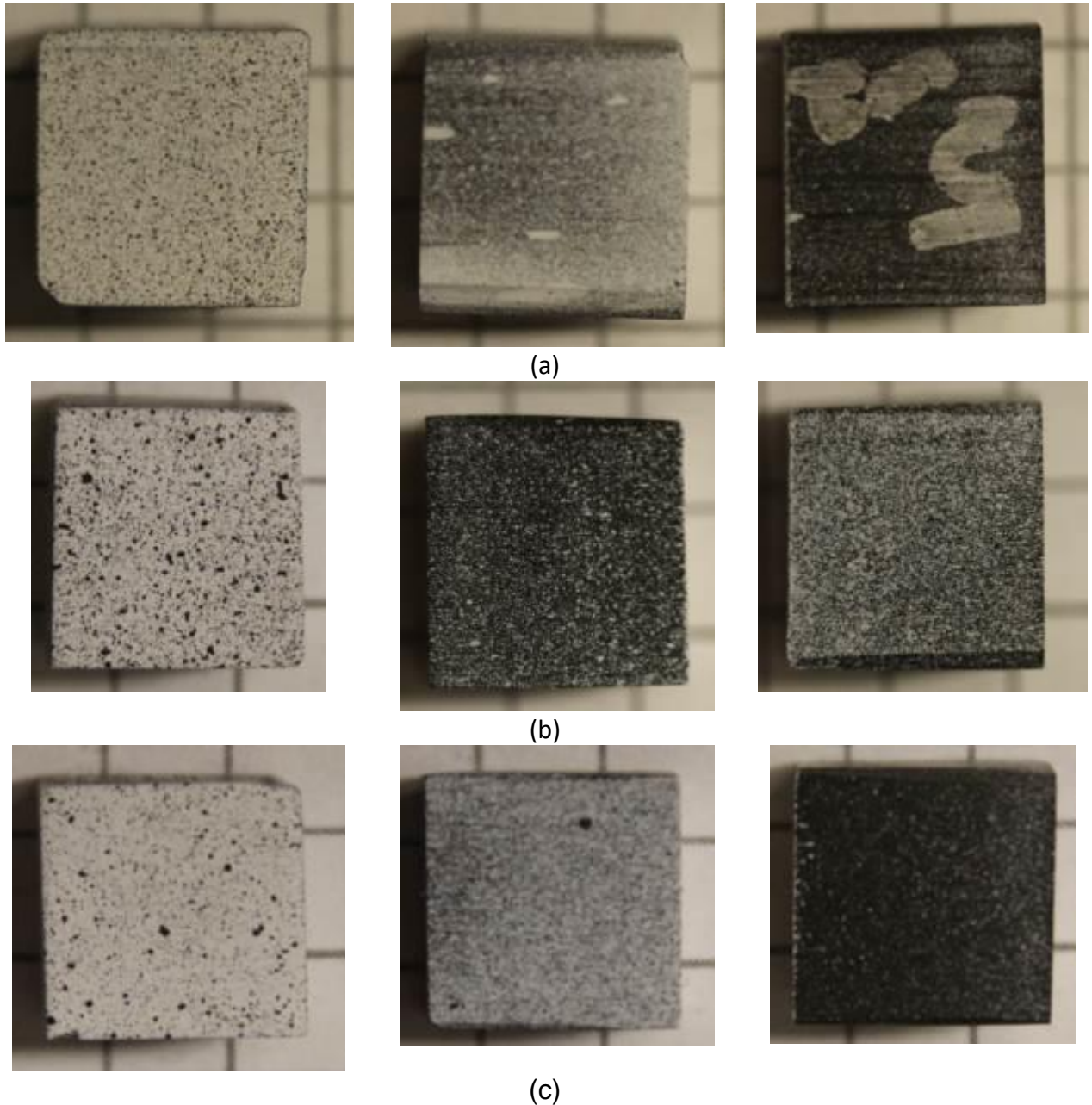


Figure 3.11-2. 2-3 plane 45° off-axis compression test specimens prior to testing  
(a) TFO23-3, (b) TFO23-4, (c) TFO23-5

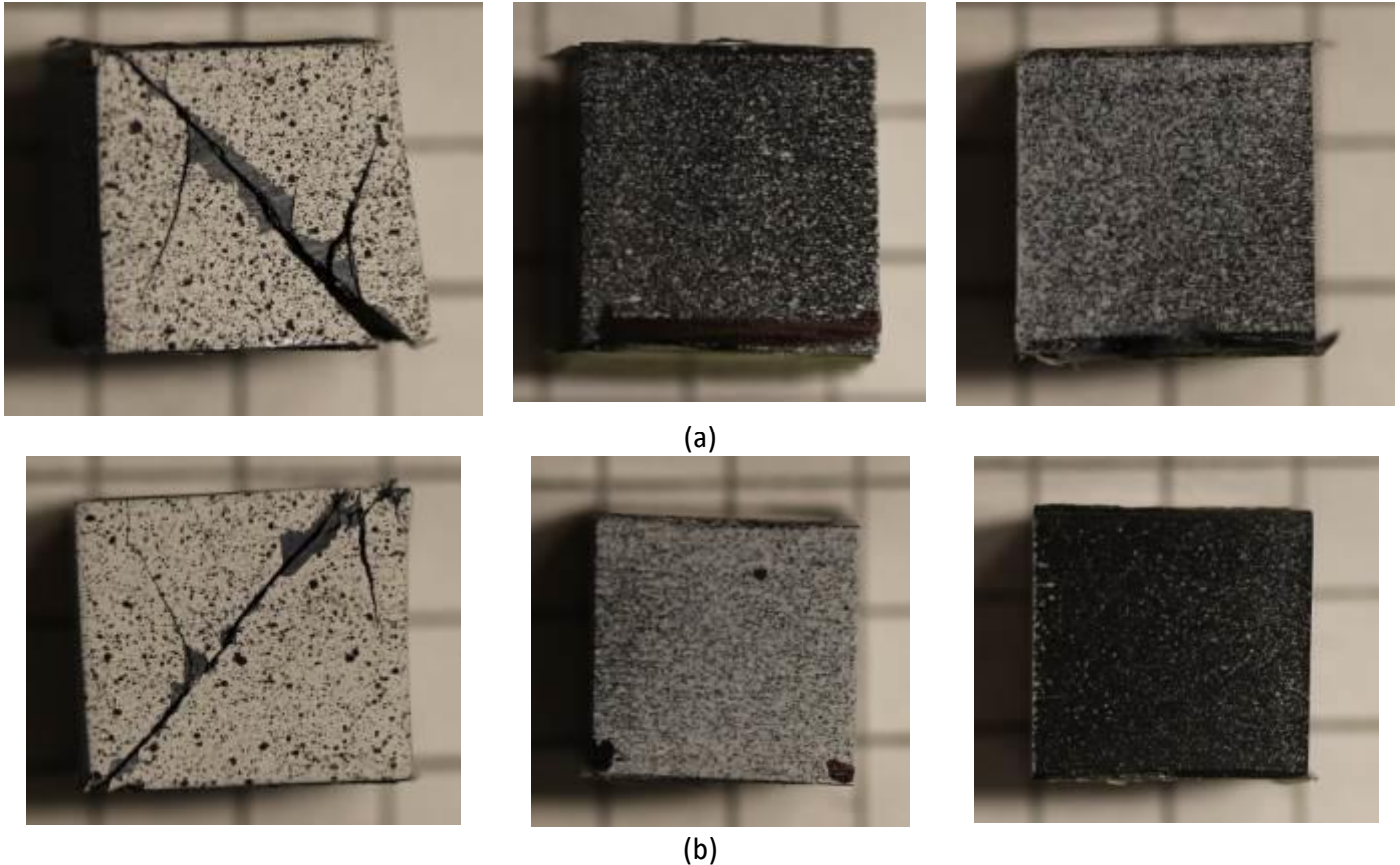


Figure 3.11-3. 2-3 plane 45° off-axis compression test specimens after testing (a) TFO23-4, (b) TFO23-5<sup>9</sup>

*Test Results:* The summary of the results from the tests is shown in table 3.11-2.

Table 3.11-2. Summary of 2-3 Plane 45° Off-Axis Compression Test Results

<b>Replicate</b>	<b>Loading Rate (in/min)</b>	<b>Strain Rate (<math>\frac{1}{s}</math>)</b>	<b>Modulus (psi)</b>	<b>Ultimate Strain</b>	<b>Peak Stress (psi)</b>
TFO23-3	0.005	1.20(10 <sup>-4</sup> )	945 437	0.05649	21 200
TFO23-4	0.005	1.20(10 <sup>-4</sup> )	1 048 242	0.05497	23 084
TFO23-5	0.005	1.30(10 <sup>-4</sup> )	850 293	0.06007	21 205
Average	-	-	947 991	0.05718	21 830
Standard Deviation	-	-	98 999	0.00262	1 086
Coefficient of Variation	-	-	10.4%	4.6%	5.0%

Figure 3.11-4 shows the individual stress-strain curves for each of the specimens as well as the model curve.

<sup>9</sup> Specimen TFO23-3 shattered at the end of the test, so there is no photograph. The specimen exhibited the same failure pattern as the other specimens.

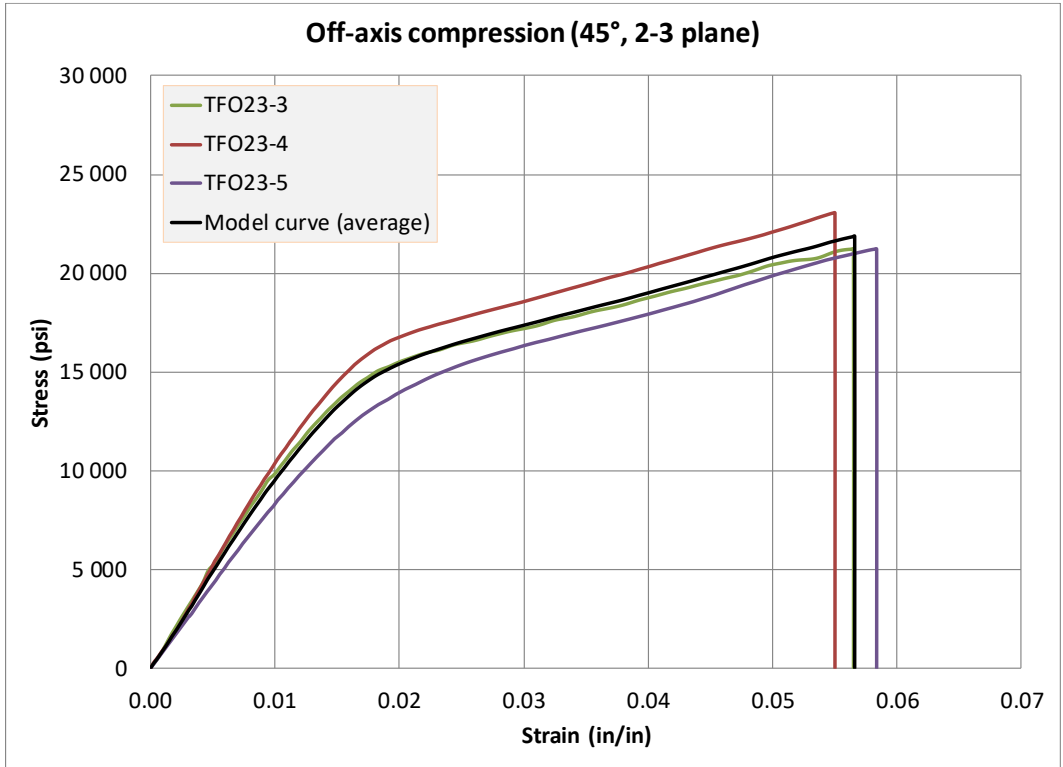


Figure 3.11-4. 2-3 plane 45° off-axis compression stress-strain curves

### 3.12 TEST T12: OFF-AXIS COMPRESSION TEST 45° IN THE 1-3 PLANE

This test is used to generate the 45° off-axis compression stress-strain curve in the 1-3 plane.

*Specimen Geometry:* The specimen dimensions and layout are shown in figure 3.12-1. The geometry shown is a modified version of the geometry set by ASTM D7291. A cube was used in place of a cylindrical specimen for ease of machining and sample preparation. However, due to the limitation of the maximum specimen size presented by the thickness of the available panels, the size of the specimen was modified by making the specimens' dimensions smaller. ASTM D7291 sets guidelines for through thickness tensile properties. This ASTM was used because there is no standard available that sets guidelines for obtaining through thickness compressive properties of fiber reinforced composites.

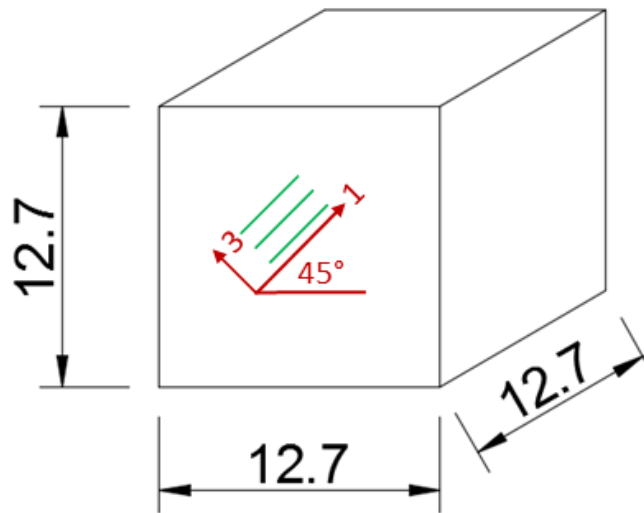


Figure 3.12-1. Specimen geometry and layout

The average specimen dimensions in the gage section are shown in table 3.12-1 for the four tested replicates.

Table 3.12-1. 1-3 Plane 45° Off-Axis Compression Test Specimen Dimensions

Replicate	Width (in)	Thickness (in)	Cross Sectional Area (in <sup>2</sup> )
TFO13-8	0.5092	0.5254	0.2675
TFO13-10	0.5083	0.5029	0.2556
TFO13-11	0.5089	0.5035	0.2562

*Specimen Photographs:* The specimen photographs before the tests are shown in figure 3.12-2. The specimens exhibited brittle failure of the matrix in the 1-3 plane between the

fibers before the tests were terminated. Figure 3.12-3 shows the specimens after testing. Each set of photos includes an image of the front, left, and right side of the respective specimen. The front of the specimen is defined as the surface that was speckled for the purpose of capturing the strain field throughout the experiment.

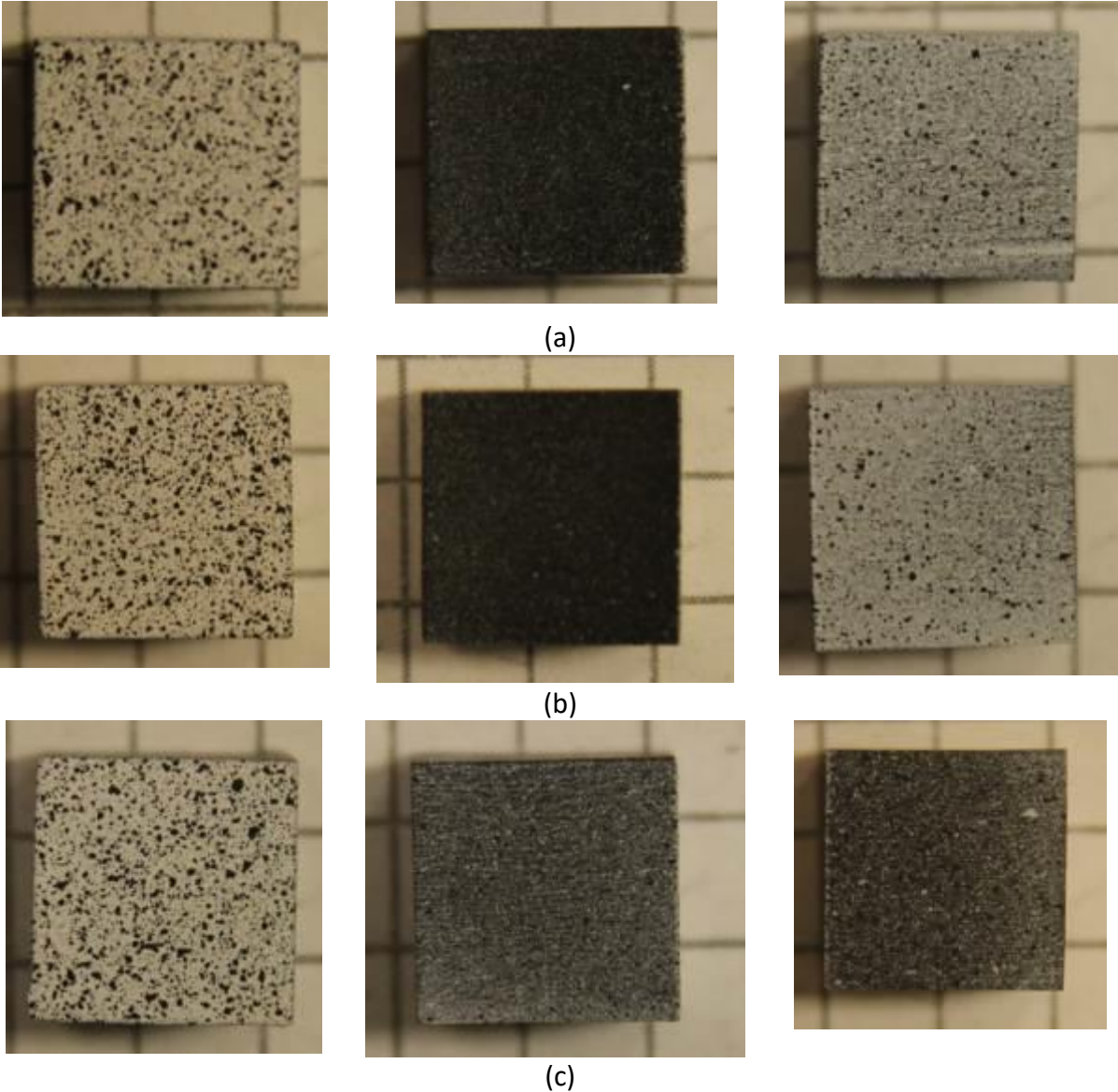
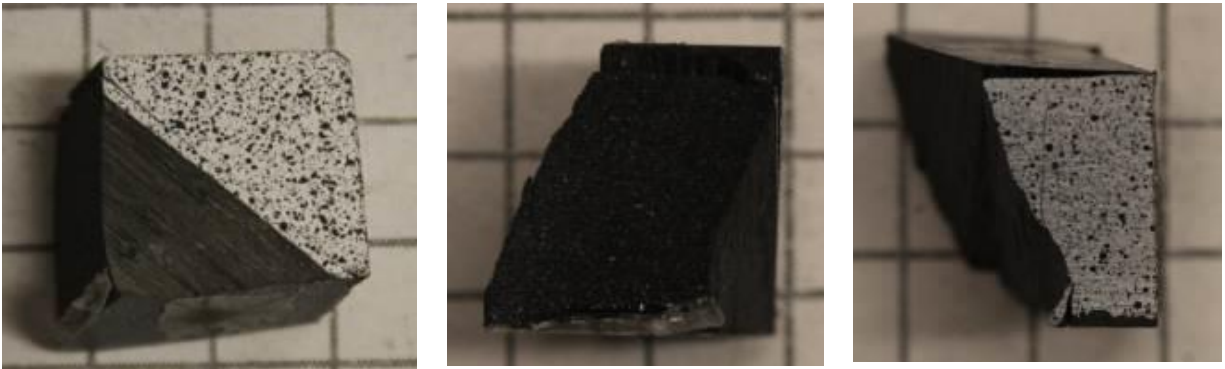


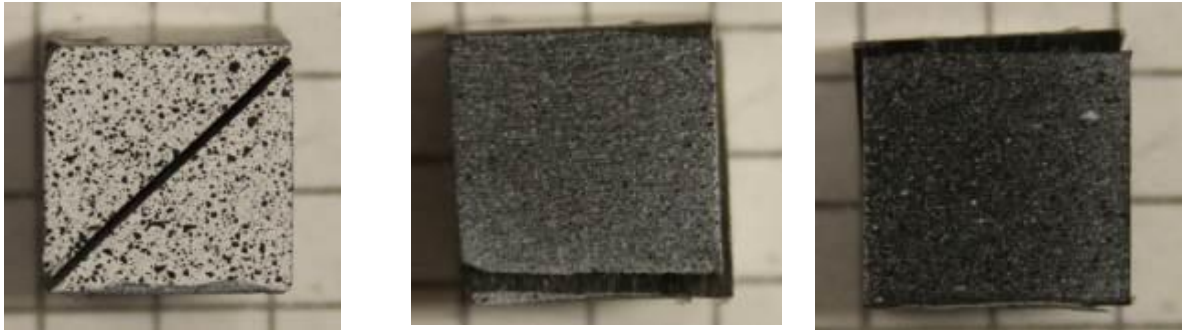
Figure 3.12-2. 1-3 plane 45° off-axis compression test specimens prior to testing  
(a) TFO13-8, (b) TFO13-10, (c) TFO13-11



(a)



(b)



(c)

Figure 3.12-3. 1-3 plane 45° off-axis compression test specimens after testing (a) TFO13-8, (b) TFO13-10, (c) TFO13-11

*Test Results:* The summary of the results from the tests is shown in table 3.12-2.

Table 3.12-2. Summary of 1-3 Plane 45° Off-Axis Compression Test Results

Replicate	Loading Rate (in/min)	Strain Rate ( $1/s$ )	Modulus (psi)	Ultimate Strain	Peak Stress (psi)
TFO13-8	0.005	$1.40(10^{-4})$	1 269 537	0.0915	29 247
TFO13-10	0.005	$1.51(10^{-4})$	1 403 289	0.0863	27 797
TFO13-11	0.005	$1.47(10^{-4})$	1 040 476	0.0958	29 282
Average	-	-	1 237 767	0.0912	28 775
Standard Deviation	-	-	149 812	0.0039	692
Coefficient of Variation	-	-	12.1%	4.3%	2.4%

Figure 3.12-4 shows the individual stress-strain curves for each of the specimens as well as the model curve.

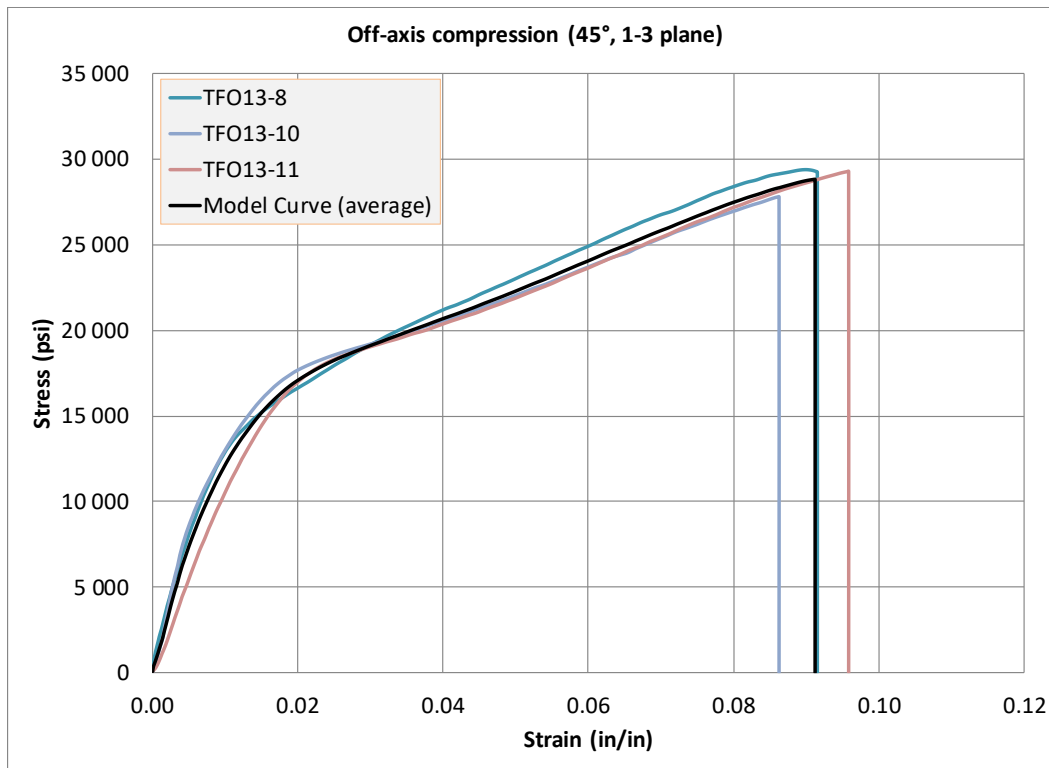


Figure 3.12-4. 1-3 plane 45° off-axis compression stress-strain curves

### 3.13 TEST T13: MASS DENSITY TEST

The mass density of the material meets ASTM D792-13. First, the mass of the specimens in air is found using a scale. Second, a beaker is filled with water and the specimens are immersed in the liquid using a wire to suspend the specimen in the liquid and to prevent the specimen from contacting the beaker. The apparent mass of the specimen and the submerged portion of the wire in water are recorded. Third, the wire is submerged up to the same point as in the second step and its apparent mass in water is recorded. Using all three measurements, the specific gravity of the material is determined using the equation below. The samples used in the experiment were taken from the edge of the panels. The process was calibrated and verified by first using aluminum. The specific gravity obtained using aluminum is 2.61, which is within the reported range.

$$S_g = \frac{a}{a + w - b}$$

$S_g$  = Specific Gravity

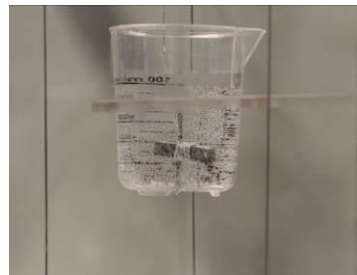
$a$  = apparent mass of specimen in air

$b$  = apparent mass of completely immersed specimen and partially immersed wire in liquid

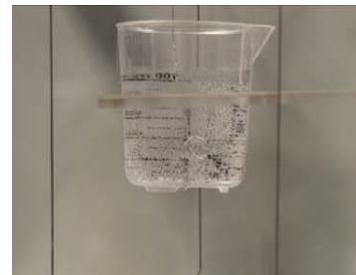
$w$  = apparent mass of partially immersed wire in liquid



(a)



(b)



(c)

Figure 3.13-1. Specific gravity test showing (a) Overall test setup, (b) specimen and wire submerged in water, and (c) wire submerged in water

Mass measurements are made using an AWS AL201S Analytical Balance<sup>10</sup> that has a resolution of 0.1 mg. The stand and beaker shown in figure 3.13-1 are part of a specific gravity kit obtained from Mineralab<sup>11</sup>.

<sup>10</sup> <http://www.awsscales.com/analytical-balances/166-al-201s-analytical-balance>

<sup>11</sup> <http://www.mineralab.com/SGK-B/>

Table 3.13-1. Specific Gravity

Sample	Mass: Specimen in Air (g)	Mass: Wire + Specimen Submerged (g)	Mass: Wire Submerged (g)	Specific Gravity
16-Ply_1	1.3496	0.8113	0.3258	1.5615
	1.3502	0.8115	0.3273	
	1.3498	0.8110	0.3245	
	Average: 1.3499	Average: 0.8113	Average: 0.3259	
	Std Dev: 0.00031	Std Dev: 0.00025	Std Dev: 0.00140	
	SD/AVG: 0.00023	SD/AVG: 0.00031	SD/AVG: 0.00430	
16-Ply_2	0.6993	0.5786	0.3258	1.5661
	0.6990	0.5773	0.3246	
	0.6996	0.5784	0.3256	
	Average: 0.6993	Average: 0.5781	Average: 0.3253	
	Std Dev: 0.00030	Std Dev: 0.00070	Std Dev: 0.00064	
	SD/AVG: 0.00043	SD/AVG: 0.00121	SD/AVG: 0.00198	
16-Ply_3	0.6867	0.5690	0.3257	1.5514
	0.6865	0.5707	0.3266	
	0.6854	0.5685	0.3242	
	Average: 0.6862	Average: 0.5694	Average: 0.3255	
	Std Dev: 0.00070	Std Dev: 0.00115	Std Dev: 0.00121	
	SD/AVG: 0.00102	SD/AVG: 0.00203	SD/AVG: 0.00372	
24-Ply_1	0.5534	0.5783	0.3845	1.5513
	0.5548	0.5845	0.3841	
	0.5536	0.5804	0.384	
	Average: 0.5539	Average: 0.5811	Average: 0.3842	
	Std Dev: 0.00076	Std Dev: 0.00315	Std Dev: 0.00026	
	SD/AVG: 0.00137	SD/AVG: 0.00543	SD/AVG: 0.00069	
24-Ply_2	0.567	0.5864	0.3846	1.5488
	0.5684	0.5839	0.3841	
	0.5678	0.5851	0.3832	
	Average: 0.5677	Average: 0.5851	Average: 0.3840	
	Std Dev: 0.00070	Std Dev: 0.00125	Std Dev: 0.00071	
	SD/AVG: 0.00124	SD/AVG: 0.00214	SD/AVG: 0.00185	
96-Ply_1	11.4349	5.1205	1.0709	1.5514
	11.4348	5.1365	1.0614	
	11.4355	5.1405	1.0722	
	Average: 11.4351	Average: 5.1325	Average: 1.0682	
	Std Dev: 0.00038	Std Dev: 0.01058	Std Dev: 0.00590	

	SD/AVG: 0.00003	SD/AVG: 0.00206	SD/AVG: 0.00552	
96-Ply_2	11.3898	5.1416	1.0659	1.5559
	11.3892	5.1441	1.0671	
	11.3902	5.1221	1.0673	
	Average: 11.3897	Average: 5.1359	Average: 1.0668	
	Std Dev: 0.00050	Std Dev: 0.01205	Std Dev: 0.00076	
	SD/AVG: 0.00004	SD/AVG: 0.00235	SD/AVG: 0.00071	

The specific gravity can be multiplied by the mass density of water to determine the mass density of the specimen.

Table 3.13-2. Specific Gravity Summary and Statistics

<b>Sample</b>	<b>Specific Gravity</b>
16-Ply_1	1.5615
16-Ply_2	1.5661
16-Ply_3	1.5514
24-Ply_1	1.5513
24-Ply_2	1.5488
96-Ply_1	1.5514
96-Ply_2	1.5559
Average	1.5552
Standard Deviation	0.0059
Coefficient of Variation	0.38%

### 3.14 TEST T14: VOLUME FRACTION TEST

The volume fraction of the composite is found using ImageJ<sup>12</sup>, an image analysis program. Images obtained from an optical microscope are processed. The software identifies the two constituents (fibers and matrix) based on their distinct colors (figure 3.14-1). It then calculates the amount of area that a phase occupies and reports the findings. The analyses are performed using 200x, 400x, and 500x magnification images. Figure 3.14-2 shows samples of the original and processed images used in the analyses.

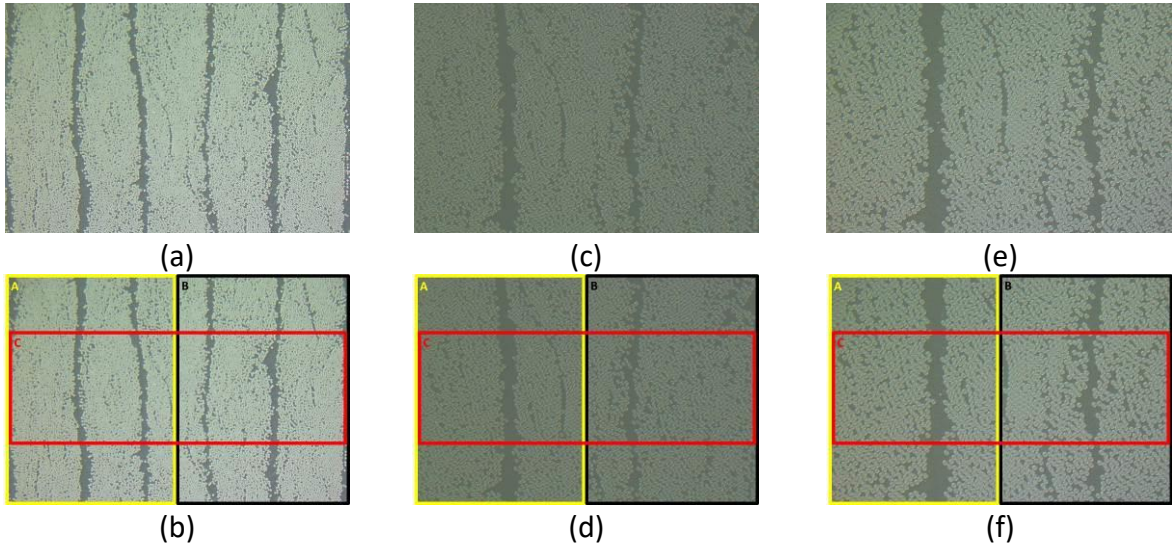


Figure 3.14-1. ImageJ volume fraction analysis 16-Ply analysis zones (a),(b) 200x, (c),(d) 400x, (e),(f) 500x

---

<sup>12</sup> <http://imagej.nih.gov/ij/>

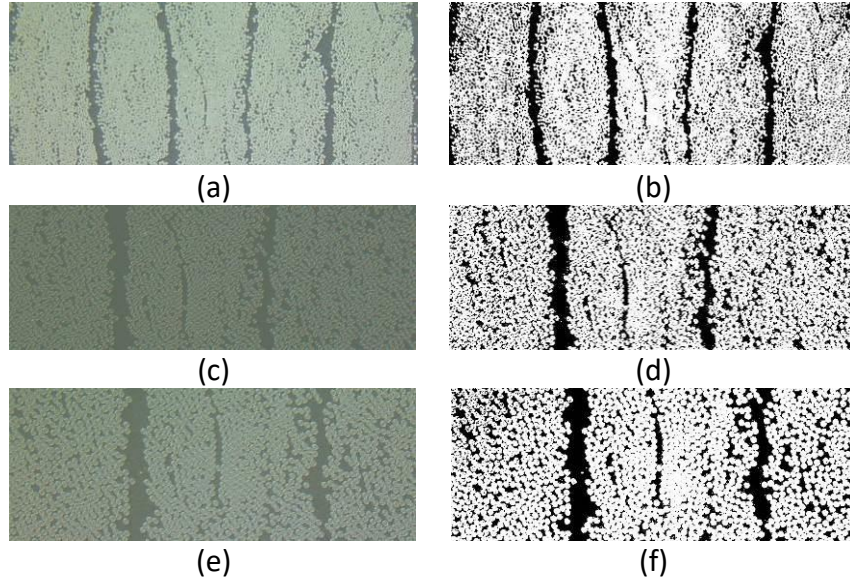


Figure 3.14-2. ImageJ volume fraction analysis original and processed images (a) 200x Original, (b) 200x processed, (c) 400x original, (d) 400x processed, (e) 500x original, (f) 500x processed

The results of the volume fraction test performed on a 16-Ply specimen are shown in Tables 3.14-1-3.14-3.

Table 3.14-1. Volume Fraction Results 16-Ply, 200x

<b>Zone</b>	<b>Matrix Volume Fraction (%)</b>
A	23.1
B	29.0
C	27.4
Average	26.
Std. Deviation	3.1

Table 3.14-2. Volume Fraction Results 16-Ply, 400x

<b>Zone</b>	<b>Matrix Volume Fraction (%)</b>
A	31.0
B	31.5
C	28.8
Average	30.4
Std. Deviation	1.4

Table 3.14-3. Volume Fraction Results 16-Ply, 500x

<b>Zone</b>	<b>Matrix Volume Fraction (%)</b>
A	29.7
B	30.6
C	29.8
Average	30.1
Std. Deviation	0.5

## 4 DAMAGE CHARACTERIZATION TEST DETAILS AND RESULTS

### 4.1 BACKGROUND

The full damage tensor can be used to relate the true stress to the effective stress as:

$$\begin{pmatrix} \sigma_{11} \\ \sigma_{22} \\ \sigma_{33} \\ \sigma_{12} \\ \sigma_{23} \\ \sigma_{13} \end{pmatrix} = \begin{bmatrix} M_{11} & M_{12} & M_{13} & M_{14} & M_{15} & M_{16} \\ M_{21} & M_{22} & M_{23} & M_{24} & M_{25} & M_{26} \\ M_{31} & M_{32} & M_{33} & M_{34} & M_{35} & M_{36} \\ M_{41} & M_{42} & M_{43} & M_{44} & M_{45} & M_{46} \\ M_{51} & M_{52} & M_{53} & M_{54} & M_{55} & M_{56} \\ M_{61} & M_{62} & M_{63} & M_{64} & M_{65} & M_{66} \end{bmatrix} \begin{pmatrix} \sigma_{11}^{eff} \\ \sigma_{22}^{eff} \\ \sigma_{33}^{eff} \\ \sigma_{12}^{eff} \\ \sigma_{23}^{eff} \\ \sigma_{13}^{eff} \end{pmatrix} \quad (3)$$

However, in the current research, a semi-coupled, directional dependent relationship is assumed, for example:  $M_{11} = M_{11}(\varepsilon_p^{11}, \varepsilon_p^{22}, \varepsilon_p^{33}, \varepsilon_p^{12}, \varepsilon_p^{23}, \varepsilon_p^{13})$ . This can then be used to construct the modified relationship as:

$$\begin{pmatrix} \sigma_{11} \\ \sigma_{22} \\ \sigma_{33} \\ \sigma_{12} \\ \sigma_{23} \\ \sigma_{13} \end{pmatrix} = \begin{bmatrix} M_{11} & 0 & 0 & 0 & 0 & 0 \\ 0 & M_{22} & 0 & 0 & 0 & 0 \\ 0 & 0 & M_{33} & 0 & 0 & 0 \\ 0 & 0 & 0 & M_{44} & 0 & 0 \\ 0 & 0 & 0 & 0 & M_{55} & 0 \\ 0 & 0 & 0 & 0 & 0 & M_{66} \end{bmatrix} \begin{pmatrix} \sigma_{11}^{eff} \\ \sigma_{22}^{eff} \\ \sigma_{33}^{eff} \\ \sigma_{12}^{eff} \\ \sigma_{23}^{eff} \\ \sigma_{13}^{eff} \end{pmatrix} \quad (4)$$

The damage parameter  $d_{ij}^{kl}$  represents damage in  $kl$  due to loading along  $ij$ , as a function of the directional plastic strain. It is assumed:

Normal damage is due to all normal and shear terms (for full generalization), for example:

$$(1 - d_{11}^{11}(\varepsilon_p^{11})) (1 - d_{22}^{11}(\varepsilon_p^{22})) (1 - d_{33}^{11}(\varepsilon_p^{33})) (1 - d_{12}^{11}(\varepsilon_p^{12})) (1 - d_{23}^{11}(\varepsilon_p^{23})) (1 - d_{13}^{11}(\varepsilon_p^{13})) = \frac{E_{11}^{dam}}{E_{11}} \quad (5)$$

Shear damage is due to all normal and shear terms (for full generalization), for example:

$$(1 - d_{11}^{12}(\varepsilon_p^{11})) (1 - d_{22}^{12}(\varepsilon_p^{22})) (1 - d_{33}^{12}(\varepsilon_p^{33})) (1 - d_{12}^{12}(\varepsilon_p^{12})) (1 - d_{23}^{12}(\varepsilon_p^{23})) (1 - d_{13}^{12}(\varepsilon_p^{13})) = \frac{G_{12}^{dam}}{G_{12}} \quad (6)$$

Using the given notation and assumptions, the expanded damage transformation can be written as:

$$\begin{aligned}
\sigma_{11} &= (1-d_{11}^{11}(\varepsilon_{11}^p))(1-d_{22}^{11}(\varepsilon_{22}^p))(1-d_{33}^{11}(\varepsilon_{33}^p))(1-d_{12}^{11}(\varepsilon_{12}^p))(1-d_{23}^{11}(\varepsilon_{23}^p))(1-d_{13}^{11}(\varepsilon_{13}^p))\sigma_{11}^{eff} \\
\sigma_{22} &= (1-d_{11}^{22}(\varepsilon_{11}^p))(1-d_{22}^{22}(\varepsilon_{22}^p))(1-d_{33}^{22}(\varepsilon_{33}^p))(1-d_{12}^{22}(\varepsilon_{12}^p))(1-d_{23}^{22}(\varepsilon_{23}^p))(1-d_{13}^{22}(\varepsilon_{13}^p))\sigma_{22}^{eff} \\
\sigma_{33} &= (1-d_{11}^{33}(\varepsilon_{11}^p))(1-d_{22}^{33}(\varepsilon_{22}^p))(1-d_{33}^{33}(\varepsilon_{33}^p))(1-d_{12}^{11}(\varepsilon_{12}^p))(1-d_{23}^{33}(\varepsilon_{23}^p))(1-d_{13}^{33}(\varepsilon_{13}^p))\sigma_{33}^{eff} \quad (7) \\
\sigma_{12} &= (1-d_{11}^{12}(\varepsilon_{11}^p))(1-d_{22}^{12}(\varepsilon_{22}^p))(1-d_{33}^{12}(\varepsilon_{33}^p))(1-d_{12}^{12}(\varepsilon_{12}^p))(1-d_{23}^{12}(\varepsilon_{23}^p))(1-d_{13}^{12}(\varepsilon_{13}^p))\sigma_{12}^{eff} \\
\sigma_{23} &= (1-d_{11}^{23}(\varepsilon_{11}^p))(1-d_{22}^{23}(\varepsilon_{22}^p))(1-d_{33}^{23}(\varepsilon_{33}^p))(1-d_{12}^{12}(\varepsilon_{12}^p))(1-d_{23}^{23}(\varepsilon_{23}^p))(1-d_{13}^{12}(\varepsilon_{13}^p))\sigma_{23}^{eff} \\
\sigma_{13} &= (1-d_{11}^{13}(\varepsilon_{11}^p))(1-d_{22}^{23}(\varepsilon_{22}^p))(1-d_{33}^{13}(\varepsilon_{33}^p))(1-d_{12}^{12}(\varepsilon_{12}^p))(1-d_{23}^{23}(\varepsilon_{23}^p))(1-d_{13}^{13}(\varepsilon_{13}^p))\sigma_{13}^{eff}
\end{aligned}$$

Eq. 7 shows that a total of 36 damage terms are required to fully characterize the damage in an orthotropic material. However, no assumptions are made as far as the symmetry of the material is concerned, meaning tension and compression is not treated

as being identical.  $\left(\frac{E_{11}^{dam}}{E_{11}}\right)^T \neq \left(\frac{E_{11}^{dam}}{E_{11}}\right)^C$ .

The asymmetry of the material means a total of 54 normal damage parameters and 27 shear damage parameters are required to characterize an orthotropic material. Three additional uncoupled damage terms for the off-axis tests are also required for converting input stress-strain curves to effective stress-effective plastic strain curves. This leads to a total of 84 damage terms that need to be determined experimentally. For preliminary damage characterization experiments, a plane stress assumption is used. This eliminates all experiments related to the 3-direction of the composite (through the thickness). Additionally, analyzing the results of the quasi-static room temperature experiments shows the 1-direction (longitudinal to the fibers) exhibits linear-elastic behavior throughout the experiment. Therefore, the experiments related to the 1-direction are also eliminated. Because no assumption is made about the symmetry of the material, both tension and compression in the 2-direction are tested separately. The experiments that must be carried out to obtain the necessary damage parameters are shown in Tables 4.1-1 through 4.1-4.

Table 4.1-1. Uncoupled Normal and Shear Damage Parameters

Parameter	Details
$d_{22_r}^{22}(\varepsilon_{22_r}^p)$	T2 unload/reload: damage 2-direction tension
$d_{22_c}^{22}(\varepsilon_{22_c}^p)$	C2 unload/reload: damage 2-direction compression
$d_{12}^{12}(\varepsilon_{12}^p)$	S12 unload/reload: damage 12-plane

Table 4.1-2. Coupled Normal-Normal Damage Parameters

Parameter	Details
$d_{22_T}^{22_c}(\varepsilon_{22_T}^p)$	T2 unload/reload: damage 2-direction compression
$d_{22_c}^{22_T}(\varepsilon_{22_c}^p)$	C2 unload/reload: damage 2-direction tension

Table 4.1-3. Coupled Normal-Shear Damage Parameters

Parameter	Details
$d_{12}^{22_T}(\varepsilon_{12}^p)$	S12 unload/reload: damage 2-direction tension
$d_{12}^{22_c}(\varepsilon_{12}^p)$	S12 unload/reload: damage 2-direction compression

Table 4.1-4. Coupled Shear-Normal Damage Parameters

Parameter	Details
$d_{22_T}^{12}(\varepsilon_{22_T}^p)$	T2 unload/reload: damage 12-plane
$d_{22_c}^{12}(\varepsilon_{22_c}^p)$	C2 unload/reload: damage 12-plane

Details of the experiments are provided in the next section. Determining the damage parameters requires the measurement of either the damaged modulus or plastic strain (by unloading the material to a state of zero stress) at several total strain values.

Table 4.1-5. Damaged Modulus and Plastic Strain (normal stress-strain relationship)

Damaged Modulus	Plastic Strain
$d_{11}^{11} = 1 - \frac{E_{11}^{d11}}{E_{11}}$	$\tilde{\sigma}_{11} = E_{11}(\varepsilon_{11} - \varepsilon_{11}^p)$
$M_{11}^{11} = 1 - d_{11}^{11}$	$M_{11}^{11} = \frac{\sigma_{11}}{\tilde{\sigma}_{11}}$
$\tilde{\sigma}_{11} = \frac{\sigma_{11}}{M_{11}^{11}}$	$d_{11}^{11} = 1 - M_{11}^{11} \quad (9)$
$\varepsilon_{11}^p = \varepsilon_{11} - \frac{\tilde{\sigma}_{11}}{E_{11}} \quad (8)$	

Using either approach, the damage parameter can be calculated at different values of total strain. It is important to note that the number of effective stress versus total strain points is equal to the amount of unloading steps taken during experimentation. Therefore, the true stress versus total strain curve may have more points than the damage parameter versus total strain curve. Therefore, consider the desired resolution of the damage parameter data when determining the number of unloading steps.

Similarly, the shear damage terms are determined using either of the following two approaches.

Table 4.1.6. Damaged Modulus and Plastic Strain (shear stress-strain relationship)

Damaged Modulus	Plastic Strain
$d_{12}^{12} = 1 - \frac{G_{12}^{d12}}{G_{12}}$	$\tilde{\sigma}_{12} = 2G_{12} (\varepsilon_{12} - \varepsilon_{12}^p)$ $M_{44}^{12} = \frac{\sigma_{12}}{\tilde{\sigma}_{12}}$ $d_{xy}^{xy} = 1 - M_{44}^{12} \quad (11)$
$M_{44}^{12} = 1 - d_{12}^{12}$	
$\tilde{\sigma}_{12} = \frac{\sigma_{12}}{M_{44}^{12}}$	
$\varepsilon_{12}^p = \varepsilon_{12} - \frac{\tilde{\sigma}_{12}}{2G_{12}} \quad (10)$	

The same approach can be used to determine the coupled terms with the following

generalized equation: 
$$d_{ij}^{kl} = 1 - \frac{E_{kl}^d(\varepsilon_{ij}^p)}{E_{kl}}$$
.

## 4.2 EXPERIMENTAL METHODS

The experiments to characterize the damaged behavior of the T800/F3900 composite were performed using the respective test fixtures as the QS-RT tests. Additionally, the post-processing techniques used to obtain strain field data were the same as the QS-RT tests. Any additional methods or fixtures used for the experiments are discussed in this section.

### 4.2.1 Uncoupled Experiments

The procedure for the experimental tests to obtain the uncoupled damage terms is described below, where the damaged modulus and plastic strain are calculated at each of the unload/reload steps. The procedure applies to the uncoupled 2-direction tension, uncoupled 2-direction compression, and uncoupled 1-2 plane shear.

Load Steps (figure 4.2-1):

- a) Load to a damaged point, i.e. point 1.
- b) Unload to a stress-free state, i.e. point 2.
- c) Perform three conditioning load/unload cycles in the current elastic regime, i.e. between point 2 and point 1a, where point 1a corresponds to 80% of the stress value observed at point 1.
- d) Reload to a strain level past the point of the previously loaded state, i.e. load to point 3.
- e) Repeat steps b and c for the desired amount of damage points.
- f) Final unload point is 2 standard deviations below the average failure strain of the respective QS-RT curves.

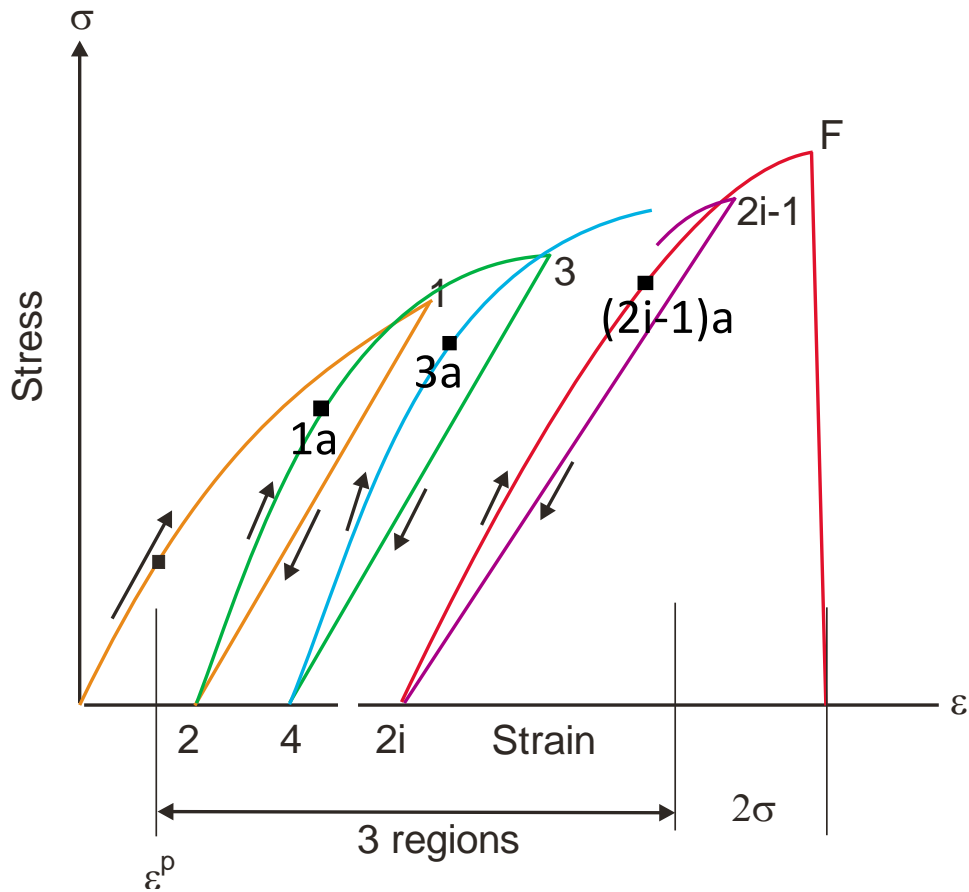


Figure 4.2-1. Loading-unloading steps for characterization of uncoupled damage parameters

Conditioning cycles serve two purposes. The first is to yield more information about the elastic modulus at the point of plastic strain. Because multiple cycles are performed, multiple measurements of the elastic modulus can be made. This information gives statistical data that can be used to determine whether the change in modulus as the test progresses is due to numerical dispersion or actual damage. If there is no clear trend, any data that lies within the average dispersion in the given cycles can be attributed to noise in the data instead of damage in the specimen. The second is that the elastic modulus seemed to approach a steady state value as the conditioning cycles were performed. The test specimens used for the uncoupled 2-direction tension, uncoupled 2-direction compression, and uncoupled 1-2 plane shear are shown in figure 4.2-2 through 4.2-4 respectively.

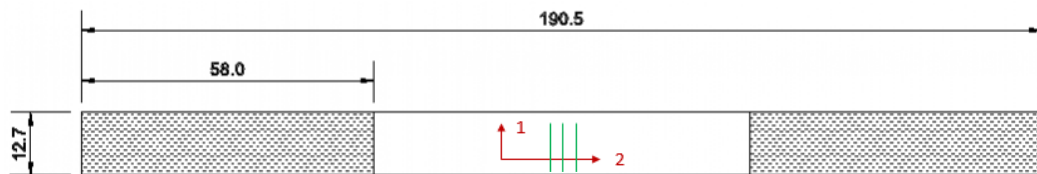


Figure 4.2-2. Uncoupled 2-direction tension test specimen (dimensions in mm)

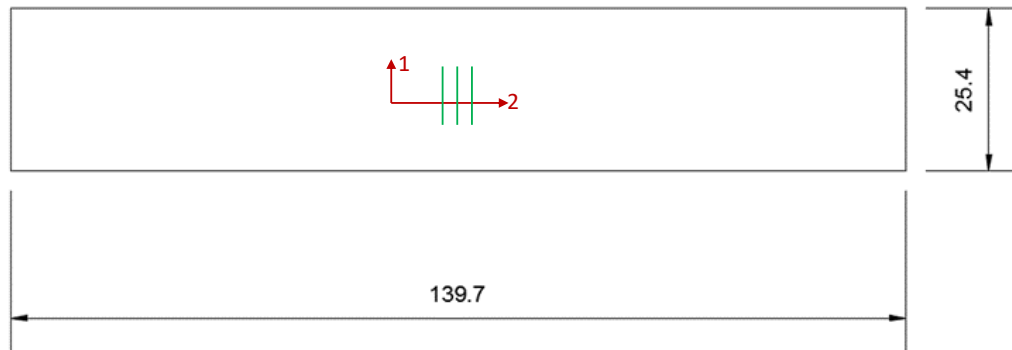


Figure 4.2-3. Uncoupled 2-direction compression test specimen without tabs (dimensions in mm)

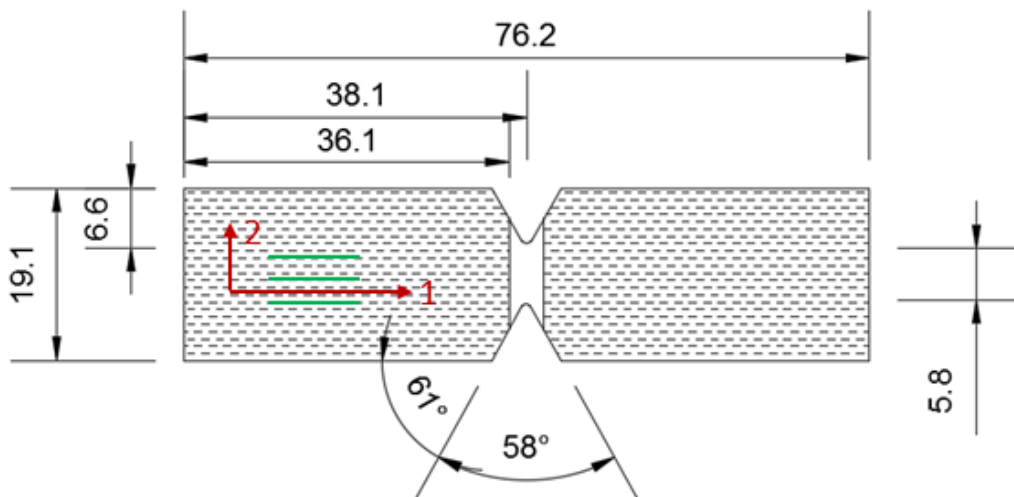


Figure 4.2-4. Uncoupled 1-2 plane shear test specimen (dimensions in mm)

#### 4.2.2 Coupled Experiments

The coupled damage terms are obtained by testing a specimen in one direction to a damaged point, then reloading in another direction elastically just enough to obtain a modulus value without inducing any additional damage. The steps to obtain the normal-normal coupled damage are described below. These steps follow the same general procedure from the uncoupled tests with an additional reloading in the damage direction of interest. The damage direction may be either another material direction/plane or loading the specimen tension/compression.

Load Steps (figure 4.2-5):

- a) Obtain initial undamaged modulus in direction  $kl$  following steps d-f.
- b) Load to a damaged point in  $ij$  direction, i.e. point 1.
- c) Unload to a stress-free state in the  $ij$  direction, i.e. point 2.
- d) **Change the loading direction to  $kl$ .** Reload elastically in the  $kl$  direction, without inducing any additional damage.

- e) Unload to a stress-free state in the  $kl$  direction.
- f) Perform three conditioning load/unload cycles in the current elastic regime of the  $kl$  direction, i.e. between point 2 and point 1a, where point 1a corresponds to 80% of the stress value observed at point 1.
- g) **Change the loading direction to  $ij$ .** Reload to a strain level past the point of the previous unloading in the  $ij$  direction.
- h) Repeat steps b-e for the desired amount of damage points.
- i) Final unload point in the  $ij$  direction is 2 standard deviations below the average failure strain of the respective QS-RT curves for the experiment where damage is being induced in the specimen.

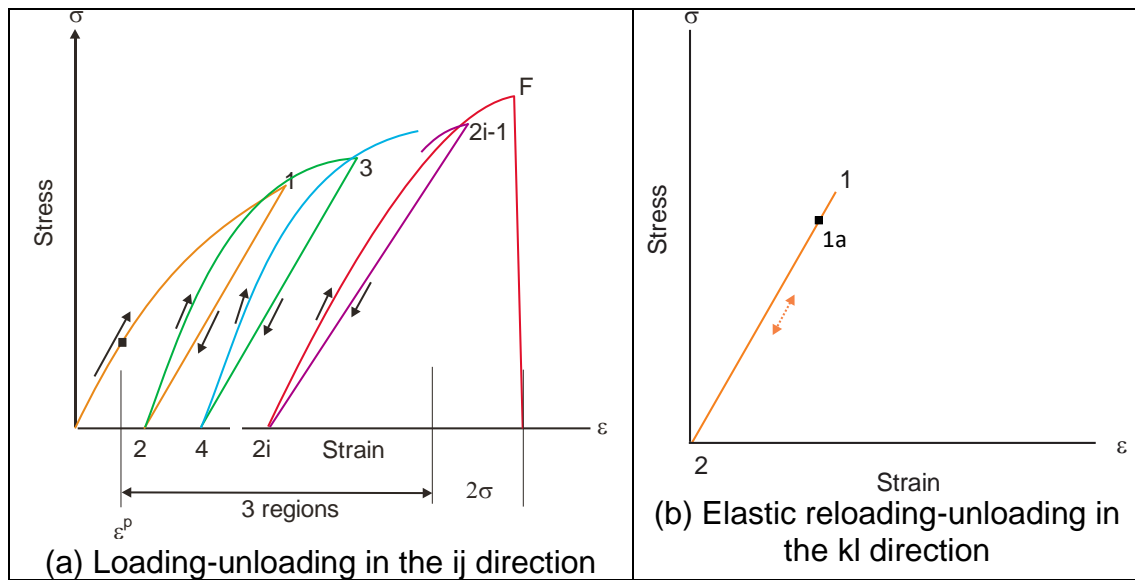


Figure 4.2-5. Loading-unloading steps for characterization of coupled damage parameter  $d_{ij}^{kl}$

The specimen dimensions shown in figure 4.2-6 are used for both coupled normal tests.

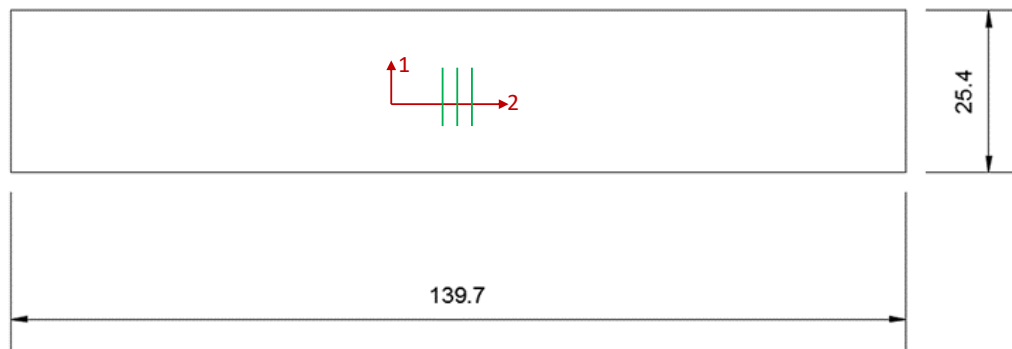


Figure 4.2-6. Specimen dimensions for coupled normal-normal tests (dimensions in mm)

The coupled damage terms for the normal-shear relation can be obtained by following the same coupled procedure for the normal-normal test cases. However, the initial loading is in the normal direction to induce damage with elastic reloading-unloading in the shear plane. The specimen for the coupled normal-shear tests is shown in figure 4.2-7.

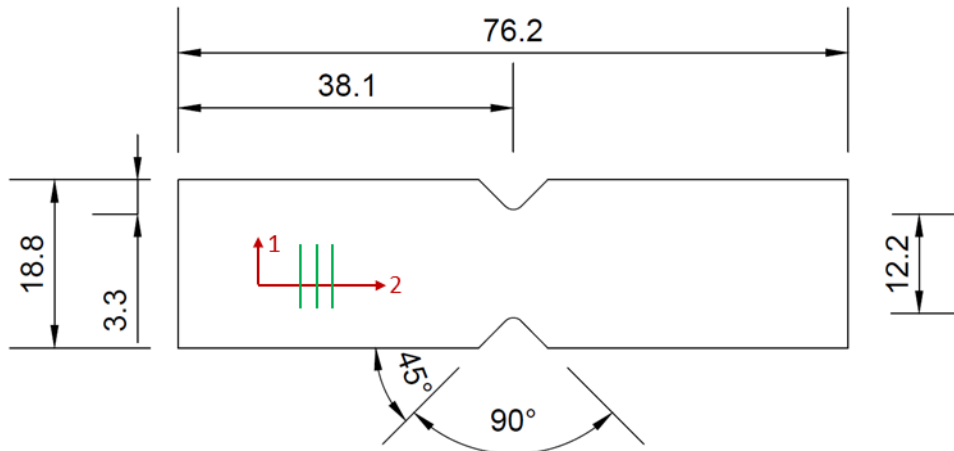


Figure 4.2-7. Specimen dimensions for coupled normal-shear tests (dimensions in mm)

The coupled shear-normal test coupons are the same as those used for the coupled normal-shear tests, but the loading steps are reversed. In other words, the specimens are loaded in the shear plane to induce damage, and the corresponding elastic reloading-unloading is performed in the normal direction.

#### 4.2.3 Computing Elastic Modulus

The elastic modulus is computed at each point of damage inducing strain. A linear regression is performed on all load and unload paths, including the conditioning cycles, at the current point of strain for which damage is measured. Figure 4.2-8 shows a typical cycle for the coupled 2-direction compression 2-direction tension test. Figure 4.2-8(a) shows the specimen being loaded in compression to a predetermined strain value and subsequently being unloaded to a stress-free state. Figure 4.2-8(b) shows the specimen being subjected to multiple load and unload cycles in the elastic regime in tension.

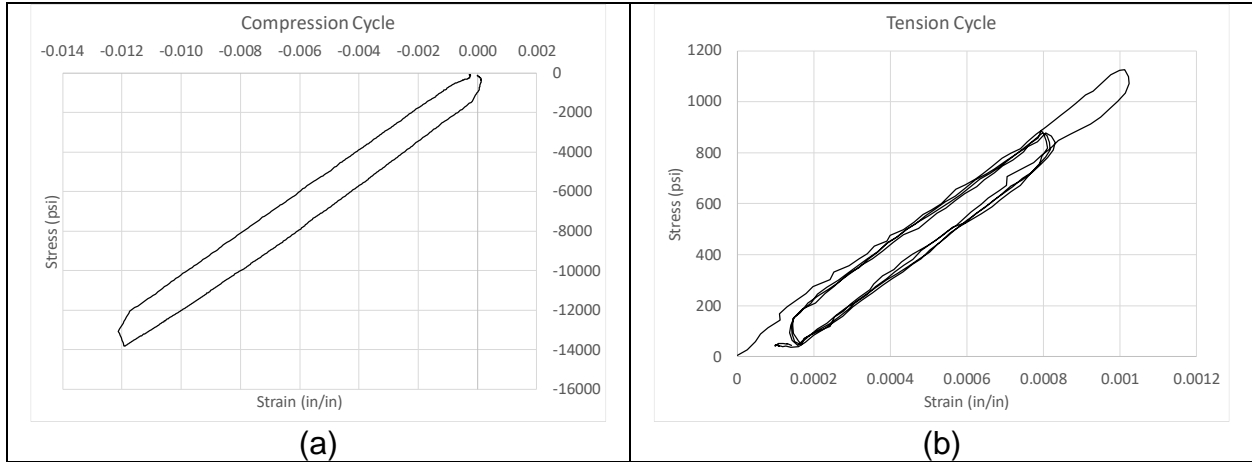


Figure 4.2-8. Standard cycle for the coupled test: 2-direction compression and 2-direction tension (a) compression loading causing damage and (b) subsequent interrogation in tension with conditioning cycles

Figure 4.2-8(b) shows curvature when the load direction reverses. This is because systems used to capture strain data and force are completely independent, which causes a discrepancy in the actual time at which the respective corresponding data was captured. The curved regions are ignored in the regression analysis. Figure 4.2-9 shows each individual load and unload path along with its corresponding regression equation.

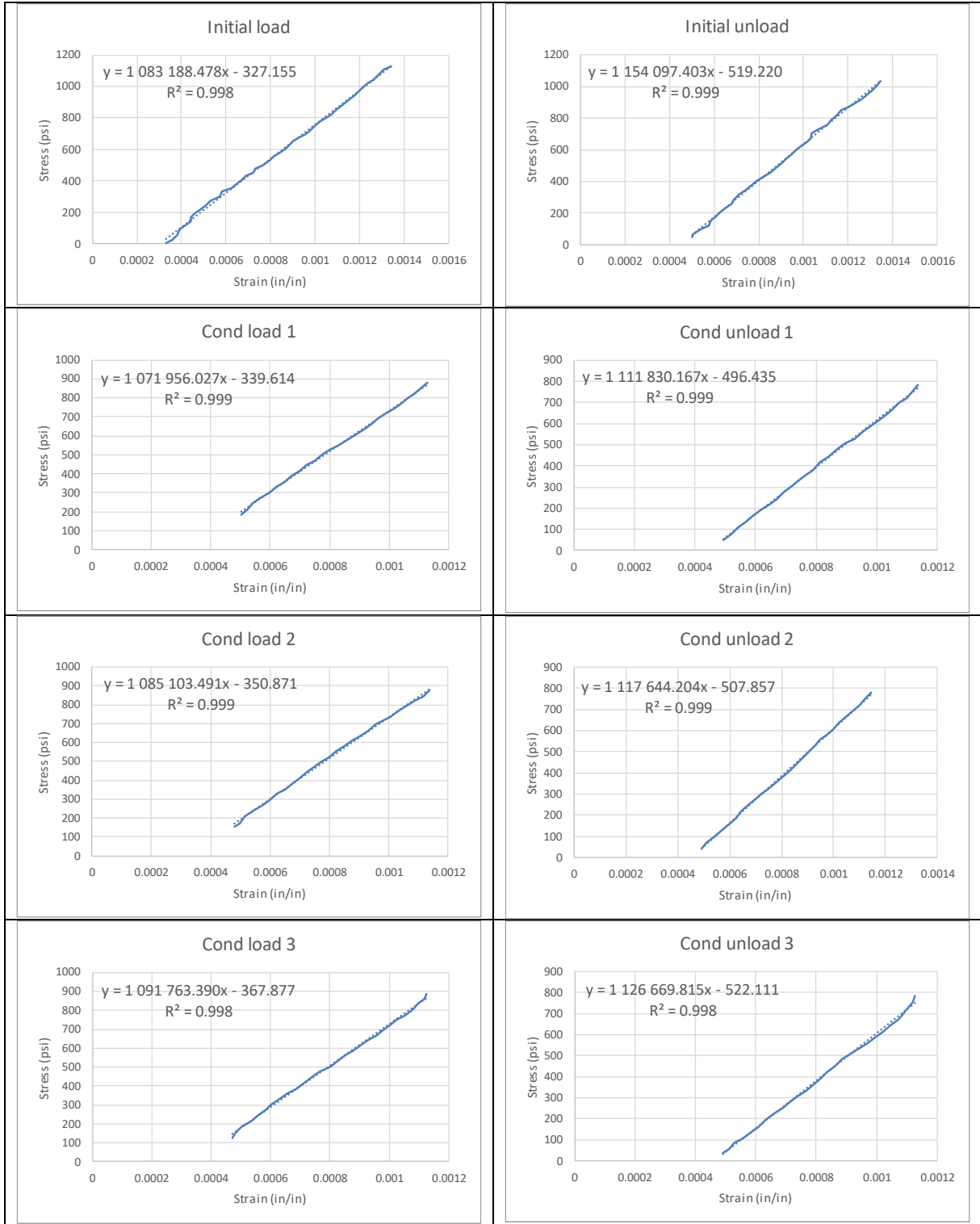


Figure 4.2-9. Individual load and unload paths in the tension cycle

The data shown in figure 4.2-9 is summarized in table 4.2-1.

Table 4.2-1. Summary of Tension Moduli

<b>Title</b>	<b>Measurement</b>	<b>Modulus (psi)</b>
1st load	1	1 083 188
1st unload	2	1 154 097
1st cond load	3	1 071 956
1st cond unload	4	1 111 830
2nd cond load	5	1 085 103
2nd cond unload	6	1 117 644
3rd cond load	7	1 091 763
3rd cond unload	8	1 126 669
Average loading		1 083 003
Average unloading		1 127 560
Average Total		1 105 281
SD loading		7 128
SD unloading		16 208
SD Total		25 556
CV loading		0.66%
CV unloading		1.44%
CV Total		2.31%

The average loading modulus is compared against the modulus from the undamaged cycle for a given specimen. This comparison is used to compute the damage parameter at the given total strain value where unloading was initiated in the damage inducing direction. The same process is used for all coupled damage tests as well as uncoupled tests unless otherwise noted. However, in uncoupled tests, the damage inducing direction and the interrogation directions are identical.

### 4.3 EXPERIMENTAL RESULTS

#### 4.3.1 Uncoupled 2-direction Tension

An uncoupled 2-direction tension load, tension reload test was performed to obtain an initial estimate of the plastic strains when the specimen is unloaded. The results of the experiment are shown in figure 4.3-1.

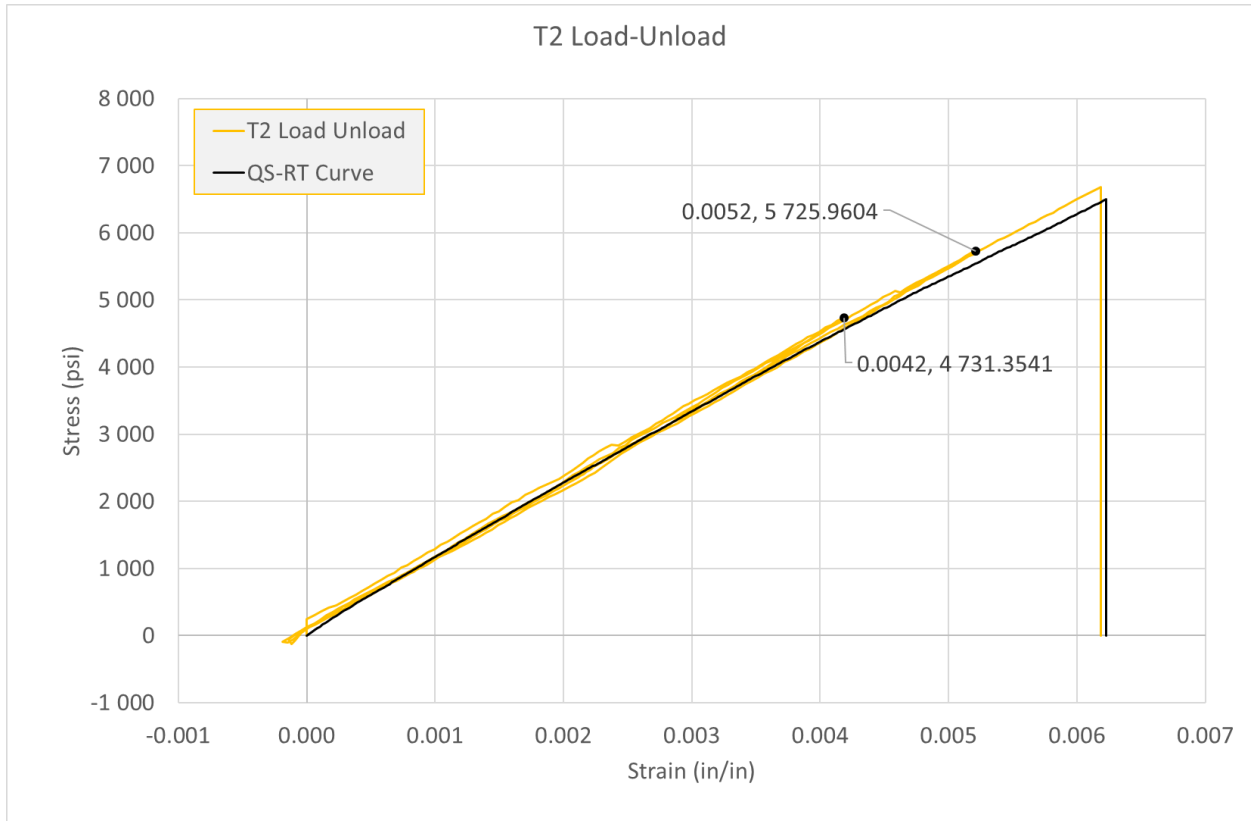
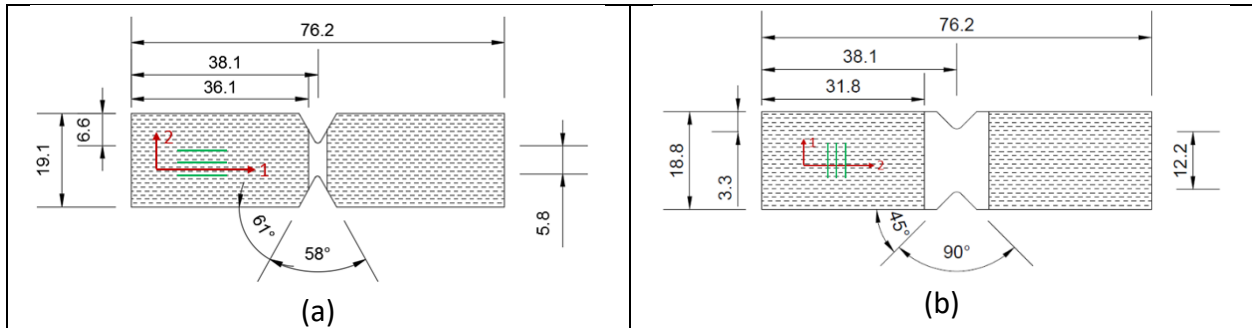


Figure 4.3-1. Uncoupled 2-direction tension test

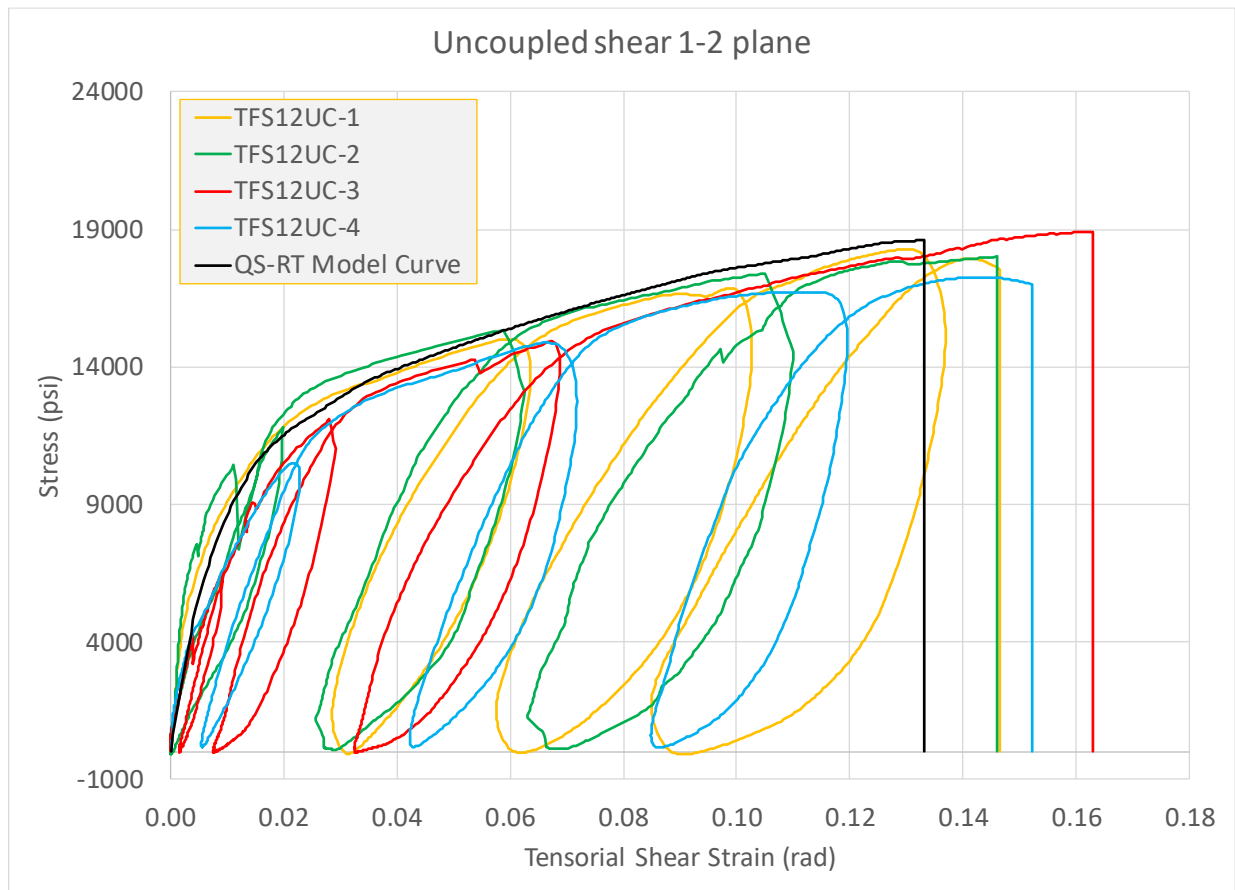
Figure 4.3-1 shows the points of unload used during the experiment as well as the average curve from the Quasi-Static Room Temperature (QS-RT) 2-direction tension experiments. After analysis of the data, the specimen showed no plasticity as it reloaded back to a state of both zero stress and zero strain. Consequently, no more experiments were performed because there is no data to obtain a damage parameter.

### 4.3.2 Uncoupled 1-2 Plane Shear

Uncoupled 1-2 plane shear tests were performed using the 1-2 shear specimen shown in figure 4.3-2(a) instead of the 2-1 shear specimen shown in figure 4.3-2(b). This was done because MAT 213 takes 1-2 shear data as input, and the damage being calculated must correspond to the input data.



Four replicates of this experiment were completed. The curves can be seen in figure 4.3-3.



All replicates showed displayed nonlinear unloading and reloading behavior. MAT 213 cannot replicate this hysteretic behavior. Instead, the code simplifies the unload and reload as a line with the slope of the damaged modulus corresponding to the total strain value where unloading was initiated. Therefore, the damaged modulus will not be a regression of any sort along either the load or unload path. Instead, the damaged modulus will be calculated as the slope between two points. The first point corresponds to where unloading was initiated, and the second point corresponds to the point where a state of zero stress is reached during the unload. The damaged moduli and corresponding total strain values are shown in table 4.3-1.

Table 4.3-1. Uncoupled 1-2 Plane Shear Summary of Results

<b>Replicate Name</b>	<b>Total Strain (in/in)</b>	<b>Modulus (psi)</b>
TFS12UC-1	0.0646050	225 167
	0.1025496	186 202
	0.1354536	190 529
TFS12UC-2	0.0603129	236 291
	0.1069462	219 007
	-	-
TFS12UC-3	0.009144	432 401
	0.028105	295 745
	0.06729	215 540
TFS12UC-4	0.022773	313 482
	0.070291	269 741
	0.118904	249 057

TFS12UC-2 only had two data points because there was an issue with the experimental procedure that governed the load and unload cycle. The damage parameter for a corresponding level of strain can be computed as the ratio of the damaged modulus to the initial elastic modulus of the given replicate. The results of this calculation are shown in figure 4.3-4.

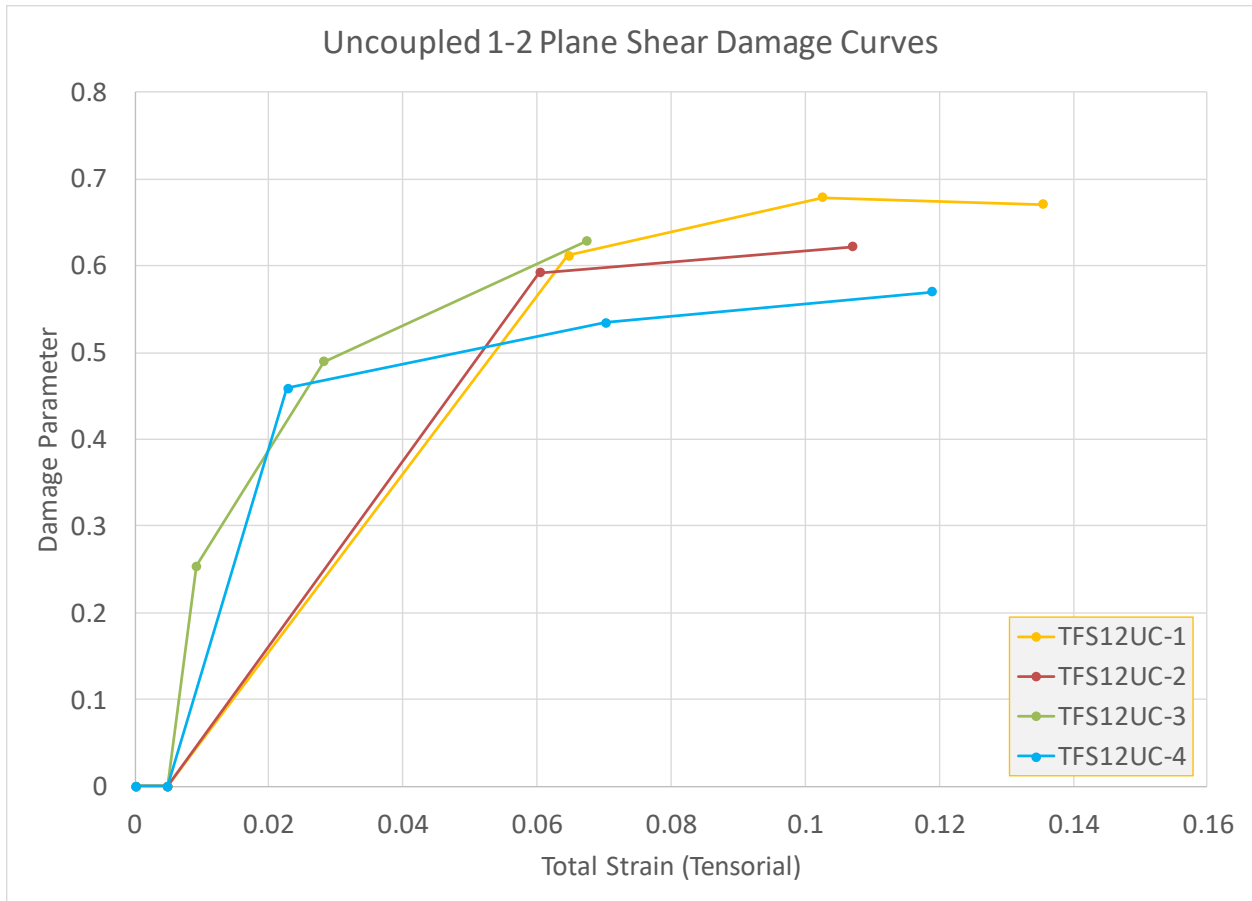


Figure 4.3-4. Uncoupled 1-2 plane shear damage curves

The trend in figure 4.3-4 leads to the conclusion that there is a large amount of initial damage and the damaged modulus asymptotically approaches some value at larger values of total strain. The damage-total strain curves must be converted into a form that MAT 213 can use as input. The damage parameters must be known for all given points of strain until failure for any given input stress-strain curve. This means the damage-total strain curves must be extrapolated to the final value of total strain of the corresponding input curve, i.e. QS-RT S12 curve. Additionally, a model damage-total strain curve must be generated because only one curve can be used to define the damage for any given material curve. The extrapolated replicate curves and the model curve are shown in figure 4.3-5.

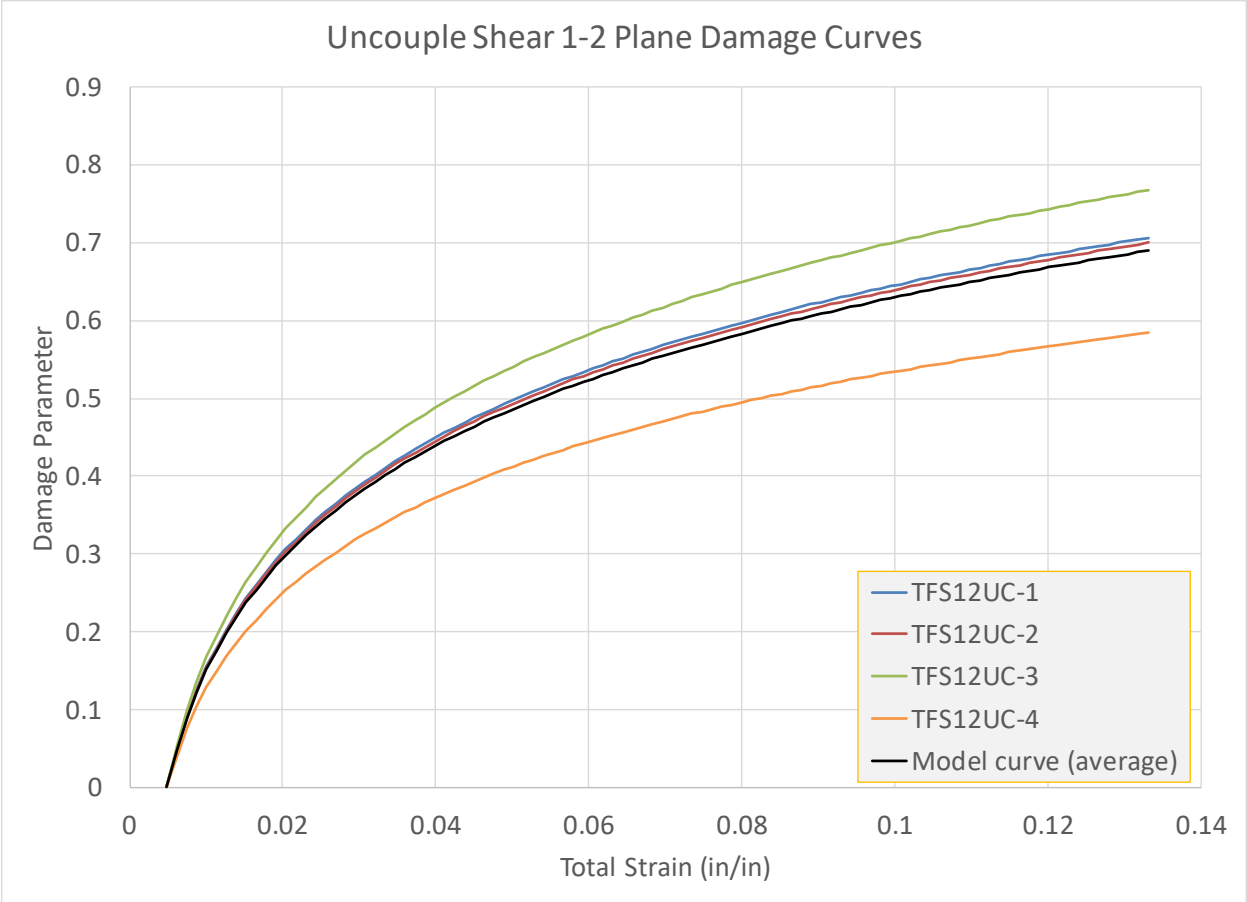


Figure 4.3-5. Damage vs. total strain: Extrapolated uncoupled 1-2 plane shear damage curves and final model curve

Figure 4.3-6 shows pictures of the tested specimens.

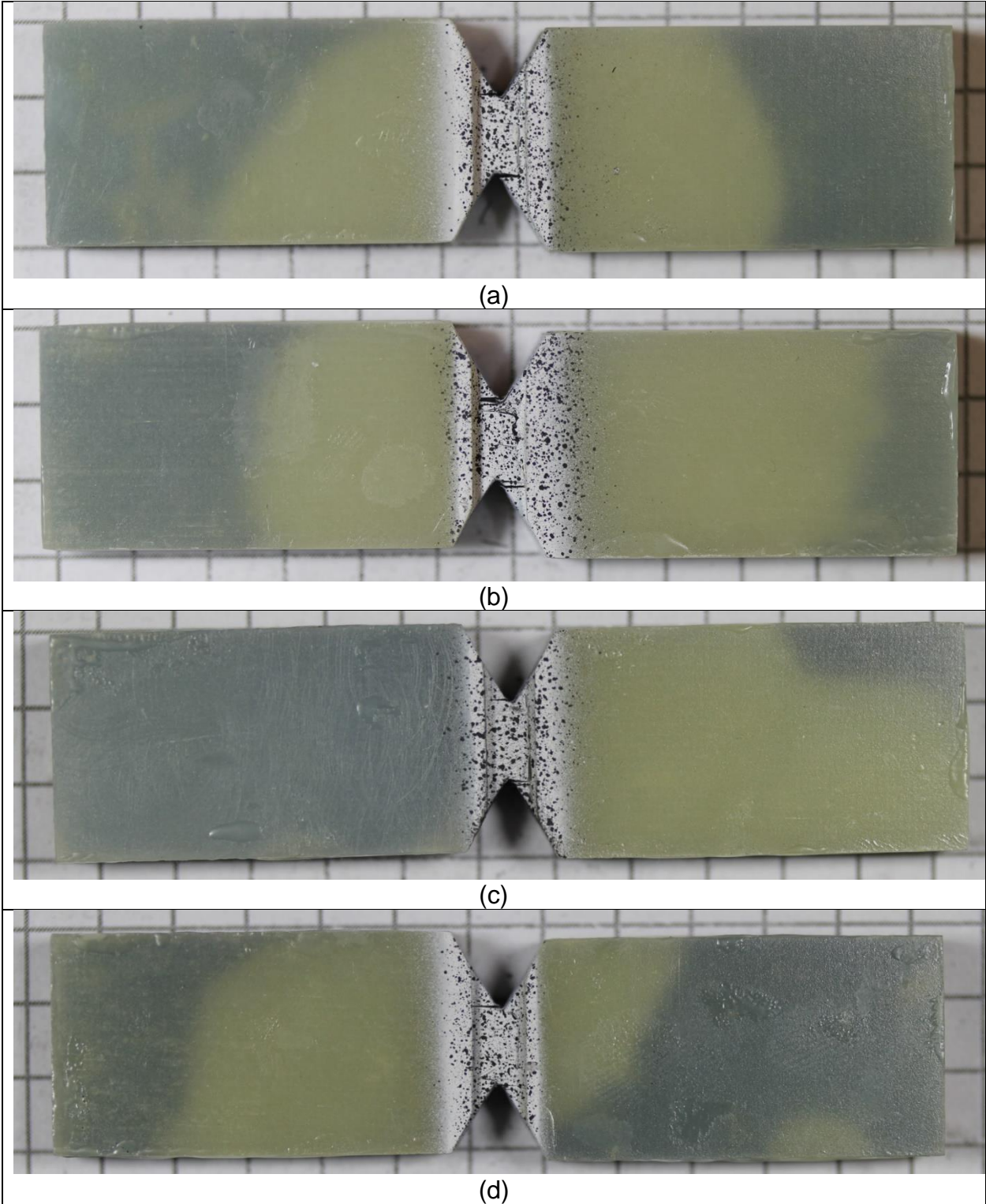


Figure 4.3-6. Uncoupled 1-2 plane shear specimens after failure (a) TFS12UC-1, (b) TFS12UC-2, (c) TFS12UC-3, and (d) TFS12UC-4

### 4.3.3 Uncoupled 2-direction Compression

Three replicates of the uncoupled 2-direction compression tests have been performed so far. The results of these tests can be seen in figure 4.3-7.

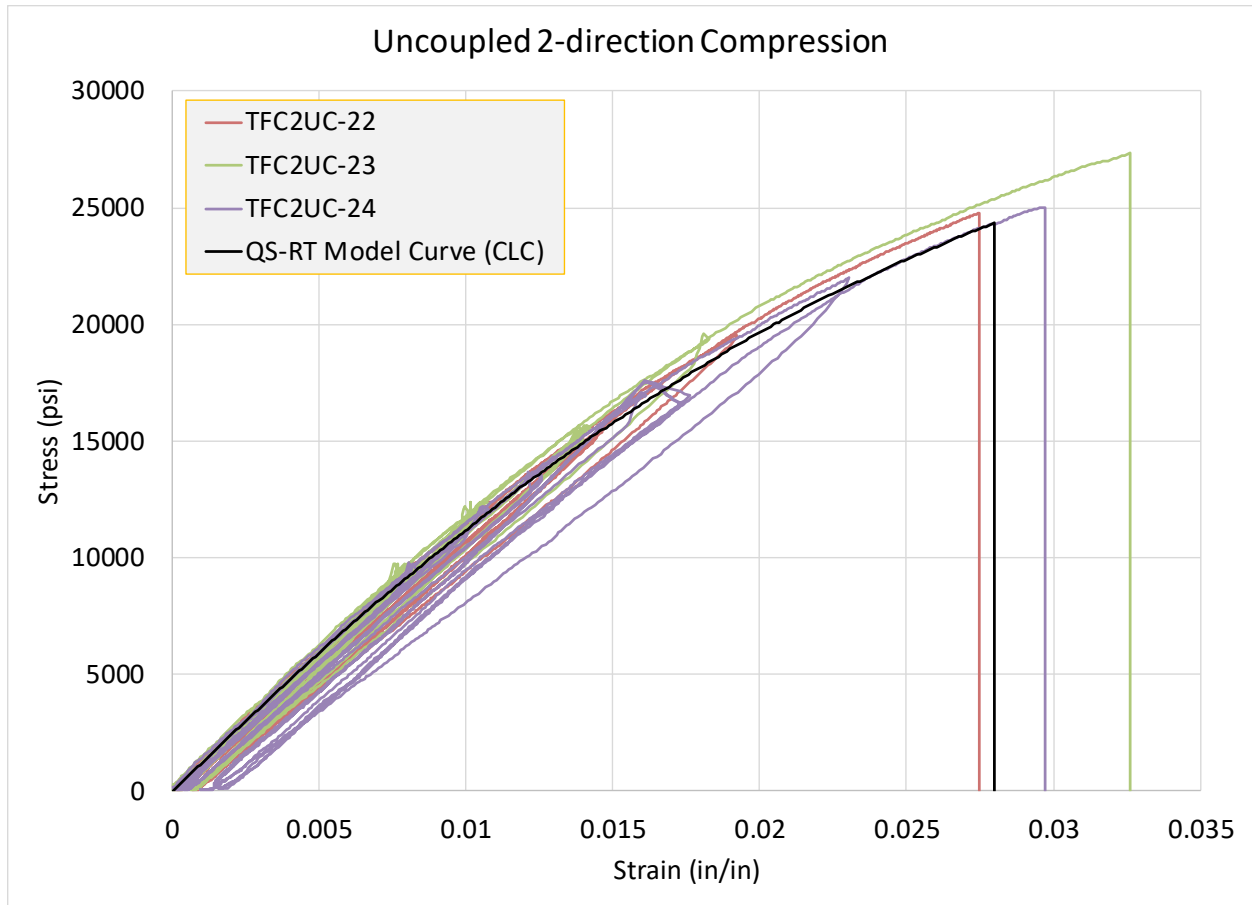


Figure 4.3-7. Uncoupled 2-direction compression experimental curves

Expectedly, the cyclic curves are, for the most part, enveloped by the QS-RT monotonic curve. Three damage points were obtained, and the damage-total strain curves are shown in figure 4.3-8.

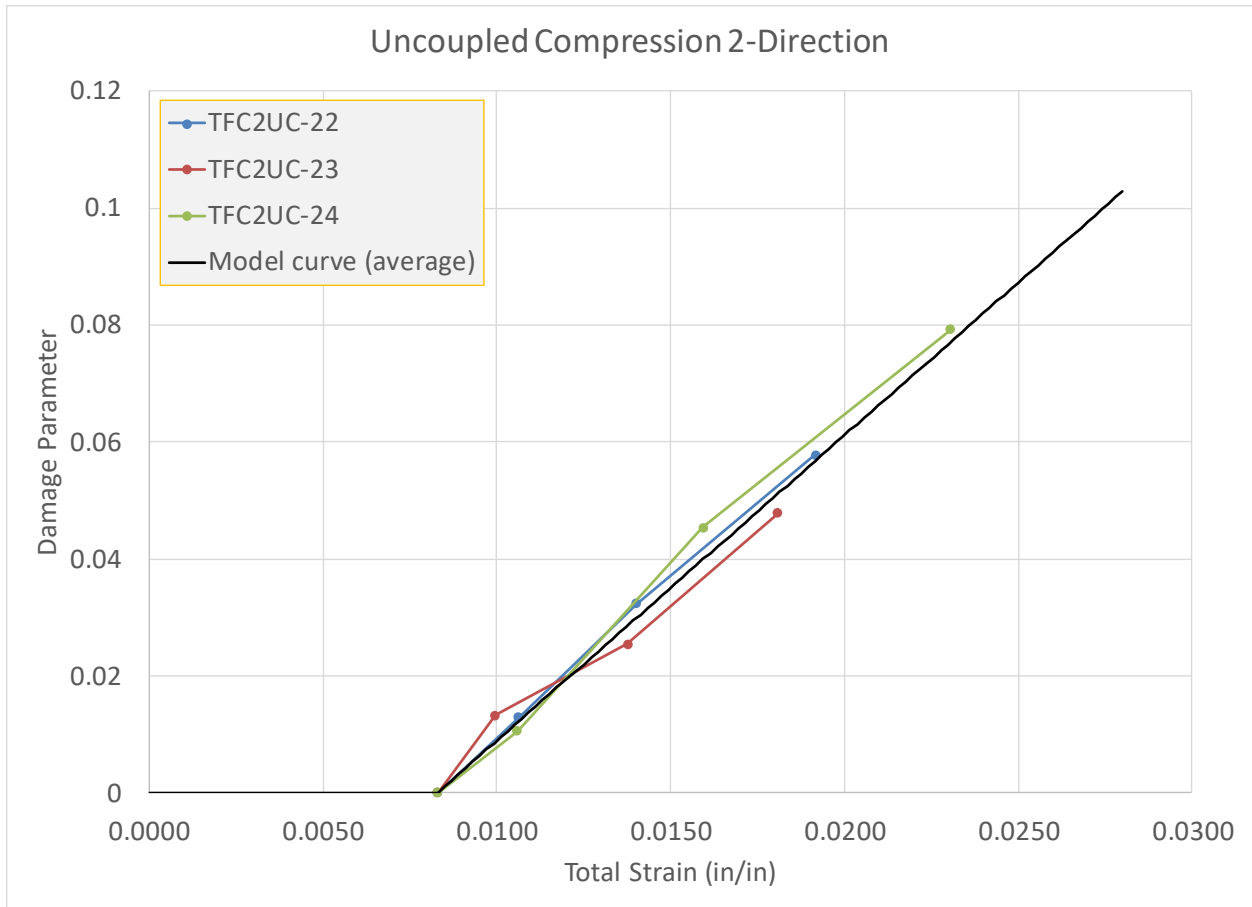


Figure 4.3-8. Uncoupled 2-direction compression damage curves

The regression equations are used to extrapolate the respective curves to the failure strain of the C2 model curve because data up to this point is needed to drive the finite element material model. The model curve is generated by performing a point by point average of the linear regression models from each of the respective replicates. A linear model was chosen over nonlinear models because the amount of available data points is too few to determine any sort of nonlinear pattern. A quadratic expression could have been used and would have yielded a better fit to the data, but there is not enough evidence to show that the damage behavior is nonlinear. Table 4.3-2 shows a summary of the experimental data.

Table 4.3-2. Uncoupled 2-direction Compression Damage Parameters

<b>Replicate Name</b>	<b>Total Strain (in/in)</b>	<b>Modulus (psi)</b>	<b>Damage Parameter</b>
TFC2UC-22	0	1 198 186	0
	0.0106	1 182 842	0.0128
	0.0140	1 159 427	0.0323
	0.0192	1 129 000	0.0577
TFC2UC-23	0	1 226 124	0
	0.0100	1 209 935	0.0132
	0.0138	1 194 917	0.0255
	0.0181	1 167 535	0.0478
TFC2UC-24	0	1 197 577	0
	0.0106	1 184 954	0.0105
	0.0159	1 143 262	0.0454
	0.0231	1 102 623	0.0793

Table 4.3-2 shows a reduction in modulus as the total strain increases during the experiment. The damage parameters continue to increase as the total strain increases and do not show the same asymptotic behavior as the uncoupled 1-2 shear damage curves. Figure 4.3-9 shows pictures of the tested specimens.

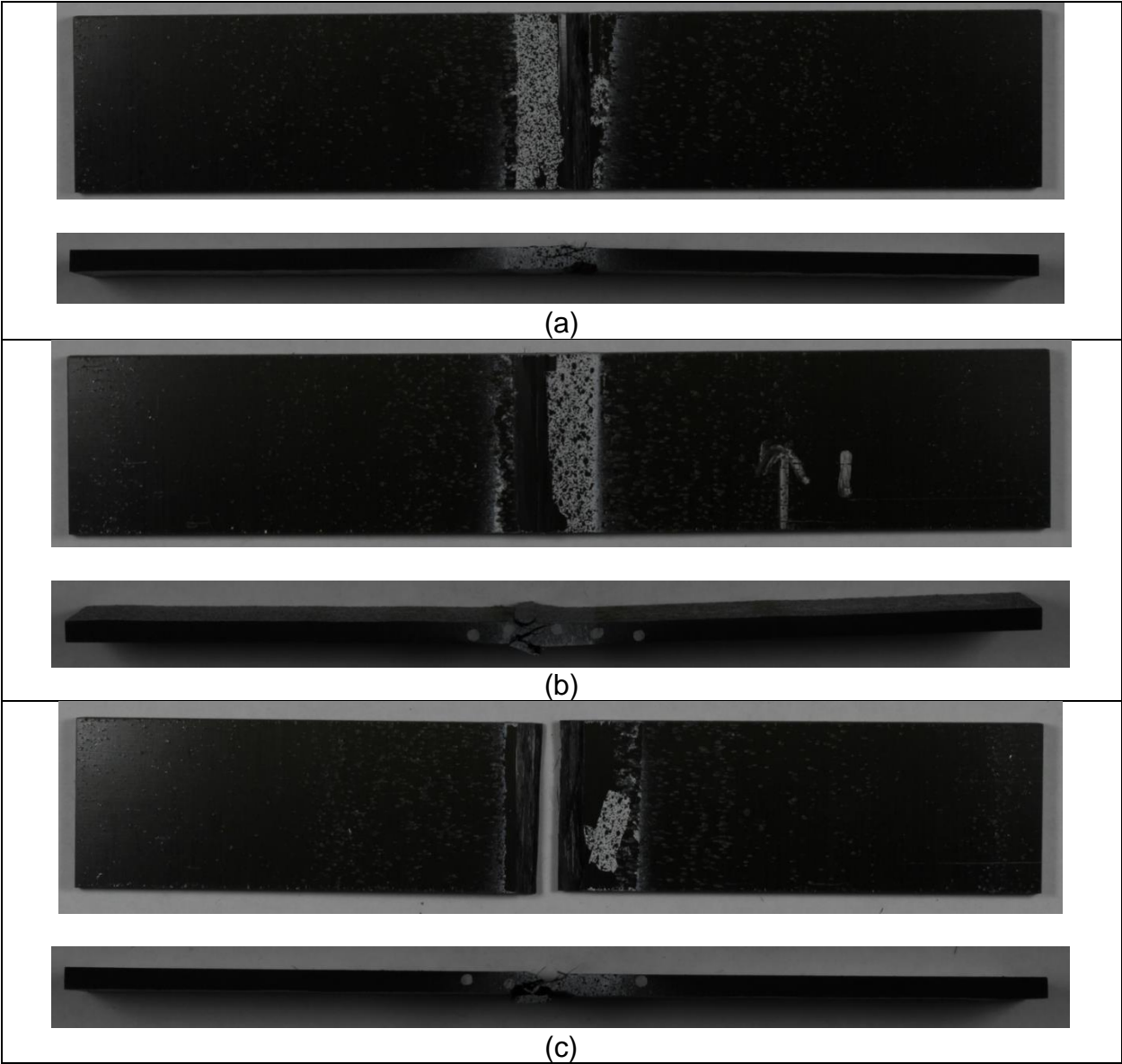
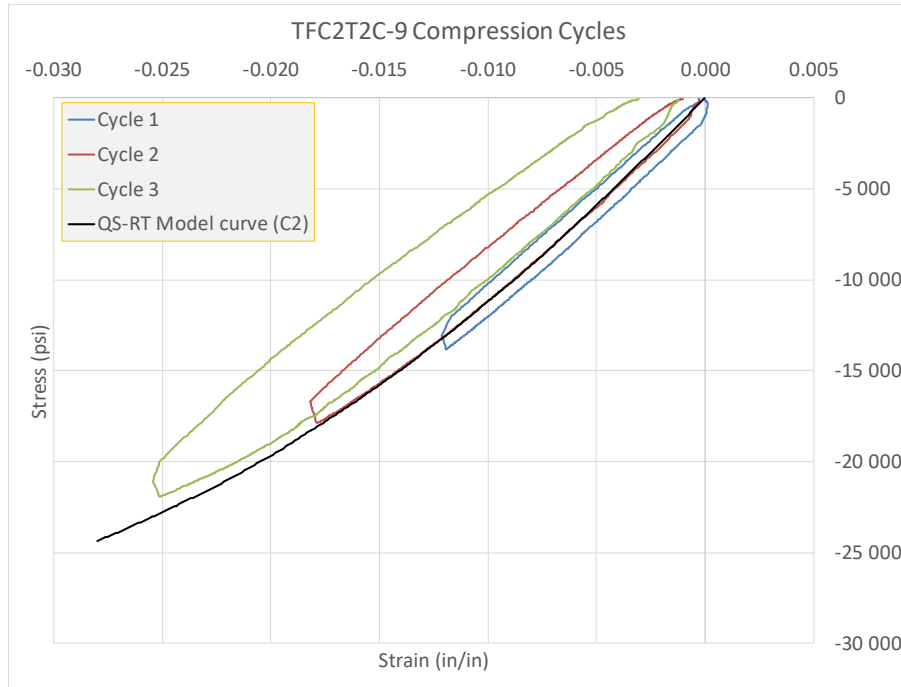


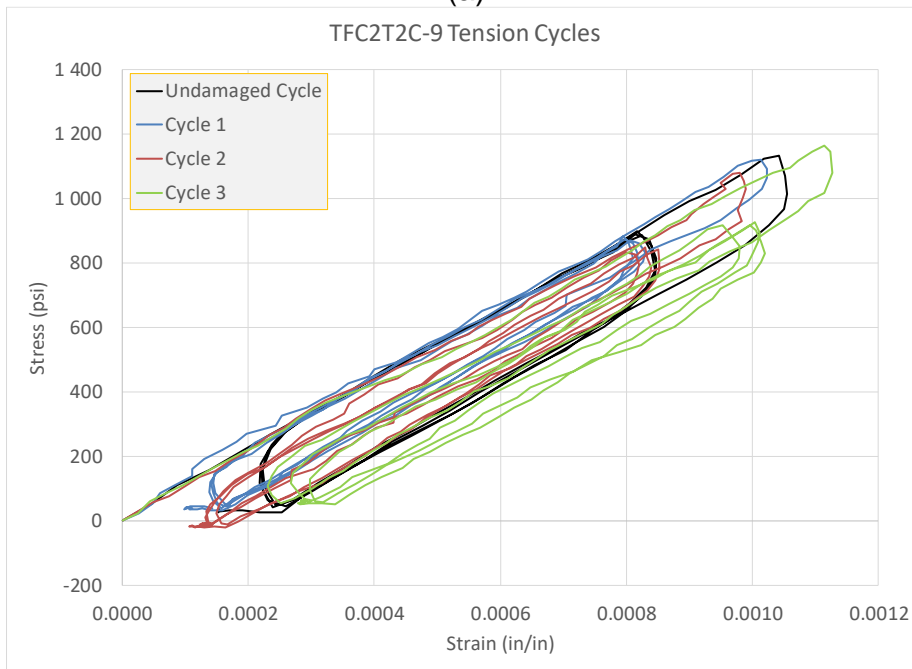
Figure 4.3-9. Uncoupled 2-direction compression specimens after failure (a) TFC2UC-22, (b) TFC2UC-23, and (c) TFC2UC-24

#### 4.3.4 Coupled 2-Direction Compression 2-Direction Tension

Three replicates of the experiment have been completed so far. The stress-strain curves for the compression and tension cycles from a single replicate are shown in figure 4.3.10.



(a)



(b)

Figure 4.3-10. Experimental stress-strain curves: Coupled 2-direction compression 2-direction tension (a) compression cycles and (b) tension cycles

The damage-total strain curves for three replicates are shown in figure 4.3.11.

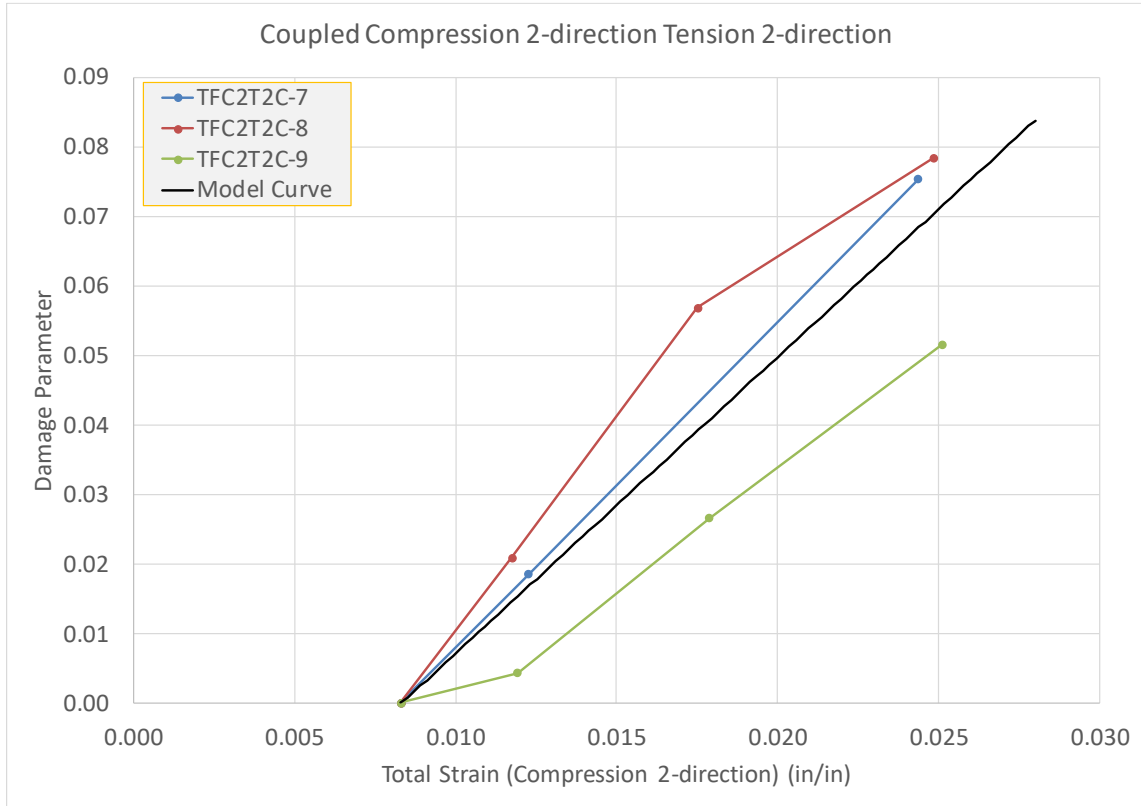


Figure 4.3-11. Coupled 2-direction compression 2-direction tension damage curves

The linear regression was performed as described in section 4.3-3. The damage parameter shows similar behavior to that of the uncoupled 2-direction compression tests in that the values do not plateau. Instead, they seem to continue increasing until failure. Table 4.3-3 shows a summary of the experimental data.

Table 4.3-3. Coupled 2-direction Compression 2-direction Tension Damage Parameters

<b>Replicate Name</b>	<b>Total Strain (in/in)</b>	<b>Modulus (psi)</b>	<b>Damage Parameter</b>
TFC2T2C-7	0	1 124 067	0.0000
	0.0123	1 103 262	0.0185
	0.0244	1 039 364	0.0754
TFC2T2C-8	0	1 156 429	0.0000
	0.0117	1 132 286	0.0209
	0.0175	1 090 646	0.0569
	0.0249	1 065 743	0.0784
TFC2T2C-9	0	1 087 851	0.0000
	0.0119	1 083 188	0.0043
	0.0179	1 058 875	0.0266
	0.0251	1 031 783	0.0515

Figure 4.3-12 shows pictures of the tested specimens and that failure was purposely not induced in the specimen.

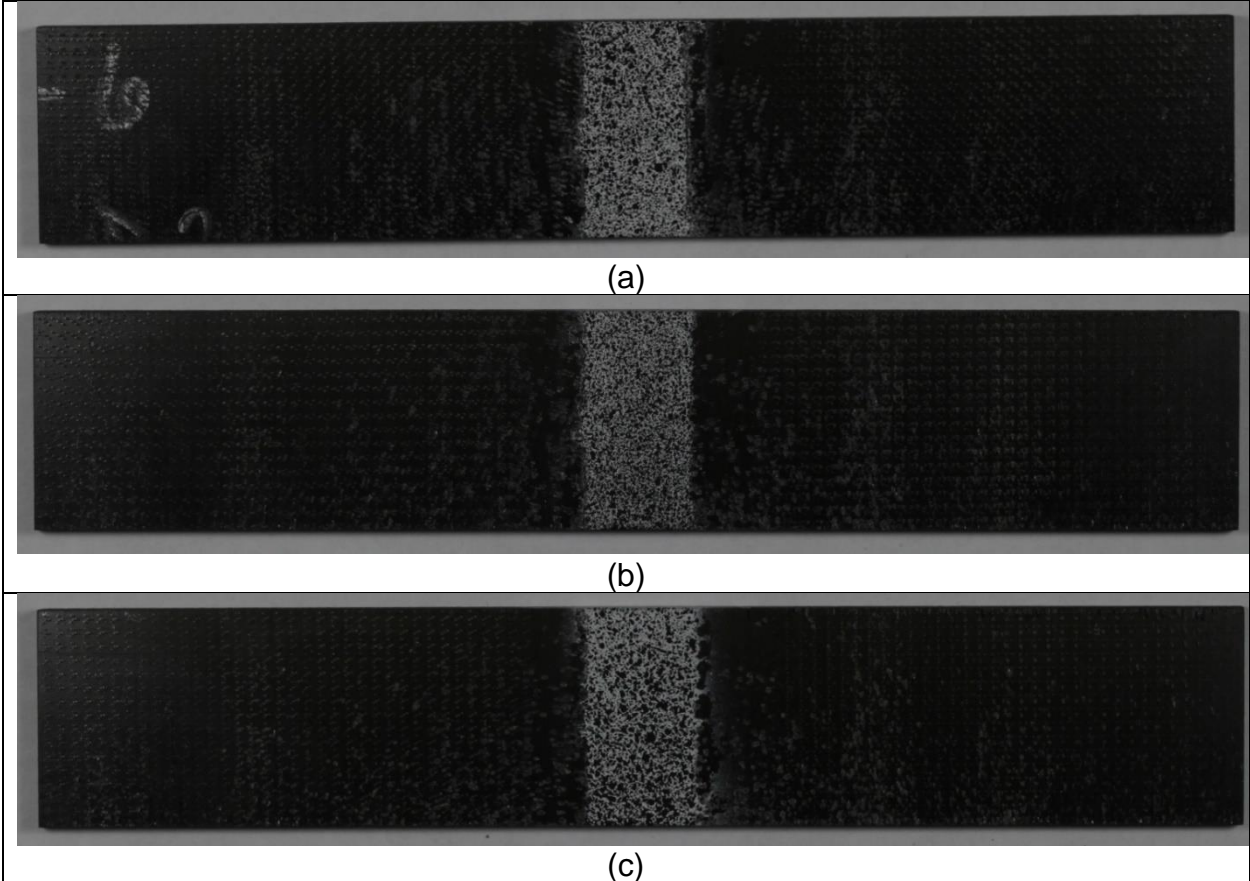


Figure 4.3-12. Coupled 2-direction compression 2-direction tension specimens after testing (a) TFC2T2C-7, (b) TFC2T2C-8, and (c) TFC2T2C-9

#### 4.3.5 Coupled 2-Direction Compression 2-1 Plane Shear

The coupled 2-direction compression 2-1 plane shear experiment involves loading the specimen in compression along the 2-direction and then unloading it to a state of zero stress. The specimen is then loaded in shear enough to obtain an estimate of the modulus. Figure 4.3.13 shows the specimen geometry that is used for the experiment.

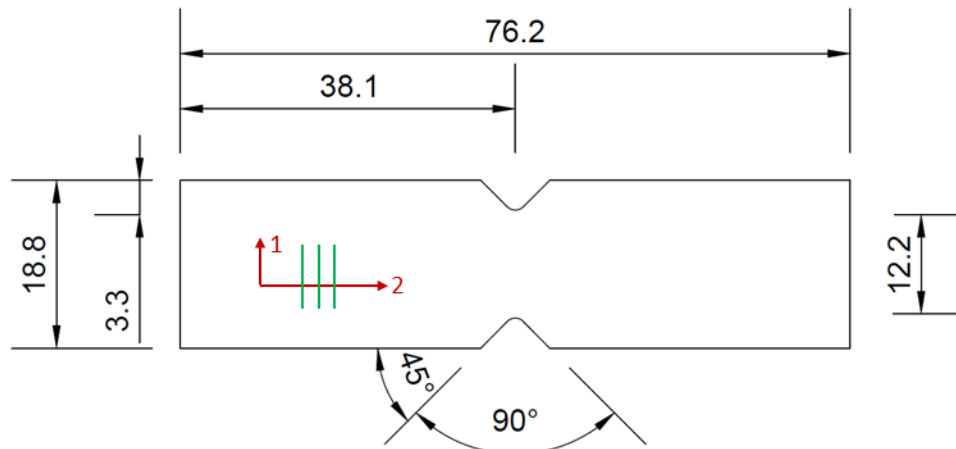


Figure 4.3-13. Specimen dimensions for coupled 2-direction 2-1 plane shear tests (dimensions in mm)

Before starting the cyclic loading experiments, an investigative experiment was performed to ensure the response of this specimen geometry in compression. This is consistent with the results of the QS-RT 2-direction compression experiments. The compression test was performed with a modified version of the CLC test fixture shown in figure 2.2-1. Consequently, all compression cycles for this test were performed with the same modified CLC fixture. The result of the investigative test is shown in figure 4.3.14.

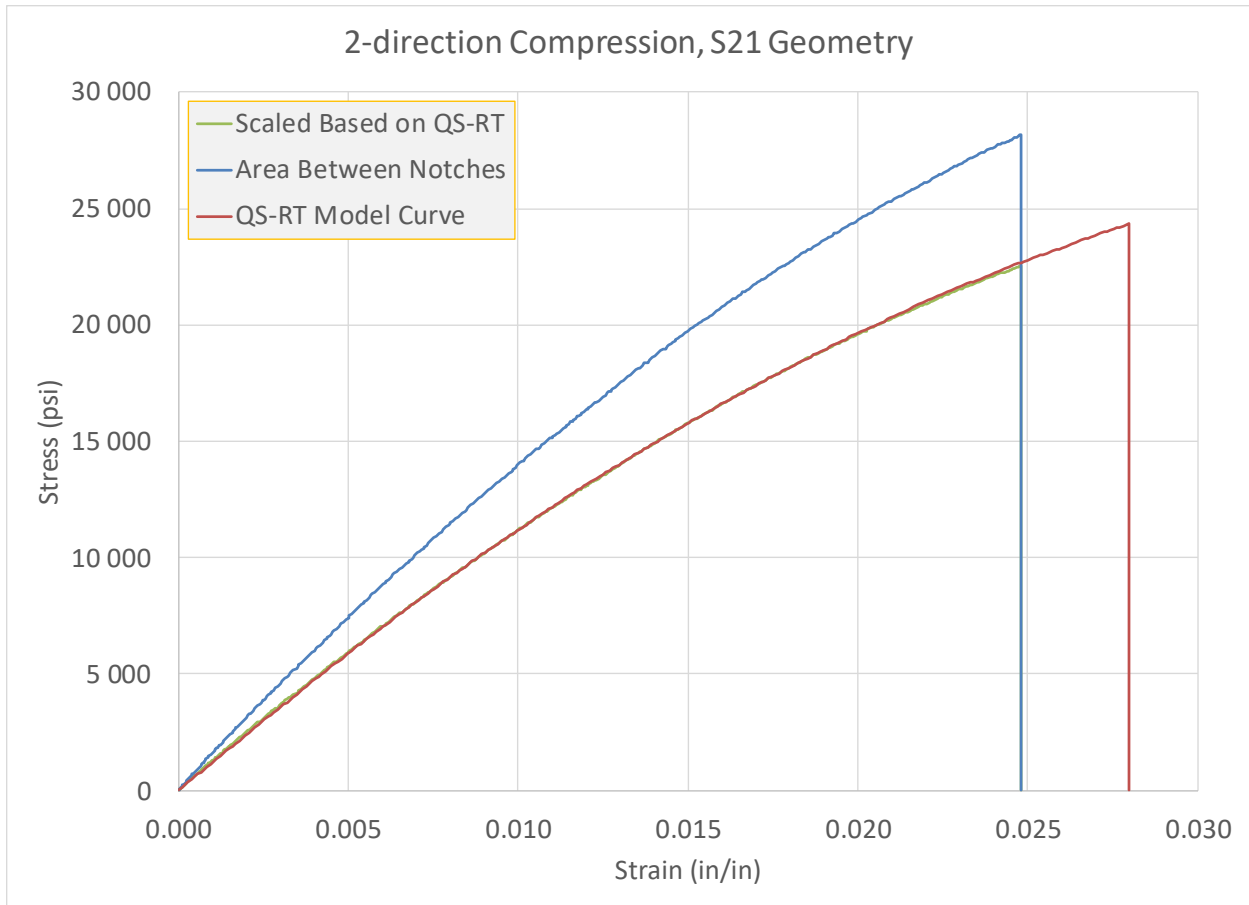


Figure 4.3-14. Investigative 2-direction compression test using 2-1 plane shear specimen geometry

The three curves in figure 4.3.14 represent the following:

- QS-RT Model Curve: The average curve computed using the replicate data obtained from QS-RT 2-direction compression tests.
- Area between notches: Using the force data obtained from the investigative test, the stress was calculated using the cross-sectional area between the notches of the specimen. This area seemed to overestimate the stress induced in the specimen.
- Scaled based on QS-RT: The curve denoted “Area between notches” was scaled down using a single factor. The factor was obtained by computing the ratio of stress at a single strain value of the “Area between notches” curve and the “QS-RT model curve”. This factor was then applied to the entirety of the “Area between notches” curve. The resulting data is the “Scaled based on QS-RT” curve. The equation below shows the process stated mathematically.

$$\frac{\sigma_{QSRT}(\varepsilon = \varepsilon_{\alpha})}{\sigma_{ABN}(\varepsilon = \varepsilon_{\alpha})} = \beta$$

$$\sigma_{SCALED}(\varepsilon) = \beta \sigma_{ABN}(\varepsilon)$$

Scaling of the experimental data was performed because the specimen is not prismatic. This means the cross-sectional area is not constant throughout the gage section. Therefore, the stress calculation is not straightforward. The specimen after testing is shown in figure 4.3.15.

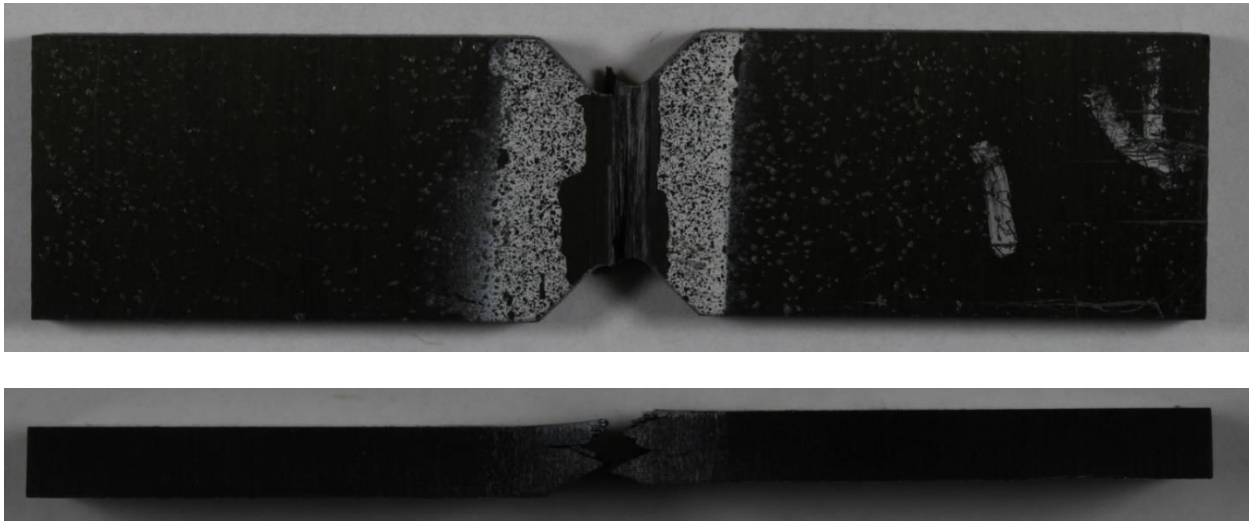


Figure 4.3-15. Coupled 2-direction compression 2-1 plane shear investigative specimen after testing.

Additionally, the specimen exhibited premature failure when compared to the QS-RT 2-direction compression curve. The failure is due to the presence of strain concentrations at the notch tips of the specimen. The strain field is shown in figure 4.3.16.

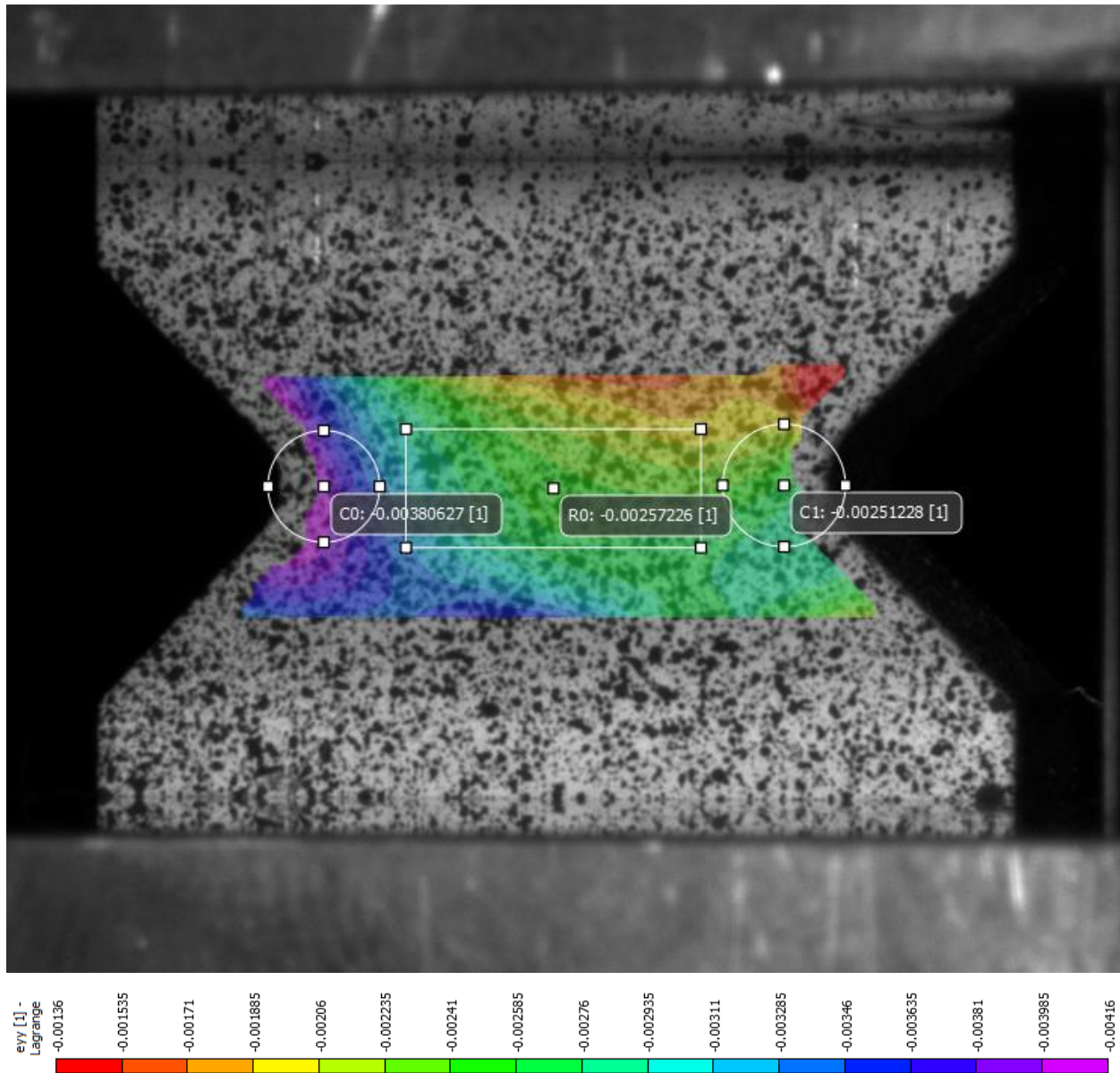


Figure 4.3-16. Strain field of C2-S21 coupled

The center rectangular region was used to generate the stress-strain curve because the compressive longitudinal strains were uniform in that section throughout the experiment. Figure 4.3.17 shows that at the instance of failure—the notch tips—the strain reaches a value approximately equal to the failure strain from the QS-RT 2-direction compression tests.

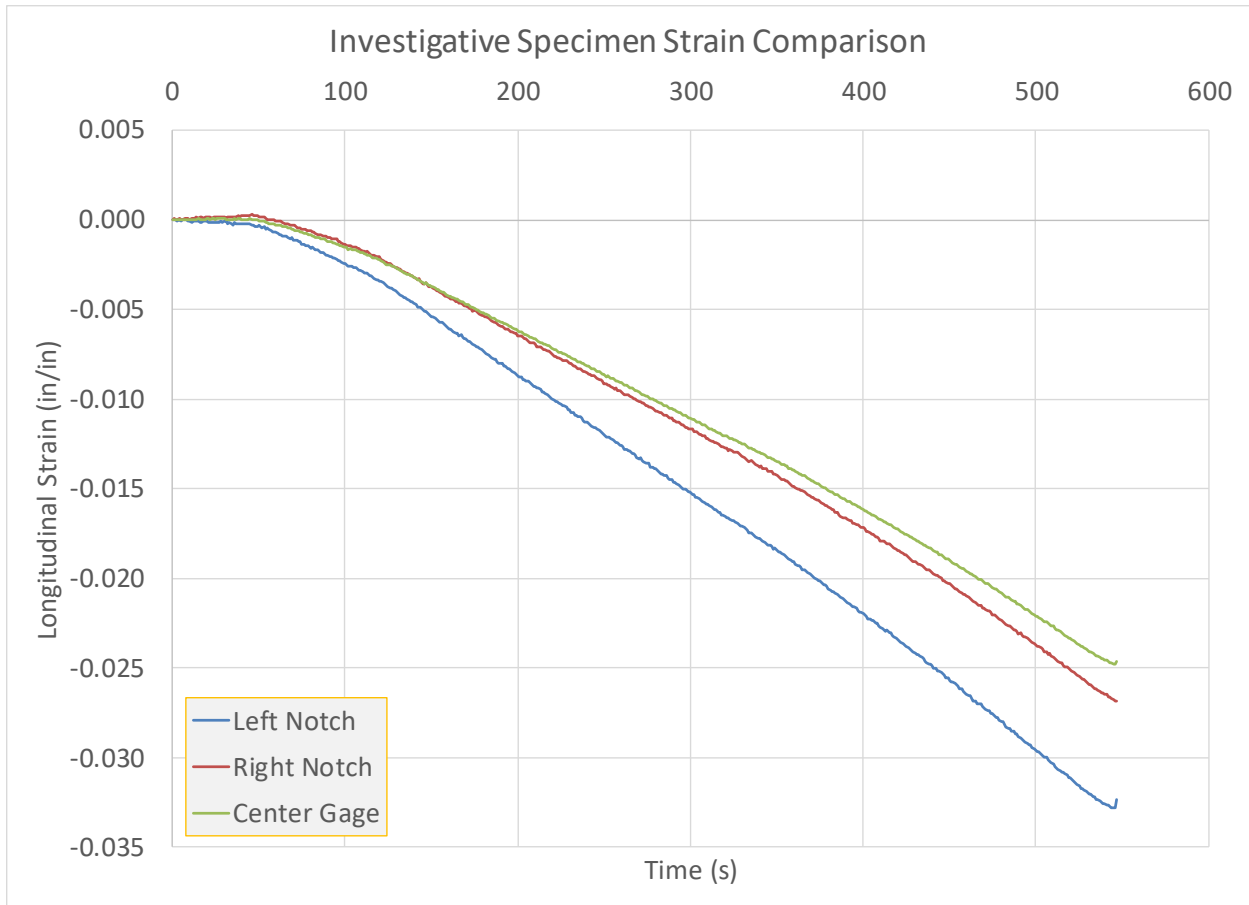


Figure 4.3-17. Strain comparison of the C2-S21 investigative compression test

The overall trend observed from the investigative curve is consistent with the QS-RT 2-direction compression curve. This leads to the conclusion that this specimen geometry suits this experiment.

The measurement of the damaged modulus comes from the 2-1 shear test instead of the 1-2 shear test. The results of the QS-RT experiments show that the initial elastic modulus values are essentially the same, although the entire stress strain curves are different. The specimen geometries are shown in figure 4.3-18 for comparison.

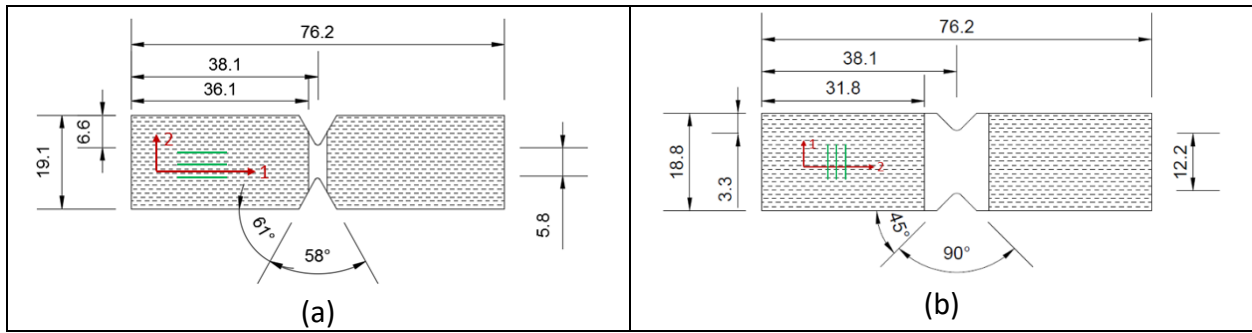


Figure 4.3-18. 1-2 shear specimen and 2-1 shear specimen: (a) 1-2 shear specimen, (b) 2-1 shear specimen

A comparison of 1-2 and 2-1 plane shear stress-strain curves are shown in figure 4.3-19.

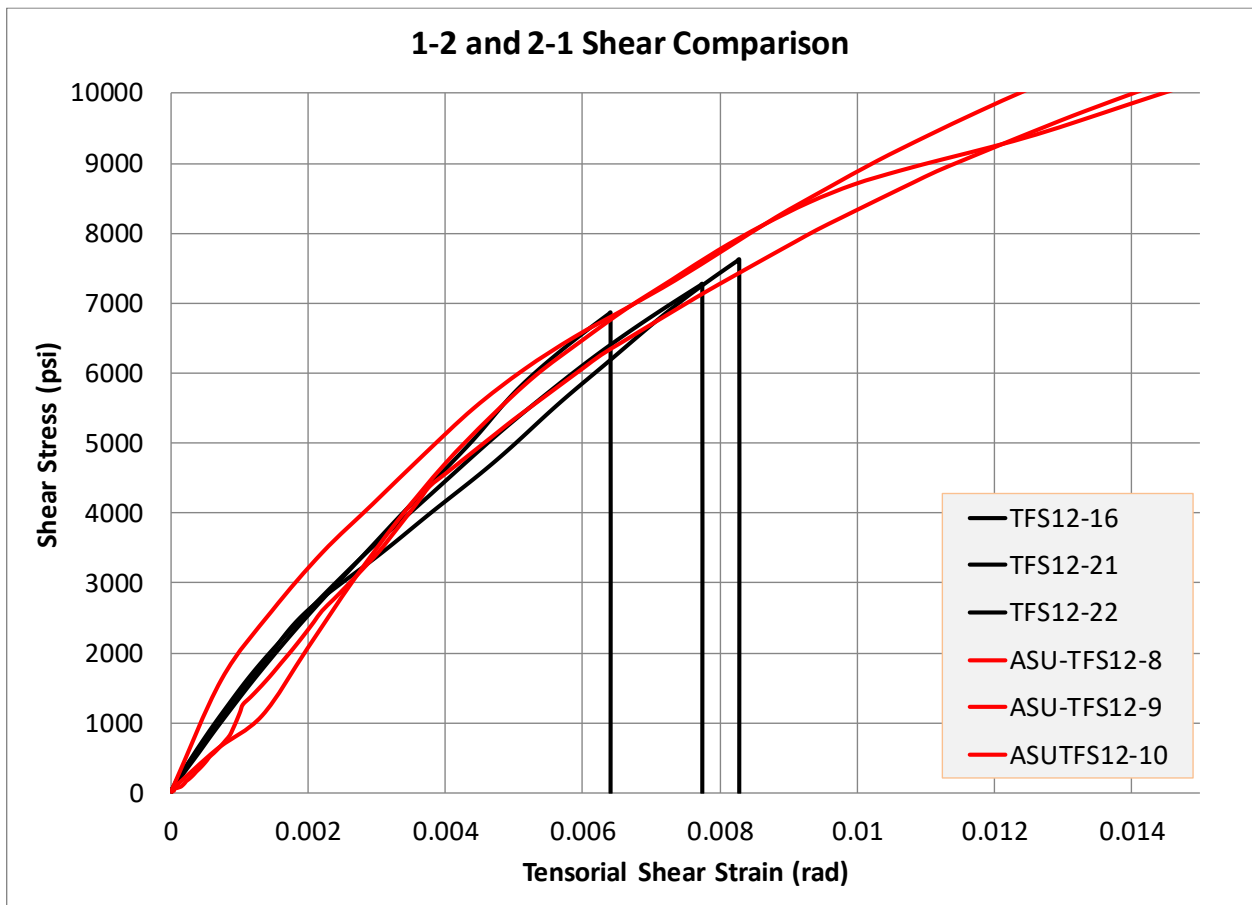
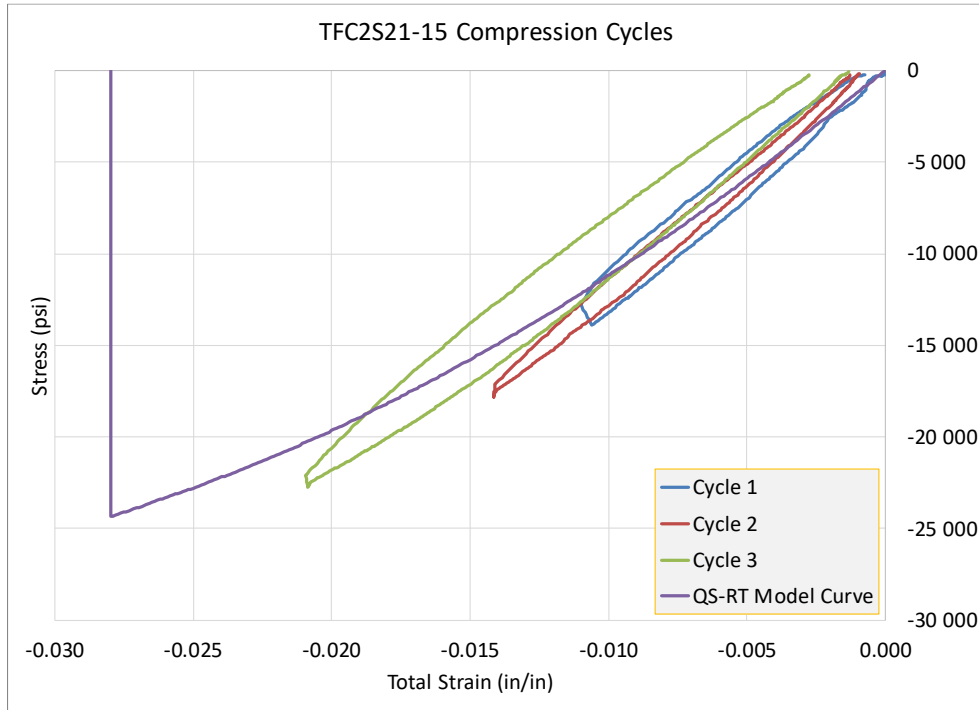


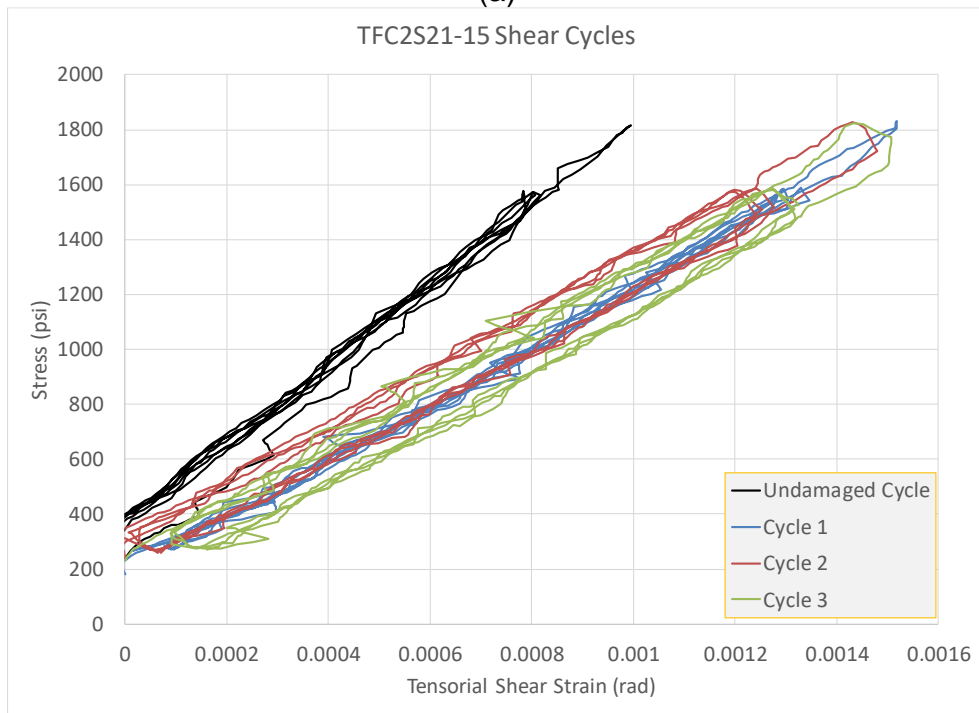
Figure 4.3-19. 1-2 and 2-1 plane shear stress-strain: comparison of initial portion of 1-2 plane shear stress-strain curves (red) with full 2-1 plane shear stress-strain curves (black)

The assumption is that the damage induced in the S21 specimen is the same that would be induced in the S12 specimen. The full coupled experiments use the 2-1 shear

specimen geometry and strategy outlined in the previous sections for coupled damage experiments. Three replicates of this experiment have been completed so far. The stress-strain curves for both the compression and shear cycles from a single replicate are shown in figure 4.3-20.



(a)



(b)

Figure 4.3-20. Coupled 2-direction compression 1-2 plane shear experimental stress-strain curves (a) compression cycles (unscaled) and (b) shear cycles

The damage-total strain curves for three replicates are shown in figure 4.3-21.

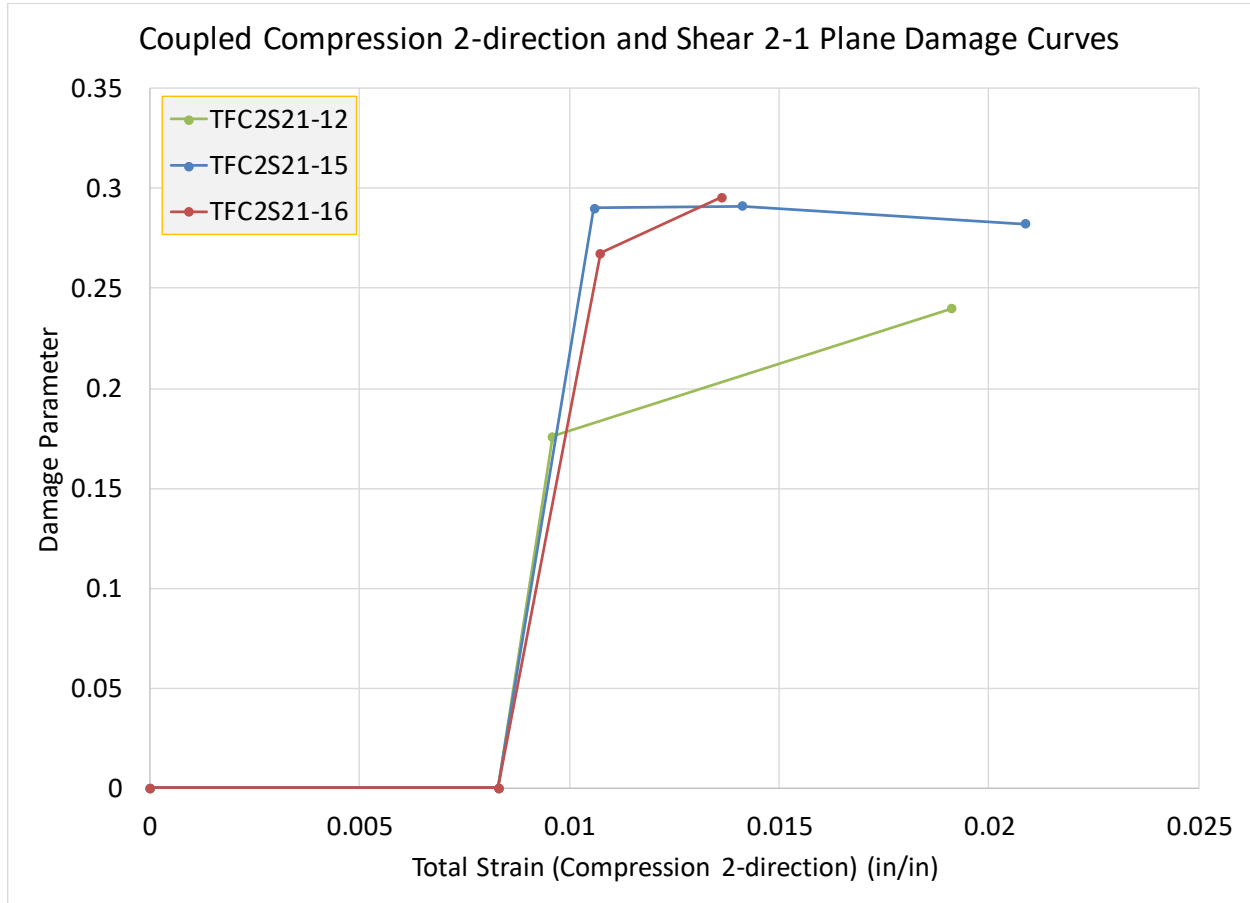


Figure 4.3-21. Coupled 2-direction compression 1-2 plane shear damage curves

The damage curves show a similar trend to the uncoupled shear 1-2 plane tests in that the damage parameter plateaus after a certain strain value. This indicates that no further effects of the damage induced in the 2-direction materializes in the 1-2 shear test. Figure 4.3-22 shows pictures of the tested specimens and that failure was purposely not induced in the specimen.

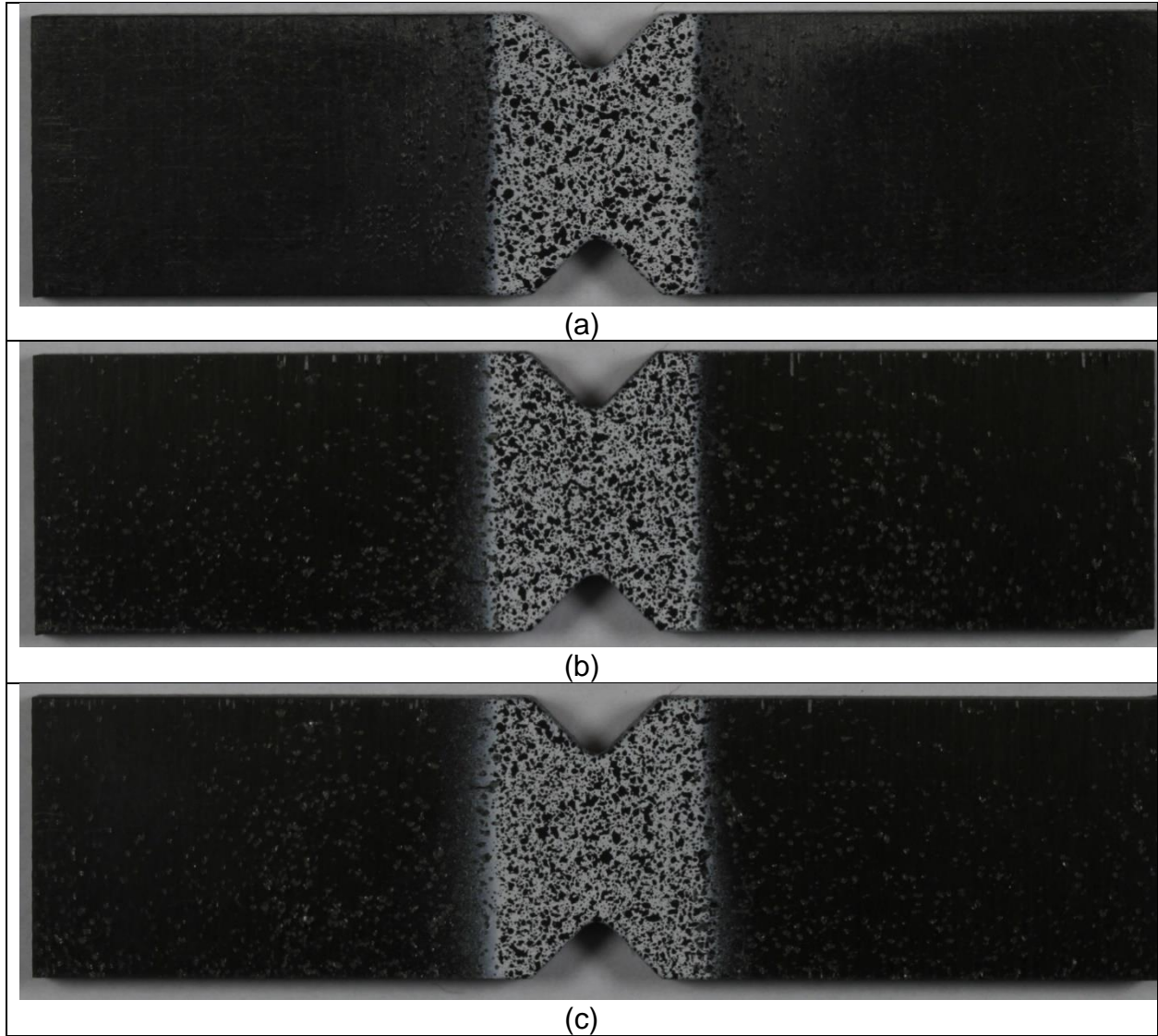


Figure 4.3-22. Coupled 2-direction compression 2-direction tension specimens after testing (a) TFC2S21-12, (b) TFC2S21-15, and (c) TFC2S21-16

#### 4.3.6 Remaining Damage Characterization Experiments

Table 4.3-4 shows a list of the experiments that have not yet been performed.

Table 4.3-4. Remaining Damage Characterization Experiments

Parameter	Description
$d_{12}^{22r}(\epsilon_{22r}^p)$	S12 unload/reload: damage 2-direction tension
$d_{12}^{22c}(\epsilon_{22c}^p)$	S12 unload/reload: damage 2-direction compression

Both of the experiments shown in table 10 correspond to experiments that require loading an S12 specimen into plasticity and then determining the damaged modulus in the normal directions. An S12 specimen must be used to conduct this experiment because it is used as input to MAT 213, and the damage terms must correspond to the strain values from the input curve. Currently, the difficulties in conducting the coupled experiments are due to the specimen geometry shown in figure 4.3-23.

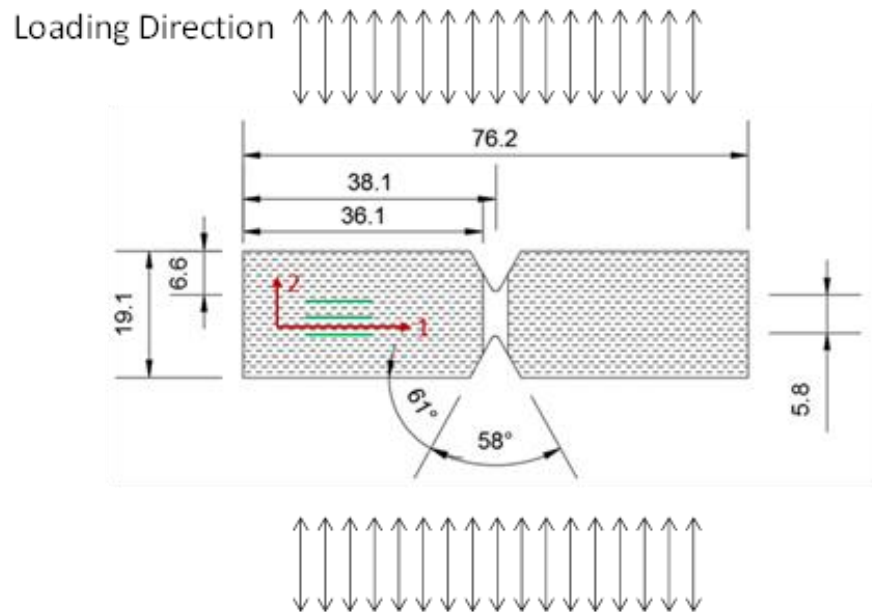


Figure 4.3-23. Specimen geometry: coupled 1-2 plane shear 2-direction compression/tension specimen geometry

The loading direction corresponds to the requirement of 2-direction compression/tension loading. This geometry does not lend itself to performing these experiments because there is not enough material to adequately grip the specimen.

## 5 CONCLUDING REMARKS

This report describes laboratory tests conducted at room temperature and at quasi-static loading conditions. The report includes:

- Data from the analysis of the laboratory tests for Toray's T800-F3900 unidirectional composite.
- The stress-strain curves from 12 different tests.
- Mass density and volume fraction of the composite.
- Curve data and mass density used as input in the MAT213 model for the composite.

## 6 REFERENCES

- Allen, D., Harris, C., & Groves, S. (1987). A thermomechanical constitutive theory for elastic composites with distributed damage-I. Theoretical development. *International Journal of Solids and Structures*, 23, 1301-1318.
- Allix, O. (2001). A composite damage meso-model for impact problems. *J. Composites Science and Technology*, 61, 2193-2205.
- America, T. C. (2018). <https://www.toraycma.com>. Retrieved March 2, 2018
- ASTM International. (2017). *ASTM D8101/D8101M-17 Standard test method for measuring the penetration resistance of composite materials to impact by a blunt projectile*. West Conshohocken, PA: ASTM International. doi:10.1520/D8101\_D8101M-17
- Barbero, E. J. (2013). *Finite element analysis of composite materials using Abaqus*. Boca Raton, FL: CRC Press.
- Bednarczyk, B. A., & Arnold, S. M. (2002). *MAC/GMC 4.0 User's Manual - Keywords Manual*. Washington, D.C.: National Aeronautics and Space Administration.
- Bergstrom, J. S. (2005). *Constitutive Modeling of Elastomers - Accuracy of Predictions and Numerical Efficiency*. Retrieved from PolymerFEM. com
- Berthelot, J. (1999). *Composite materials: mechanical behavior and structural analysis*. New York, U.S.A.: Springer.
- Bogert, P. B., Satyanarayana, A., & Chunchu, P. (2006). Comparison of Damage Path Predictions for Composite Laminates by Explicit and Standard Finite Element Analysis Tools. *47th AIAA/ASME/ASCE/AHS/ASC Structures, Structural Dynamics, and Materials Conference*. Washington D.C.: American Institute for Aeronautics and Astronautics.
- Bogetti, T. A., Staniszewski, J., Burns, B. P., Hoppel, C. P., Gillespie Jr, J. W., & Tierney, J. (2012). Prediction of the nonlinear response and progressive failure of composite laminates under triaxial loading: Correlation with experimental results. *Journal of Composite Materials*, 47(6-7), 793-804.
- Boutaous, A., Peseux, B., Gornet, L., & Belaidi, A. (2006). A new modeling of plasticity coupled with damage and identification for carbon fibre composite laminates. *Composite Structures*, 74, 1-9.
- Brent's Method*. (2018, August 10). Retrieved from Wikipedia: [https://en.wikipedia.org/wiki/Brent%27s\\_method](https://en.wikipedia.org/wiki/Brent%27s_method)
- Buyuk, M. (2014). *Development of a New Metal Material Model in LS-DYNA, Part 2: Development of a Tabulated Thermo-Viscoplastic Material Model with Regularized Failure for Dynamic Ductile Failure Prediction of Structures Under Impact Loading*. Atlantic City: Federal Aviation Administration.
- Chang, F. K., & Chang, K. Y. (1987a). Post-failure Analysis of Bolted Composite Joints in Tension and Shear-Out Mode Failure. *J of Composite Materials*(21), 834-855.
- Chang, F. -K., & Chang, K. -Y. (1987b). A Progressive Damage Model for Laminated Composites Containing Stress Concentrations. *Journal of Composite Materials*, 21, 834-855.
- Chen, H.-S., & Hwang, S.-F. (2009). A Fatigue Damage Model for Composite Materials. *Polymer Composites*, 301-308.

- Cheng, J. (2006). *Material Modeling of Strain Rate Dependent Polymer and 2D Triaxially Braided*. Akron, OH: University of Akron.
- Cho, J., Fenner, J., Werner, B., & Daniel, I. M. (2010). A Constitutive Model for Fiber-reinforced Polymer Composites. *Journal of Composite Materials*, *44*, 3133-3150.
- Christensen, R. (2009, August 8). *Failure of Fiber Composite Laminates- Progressive damage and polynomial invariants*. Retrieved April 7, 2018, from [www.failurecriteria.com](http://www.failurecriteria.com):  
[http://www.failurecriteria.com/Media/Failure\\_of\\_Fiber\\_Composite\\_Laminates-\\_Progressive\\_Damage\\_and\\_Polynomial\\_Invariants.pdf](http://www.failurecriteria.com/Media/Failure_of_Fiber_Composite_Laminates-_Progressive_Damage_and_Polynomial_Invariants.pdf)
- Christensen, R. (2008, January 27). *Failure Criteria*. Retrieved April 7, 2018, from [http://www.failurecriteria.com/Media/Failure\\_Criteria\\_for\\_Anisotropic\\_Fiber\\_Composite\\_Materials.pdf](http://www.failurecriteria.com/Media/Failure_Criteria_for_Anisotropic_Fiber_Composite_Materials.pdf)
- Correlated Solutions Inc. (2016). Retrieved February 24, 2018, from <http://correlatedsolutions.com/vic-3d/>
- Daniel, I. M., & Ishai, O. (2006). *Engineering Mechanics of Composite Materials*. New York: Oxford University Press.
- Deuschle, H. M., & Kropline, B.-H. (2012). Finite element implementation of Puck's failure theory for fiber-reinforced composites under three-dimensional stress. *Journal of Composite Materials*, *46*(19-20), 2485-2513.
- Deuschle, H. M., & Puck, A. (2012). Application of the Puck failure theory for fiber-reinforced composites under three-dimensional stress: Comparison with experimental results. *Journal of Composite Materials*, *47*(6-7), 827-846.
- Fouinneteau, M., & Pickett, A. K. (2007). Shear mechanism modelling of heavy tow braided composites using a meso-mechanical damage model. *Composites: Part A*, *38*(11), 2294-2306.
- Gama, B. A., Xiao, J.-R., Haque, M. J., Yen, C.-F., & Gillespie, J. W. (2004). *Experimental and Numerical Investigations on Damage and Delamination in Thick Plain Weave S-2 Glass Composites Under Quasi-Static Punch Shear Loading*. Aberdeen Proving Ground: U.S. Army Research Laboratory.
- Ganjani, M., Naghdabadi, R., & Asghari, M. (2012). An elastoplastic damage-induced anisotropic constitutive model at finite strains. *International Journal of Damage Mechanics*, *22*, 499-529.
- Goldberg, R. K., Carney, K. S., DuBois, P., Hoffarth, C., Khaled, B., Rajan, S., & Blankenhorn, G. (2018). Analysis and Characterization of Damage Using a Generalized Composite Material Model Suitable for Impact Problems. *Journal of Aerospace Engineering*, doi: 10.1061/(ASCE)AS.1943-5525.0000854.
- Goldberg, R., Carney, K., DuBois, P., Hoffarth, C., Harrington, J., Rajan, S., & Blankenhorn, G. (2014). Theoretical Development of an Orthotropic Three-Dimensional Elasto-Plastic Generalized Composite Material Model. *13th International LS-DYNA User's Conference*. Detroit, MI.
- Goldberg, R., Carney, K., DuBois, P., Hoffarth, C., Harrington, J., Rajan, S., & Blankenhorn, G. (2015). Development of an orthotropic elasto-plastic generalized composite material model suitable for impact problems. *Journal of Aerospace Engineering*, *29*(4), 04015083-1-04015083-11.
- Goldberg, R., Carney, K., DuBois, P., Hoffarth, C., Harrington, J., Rajan, S., & Blankenhorn, G. (2016, July). Development of an Orthotropic Elasto-Plastic

- Generalized Composite Material Model Suitable for Impact Problems. *ASCE J of Aerospace Engineering*, 29(4).
- Griffin, O., Kamat, M., & Herakovich, C. (1981). Three-dimensional inelastic finite element analysis of laminated composites. *Journal of Composite Materials*, 5, 543-560.
- Hallquist, J. (2013). *LS-DYNA Keyword User's Manual - Volume II: Material Models*. Livermore Software Technology Corporation.
- Harrington, J., & Rajan, S. D. (2014). *Test Results from Virtual Testing Software System*. Technical Report, ASU, School of Sustainable Engineering and the Built Environment.
- Harrington, J., Hoffarth, C., Rajan, S. D., Goldberg, R., Carney, K., DuBois, P., & Blankenhorn, G. (2017). Using virtual testing to complete the description of a three-dimensional orthotropic material. *Journal of Aerospace Engineering*, 30(5), 04017025-1-04017025-14.
- Hoffarth, C. (2016a). *A Generalized Orthotropic Elasto-Plastic Material Model for Impact Analysis*. Tempe, AZ, USA: PhD Dissertation, Arizona State university.
- Hoffarth, C., Harrington, J., Rajan, S. D., Goldberg, R., Carney, K., Du Bois, P., & Blankenhorn, G. (2014). Verification and Validation of a Three-Dimensional Generalized Composite Material Model. *13th International LS-DYNA User's Conference*. Detroit, MI.
- Hoffarth, C., Khaled, B., Shyamsunder, L., Rajan, S. D., Goldberg, R., Carney, K., . . . Blankenhorn, G. (2017). Verification and Validation of a Three-Dimensional Orthotropic Plasticity Constitutive Model Using a Unidirectional Composite. *Fibers*, 5(1), 1-13. doi:10.3390/fib5010012
- Hoffarth, C., Rajan, S. D., Goldberg, R., Carney, K., DuBois, P., & Blankenhorn, G. (2016b, December). Implementation and Validation of a Three Dimensional Plasticity Based Deformation Model for Orthotropic Composites. *Composites A*, 91, 336-350.
- Holzapfel, G. A., & Gasser, T. C. (2001). A viscoelastic model for fiber-reinforced composites at finite strains: Continuum basis, computational aspects and applications. *Computer methods in applied mechanics and engineering*, 190, 4379-4403.
- Johnson, A. F., Pickett, A. K., & Rozycki, P. (2001). Computational methods for predicting impact damage in composite structures. *Composites Science and Technology*, 61, 2183-2192.
- Kan, S. (2018). *Final Report on Probabilistic Modeling and Implementation in MAT 213*. George Mason University, Center for Collision Safety and Analysis, Fairfax.
- Khaled, B., Shyamsunder, L., Hoffarth, C., Rajan, S. D., Goldberg, R. K., Carney, K. S., . . . Blankenhorn, G. (2018b). Experimental characterization of composites to support an orthotropic plasticity material model. *Journal of Composite Materials*, 52(14), 1847-1872. doi:10.1177/0021998317733319
- Khaled, B., Shyamsunder, L., Hoffarth, C., Rajan, S., Goldberg, R., Carney, K., . . . Blankenhorn, G. (2018a). Damage characterization of composites to support an orthotropic plasticity material model. *Journal of Composite Materials*, 1-27. doi:10.1177/0021998318793506

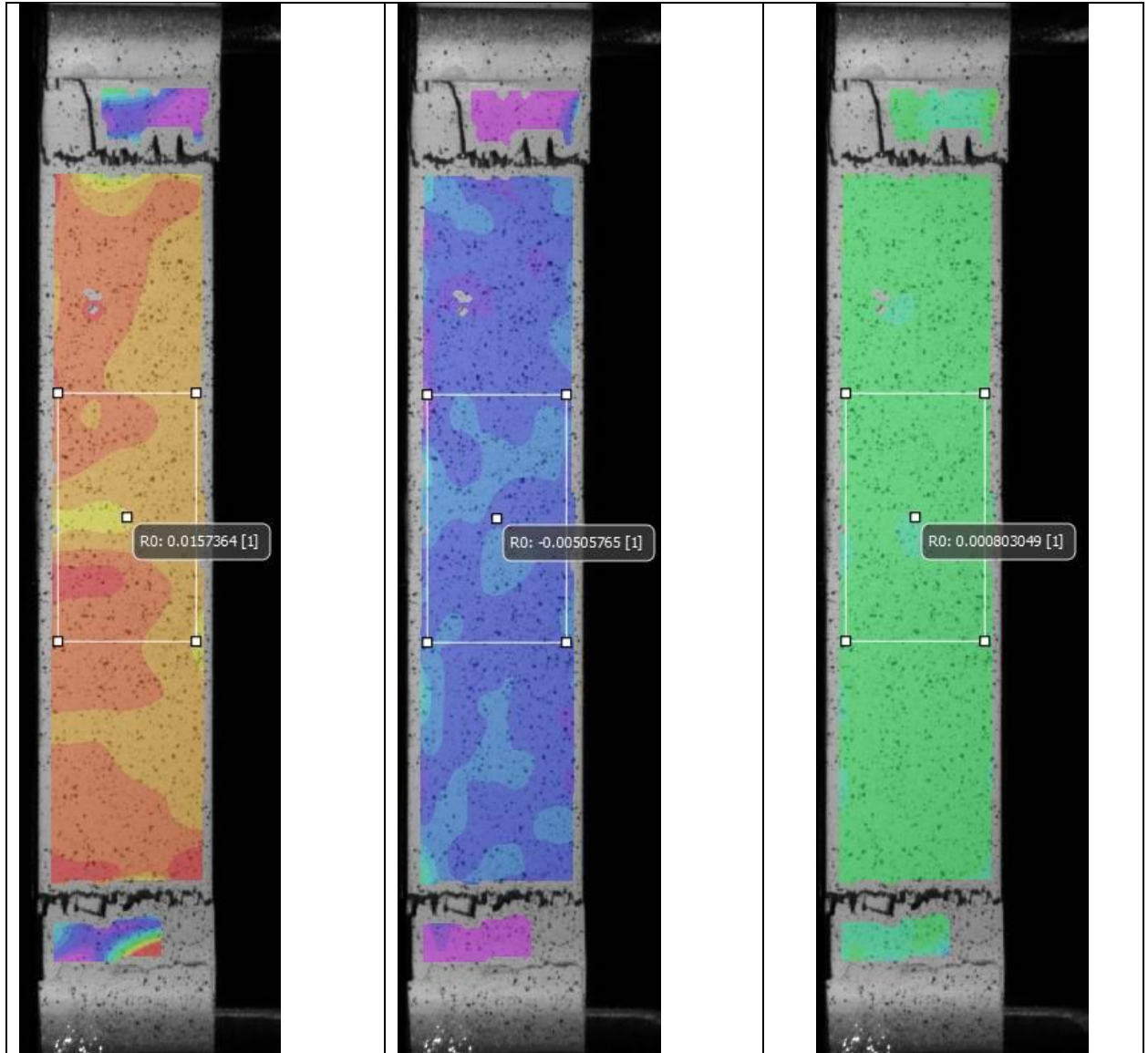
- Khaled, B., Shyamsunder, L., Schmidt, N., Hoffarth, C., & Rajan, S. (2018c). *Experimental Tests to Characterize the Behavior and Properties of T800-F3900 Toray Composite*. Arizona State University, School of Sustainable Engineering and the Built Environment, Tempe.
- Khan, A. S., & Huang, S. (1995). *Continuum Theory of Plasticity*. New York: John Wiley and Sons.
- Kodagali, K., Tessema, A., & Kidane, A. (2017). Progressive failure analysis of a composite lamina using Puck Failure Criteria. *Thirty-Second Technical Conference, American Society for Composites*. West Lafayette, Indiana.
- Ladeveze, P., & Le Dantec, E. (1992). Damage modeling of the elementary ply for laminated composites. *Compos. Sci. Technol.*, 43(3), 257-267.
- Lemaitre, J., & Desmorat, R. (2005). *Engineering Damage Mechanics: Ductile, Creep and Brittle Failures*. Berlin: Springer.
- Li, S., & Lim, S. (2005). Variational principles for generalized plane strain problems and their applications. *Composites A*, 36(3), 353-365.
- Littell, J. D., Binienda, W. K., Arnold, W. A., Roberts, G. D., & Goldberg, R. K. (2010). *Effect of Microscopic Damage Events on Static and Ballistic Impact Strength of Triaxial Braid Composites*. Washington: NASA.
- Livermore Software Technology Corporation. (2018). Retrieved from <http://ftp.lstc.com/anonymous/outgoing/lsprepost/dev/>
- Lourenco, P. B., Borst, R. D., & Rots, J. G. (1997). A Plane Stress Softening Plasticity Model for Orthotropic Materials. *International Journal for Numerical Methods in Engineering*, 4033-4057.
- LSTS. (2016). *LS-DYNA Version R8*.
- Maimi, P., Camanho, P. P., Mayugo, J. A., & Davila, C. G. (2007). A continuum damage model for composite laminates: Part I – Constitutive model. *Mechanics of Materials*, 39, 897-908.
- Maimi, P., Camanho, P. P., Mayugo, J. A., & Davila, C. G. (2007). A continuum damage model for composite laminates: Part II – Computational implementation and validation. *Mechanics of Materials*, 39, 909-919.
- Matzenmiller, A., Lubliner, J., & Taylor, R. L. (1995). A constitutive model for anisotropic damage in fiber-composites. *Mechanics of Materials*, 20, 125-152.
- Micallef, K., Fallah, A. S., Curtis, P. T., & Louca, L. A. (2013). A homogenised continuum constitutive model for visco-plastic deformation of uni-directional composites. *Composite Structures*, 99, 404-418.
- Moreira, L. P., & Ferron, G. (2007). Finite element implementation of an orthotropic plasticity model for sheet metal forming simulations. *Latin American Journal of Solids and Structures*, 4, 149-176.
- NASA. (2015, April 2). *Future Aircraft*. Retrieved from NASA Web Site: <https://www.nasa.gov/press/2015/april/nasa-creates-partnership-to-advance-composite-materials-for-aircraft-of-the-future>
- Notta-Cuvier, D., Lauro, F., & Bennani, B. (2014). An original approach for mechanical modelling of short fiber reinforced composites with complex distribution of fibre orientation. *Composites Part A*, 62, 60-66.

- Ogasawara, T., Ishikawa, T., Yokozeki, T., Shiraishi, T., & Watanabe, N. (2005). Effect of on-axis tensile loading on shear properties of an orthogonal 3D woven SiC/SiC composite. *Comp. Sci. Technol.*, 65(15-16), 2541-2549.
- Ozbolt, J., Lackovic, V., & Krolo, J. (2011). Modeling fracture of fiber reinforced polymer. *International Journal of Fracture*, 170, 13-26.
- Petit, P., & Waddoups, M. (1969). A method of predicting the nonlinear behavior of laminated composites. *Journal of Composite Materials*, 3, 2-19.
- Pindera, M., & Herakovich, C. (1982). An endochronic model for the response of unidirectional composites under off-axis tensile loads. *Mechanics of Composite Materials: Recent Advances, Proceedings of the IUTAM Symposium on Mechanics of Composite Materials*, (pp. 367-381). Blacksburg.
- Pinho, S. T., Iannucci, L., & Robinson, P. (2006). Physically-based failure models and criteria for laminated fibre-reinforced composites with emphasis on fibre kinking: Part I: Development. *Composites: Part A*, 37, 63-73.
- Pinho, S. T., Iannucci, L., & Robinson, P. (2006). Physically-based failure models and criteria for laminated fibre-reinforced composites with emphasis on fibre kinking: Part II: FE implementation. *Composites: Part A*, 37, 766-777.
- Puck, A., & Schurmann, H. (2002). Failure analysis of FRP laminates by means of physically based phenomenological models. *Composites Science and Technology*, 62(12-13), 1633-1662.
- Rajan, V., Shaw, J., Rossol, M., & Zok, F. (2014). An elastic-plastic constitutive model for ceramic composite laminates. *Composites Part A*, 66, 44-57.
- Raju, K. S., & Acosta, J. F. (2010). *Crashworthiness of Composite Fuselage Structures - Material Dynamic Properties, Phase I*. Washington, DC: U.S. Department of Transportation: Federal Aviation Administration.
- Roberts, G. D., Goldberg, R. K., Binienda, W. K., Arnold, W. A., Littell, J. D., & Kohlman, L. W. (2009). *Characterization of Triaxial Braided Composite Material Properties for Impact Simulation*. Washington: NASA.
- Salavatian, M., & Smith, L. V. (2014). The effect of transverse damage on the shear response of fiber reinforced laminates. *Comp. Sci. Technol.*, 95, 44-49.
- Santhosh, U., Ahmad, J., Ojard, G., Miller, R., & Gowayed, Y. (2016). Deformation and damage modeling of ceramic matrix composites under multiaxial stresses. *Composites Part B: Engineering*, 90, 97-106.
- Smith, D. L., & Dow, M. (September 1991). *Properties of Three Graphite/Toughened Resin Composites*. NASA Technical Paper 3102.
- Solecki, R., & Conant, R. J. (2003). *Advanced Mechanics of Materials*. New York, New York: Oxford University Press, Inc.
- Song, S., Waas, A. M., Shahwan, K. W., Faruque, O., & Xiao, X. (2010). Effects of Matrix Microcracking on the Response of 2D Braided Textile Composites Subjected to Compression Loads. *Journal of Composite Materials*, 44(2), 221-240.
- Sun, C. T., & Chen, J. L. (1989). A Simple Flow Rule for Characterizing Nonlinear Behavior of Fiber Composites. *Journal of Composite Materials*.
- Tabiei, A., & Wu, J. (2000). Three-dimensional nonlinear orthotropic finite element material model for wood. *Composite Structures*, 50, 143-149.

- Tsai, S. W., & Wu, E. M. (1971). A General Theory of Strength for Anisotropic Materials. *J. Composite Materials*, 5, 58-80.
- Tsai, S., & Wu, E. (1971). A General Theory of Strength for Anisotropic Materials. *Journal of Composite Materials*, 5(1), 58-80.
- Van der Meer, F. P. (2012). Mesolevel Modeling of Failure in Composite Laminates: Constitutive, Kinematic and Algorithmic Aspects. *Archives of Computational Methods in Engineering*, 19, 381-425.
- Vaziri, R., Olson, M. D., & Anderson, D. L. (1991). A Plasticity-Based Constitutive Model for Fibre-Reinforced Composite Laminates. *Journal of Composite Materials*, 512-535.
- Wang, C., Liu, Z., Xia, B., Duan, S., Nie, X., & Zhuang, Z. (2015). Development of a new constitutive model considering the shearing effect for anisotropic progressive damage in fiber-reinforced composites. *Composites Part B: Engineering*, 75, 288-297.
- Williams, K. V., Vaziri, R., & Poursartip, A. (2003). A physically based continuum damage mechanics model for thin laminated composite structures. *International Journal of Solids and Structures*, 40, 2267-2300.
- Wu, F., & Yao, W. (2010). A fatigue damage model of composite materials. *International Journal of Fatigue*, 134-138.
- Xiao, X. (2009). Modeling Energy Absorption with a Damage Mechanics Based Composite Material Model. *Journal of Composite Materials*, 43, 427-444.
- Xu, J., Askari, A., Weckner, O., & Silling, S. (2008). Peridynamic Analysis of Impact Damage in Composite Laminates. *J. Aerosp. Eng.*, 21, 187-194.
- Yang, W. H., & Feng, W. W. (1984). General and Specific Quadratic Yield Functions. *Journal of Composites*, 6(1), 19-21.
- Ye, J., & Zhang, D. (2012). Prediction of failure envelopes and stress-strain curves of fiber composite laminates under triaxial loads. *Journal of Composite Materials*, 46(19-20), 2417-2430.
- Yen, C.-F. (2002). Ballistic Impact Modeling of Composite Materials. *7th International LS-DYNA Users Conference*, (pp. 15-26).
- Zhang, D., Xu, L., & Ye, J. (2012). Prediction of failure envelopes and stress-strain curves of fiber composite laminates under triaxial loads: Comparison with experimental results. *Journal Composite Materials*, 47(6-7), 763-776.

## APPENDIX A—ANALYSIS OF DIC-OBTAINED STRAIN FIELD

During the experiments, all the components of the strain field are monitored. This ensures test data are reliable. For tension and compression tests, the critical strain is defined as the strain in the direction of loading. For shear tests, the critical strain is the shear strain induced in the principal plane being tested. The other strain components are relatively much smaller, which indicates the test results are reliable. Figure A.1-1 shows the longitudinal, transverse, and shear strain fields of a 1-direction tension specimen at failure. Note that the magnitude of the scales for each strain field is the same.



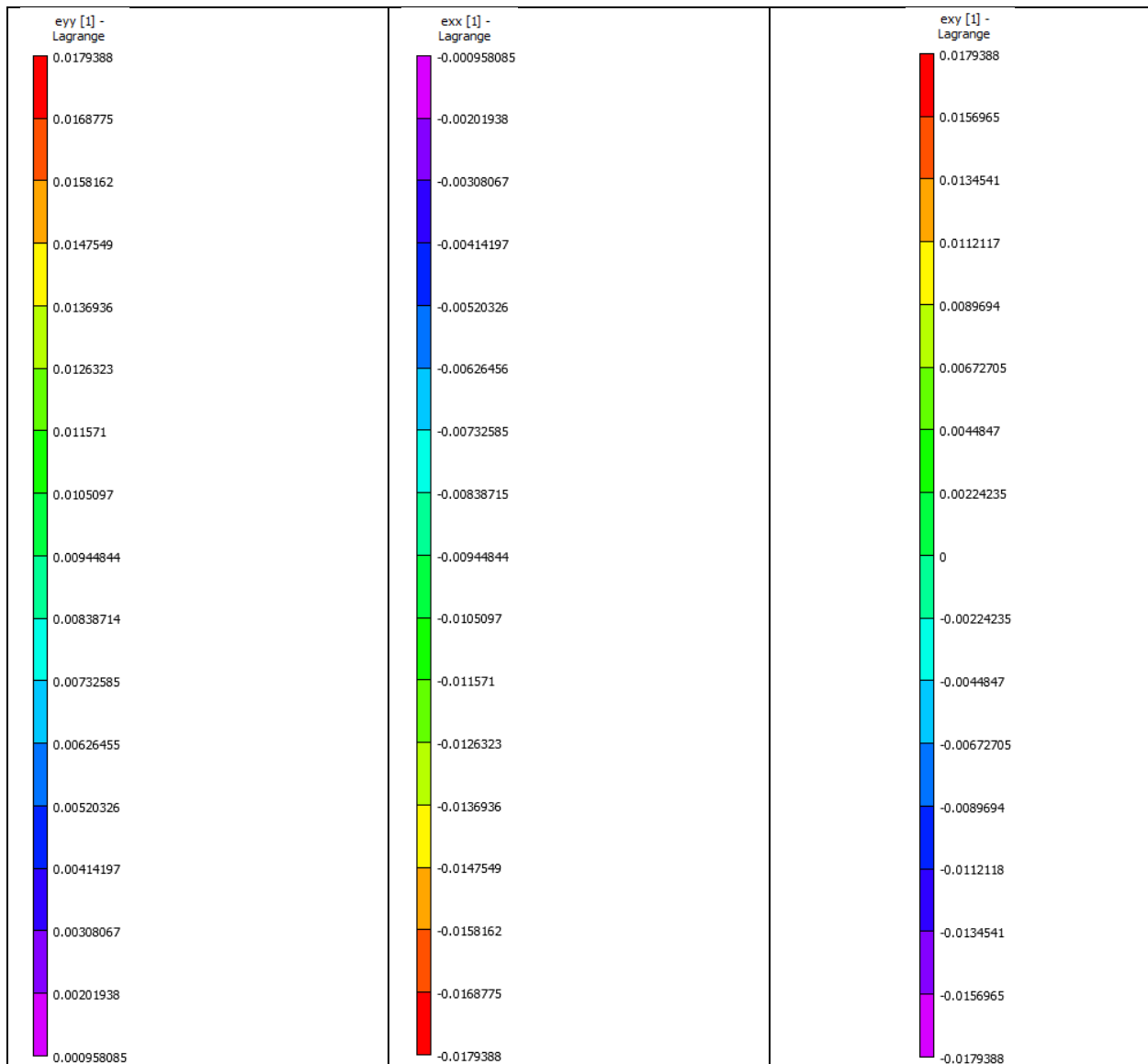


Figure A.1-1. TF16-5 strain fields (a) Longitudinal strain, (b) Transverse strain, (c) Tensorial shear strain

Table A.1-1 shows the maximum strain components at peak stress for a typical specimen from the tests. The critical strain may be either failure or ultimate depending on how it is labeled in its respective section. The critical strain for each test is highlighted.

Table A.1-1. Summary of the Maximum Strains for Each Test at Peak Stress

<b>Test Type</b>	<b>Replicate</b>	<b>Longitudinal Strain</b>	<b>Transverse Strain</b>	<b>Tensorial Shear Strain</b>
1-direction tension	TF16-5	0.01579	-0.00508	0.000763
2-direction tension	TFT2-5	0.00641	-0.00007030	-0.0000293
3-direction tension	TFT3-13	0.00395	-0.00176	-0.00000367
1-direction compression	TFC1-9	-0.00622	0.00263	-0.00058
2-direction compression	TFC2-15	-0.02817	0.00069	-0.00024
3-direction compression	TFC3-8	-0.02306	0.016705	-0.00178
1-2 plane shear	TFS12-8	0.002845	-0.00401	0.12946
2-3 plane shear	TFS23-5	0.000394	-0.00041	0.00493
1-3 plane shear	TFS13-2	0.002832	0.003957	0.06827
1-2 off axis tension	TFO12-5	0.00712	-0.00218	0.002251
2-3 off axis compression	TFO23-4	0.05497	0.054675	-0.00019
1-3 off axis compression	TFO13-8	0.0915	0.083225	-0.00805